JRC TECHNICAL REPORTS

JRC – Ispra Atmosphere – Biosphere – Climate Integrated monitoring Station

2012 report

J.P. Putaud, C. Belis, P. Bergamaschi, F. Cavalli, A. Cescatti, D. Daou, A. Dell'Acqua, K. Douglas, M. Duerr, I. Goded, F. Grassi, C. Gruening, J. Hjorth, N. R. Jensen, F. Lagler, G. Manca, S. Martins Dos Santos, R. Passarella, V. Pedroni, P. Rocha e Abreu, D. Roux, B. Scheeren

2014

Report EUR 26571 EN

Joint Research Centre

European Commission
Joint Research Centre
Institute for Environment and Sustainability

Contact information
Jean-Philippe Putaud
Address: Joint Research Centre, Via Enrico Fermi 2749, TP 050, 21027 Ispra (VA), Italy
E-mail: jean.putaud@jrc.ec.europa.eu
Tel.: +39 0332 78 50 41
Fax: +39 0332 78 50 22

http://ccaqu.jrc.ec.europa.eu/
http://www.jrc.ec.europa.eu/

This publication is a Technical Report by the Joint Research Centre of the European Commission.

JRC 87372

EUR 26571 EN

ISBN 978-92-79-33603-4 (PDF)

ISSN 1831-9424 (online)

doi:10.2788/38242

Luxembourg: Publications Office of the European Union, 2014

Printed in Italy

Contents

ABC-IS mission

The aim of the Atmosphere-Biosphere-Climate Integrated monitoring Station (ABC-IS) is to measure changes in atmospheric variables to obtain data that are useful for the conception, development, implementation, and monitoring of the impact of European policies and International conventions on air pollution and climate change. Measurements include greenhouse gas concentrations, forest ⇆ atmosphere fluxes, and concentrations of pollutants in the gas phase, the particulate phase and precipitations, as well as aerosol physical and optical characteristics. The goal of ABC-IS is to establish real world interactions between air pollution, climate change and the biosphere, for highlighting possible trade-offs and synergies between air pollution and climate change related policies. Interactions include the role of pollutants in climate forcing and CO_2 uptake by vegetation, the impact of climate change and air pollution on CO_2 uptake by vegetation, the effect of biogenic emission on air pollution and climate forcing, etc.

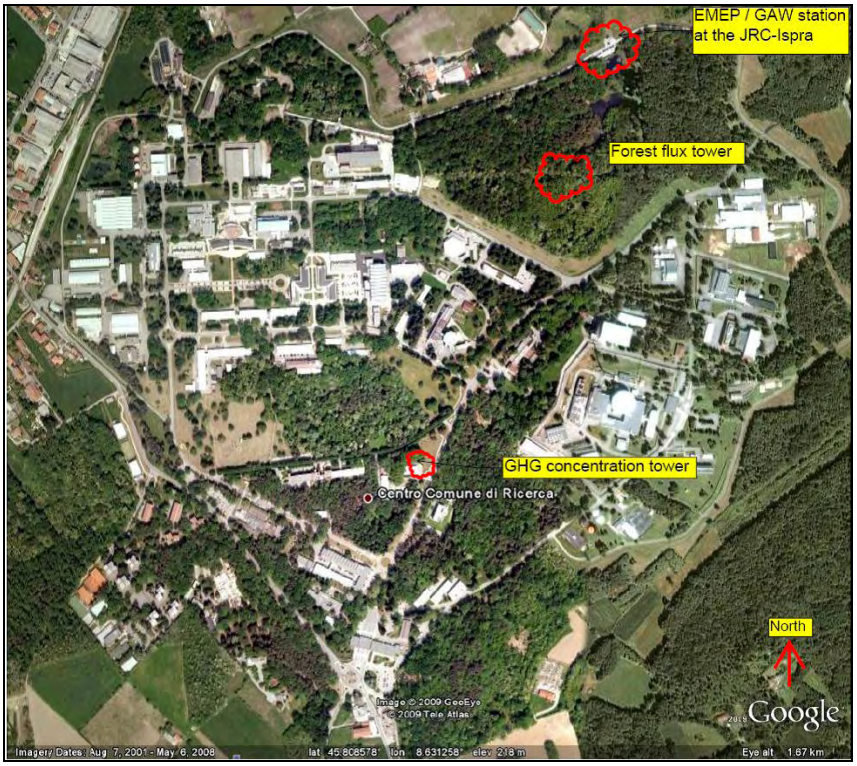

Fig. 1. *JRC-Ispra site and the location of the laboratory for greenhouse gas monitoring and the EMEP-GAW station within the site.*

Measurements are performed in the framework of international monitoring programs like the future ESFRI (European Strategy Forum on Research Infrastructures) project ICOS (Integrated Carbon Observation System), EMEP (Co-operative program for monitoring and evaluation of the long range transmission of air pollutants in Europe of the UN-ECE *Convention on Long-Range Transboundary Air Pollution* CLRTAP) and GAW (the Global Atmosphere Watch program of the World Meteorological Organization). The ABC-IS infrastructure is also used in competitive projects (e.g ACTRIS, ECLAIRE, InGOS). The participation of ABC-IS in international networks leads its staff to conduct inter-laboratory

comparisons and developments of standard methods in collaboration with the European Reference Laboratory for Air Pollution of the JRC.

Quality management system

ABC-IS is a research infrastructure of JRC's Institute for Environment and Sustainability. JRC-IES achieved the ISO 9001 certification in May 2012, which is also valid for the year 2012 (ISO 9001 is mainly about "project management").

In addition, in Nov. 2010 the JRC-Ispra also achieved the ISO 14001 certificate (ISO 14001 is mainly about "environmental issues"), which is also valid for 2012.

Every year there are internal/external audits for the certificates (ISO 9001 / ISO 14001), which were also performed in 2012.

The "quality management system (QMS) for the ABC-IS regional station" includes server space at the following links:

\\ccunas3.jrc.it\H02QMS_year_2012_
\\Ccunas3.jrc.it\largefacilities\ABC-IS
\\ccunas3.jrc.it\Laboratories

where the following information can be found: list of instruments; information about calibrations; standards used and maintenance; standard operational procedures (SOP's); instrument lifecycle sheets and log-books; manuals for the instruments; *etc*. For additional specific details about QMS, for the year 2012 and the ABC-IS station, see e.g. the file 2012_Instruments'_calibration_&_standards_&_maintenance.xls, that can be found under \\Ccunas3.jrc.it\largefacilities\ABC-IS\Quality_management.

More QMS information/details can also be found in the sections "Measurement techniques" in this report.

More general QMS information/documentations about how the IES-AC Unit (H02) is run, the management of all of the projects within the Unit and the running of the ABC-IS station can also be found at

\\ccunas3.jrc.it\H02QMS_year_2012_
\\ccunas3.jrc.it\H02QMS_year_2013_

especially in the six H02 Unit QMS documents listed here:

QMS_H02_SUMM_Scientific_Unit_Management_Manual_v7_0.pdf
QMS_H02_MANPROJ_PROJ_Laboratory_Management_v6_0.pdf
QMS_H02_MANPROJ_PROJ_Model_Management_v6_0.pdf
QMS_H02_MANPROJ_PROJ_Informatics_Management_v6_0.pdf
QMS_H02_MANPROJ_PROJ_Knowledge_Management_v6_0.pdf
QMS_H02_MANPROJ_PROJ_Review_Verification_Validation_Approval_v2_0.pdf

The latest versions of the documents are available at

\\ccunas3.jrc.it\H02QMS_year_2013_\1_UNIT\QMS_info\QMS_documents_H02

Fig. 2: the laboratory for greenhouse gas concentration monitoring (Bd 5)

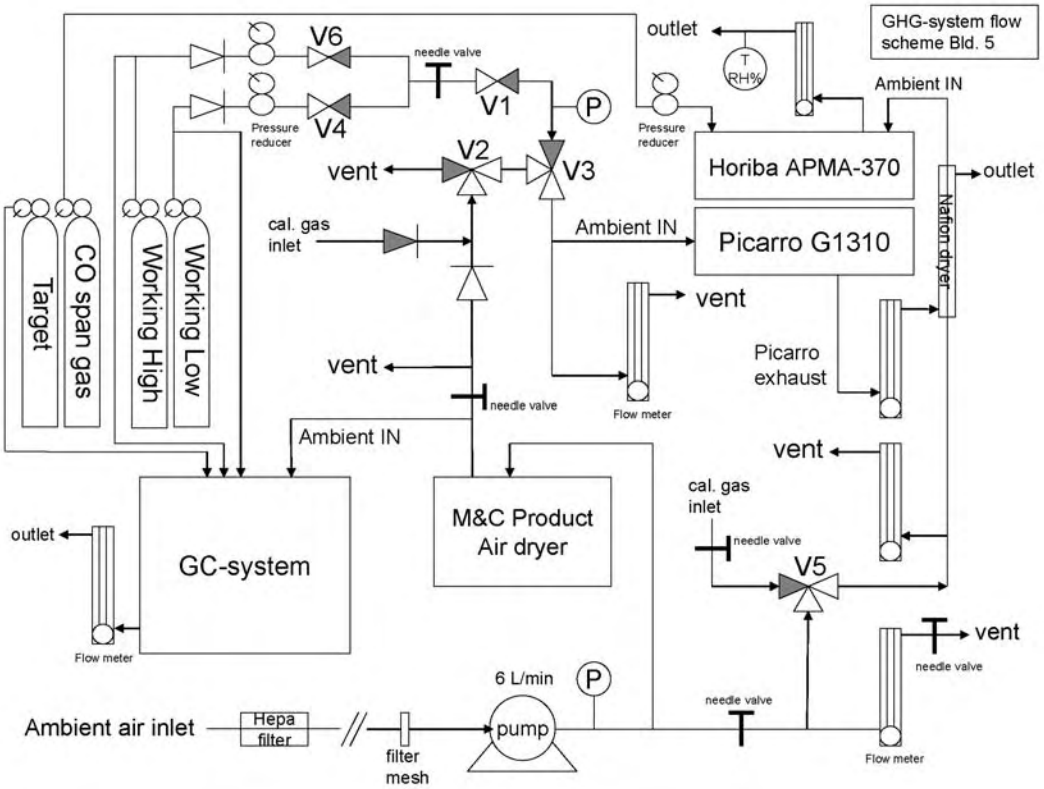

Fig. 3: *Building 5 GHG-system flow scheme.*

Greenhouse gas concentration monitoring at the JRC-Ispra site

Introduction

Location

The GHG monitoring station is located at Building 5 of the JRC site Ispra (45.807°N, 8.631°E, 223 m asl). The station is currently the only low altitude measurement site for greenhouse gases near the Po Valley. The unique location of the station at the Eastern border of Lake Maggiore in a semi-rural area at the North-Western edge of the Po Valley allows sampling of highly polluted air masses from the Po Valley during meteorological conditions with southerly flow, contrasted by situations with northerly winds bringing relatively clean air to the site. The main cities around are Varese, 20 km to the East, Novara, 40 km South, Gallarate - Busto Arsizio, about 20 km southeast and Milan, 60 km to the south-east.

Measurement program

The GHG monitoring station is in operation since October 2007 and is complementary to the JRC-Ispra EMEP-GAW (European Monitoring and Evaluation Programme - Global Atmospheric Watch) air quality station which started in 1985. Both activities together with biosphere atmosphere fluxes are referred to as ABC-IS (Atmosphere, Biosphere, Climate Integrated Monitoring Station), and will be merged in 2014 into a single monitoring and research platform with a new station building and tall tower for atmospheric sampling. The measurement program follows the recommendations of ICOS (www.ICOS-infrastructure.eu) for level 2 stations.

Instrumentation

Here we summarize the most important aspects of the GHG and ^{222}Radon measurement system. A more detailed description is given by Scheeren et al. (2010).

Sampling

Air is sampled from a 15 m high mast using a 50 m 6 mm i.d. Teflon tube at a flow rate of ~6 L /min using a KNF membrane pump (KNF N811KT.18). The sampled air is filtered from aerosols by a Pall Hepa filter (model PN12144) positioned 10 m downstream of the inlet and dried cryogenically by a commercial system from M&C products (model EC30 FD) down to a water vapour content of <0.015%v before being directed to the different instruments. The remaining water vapour is equivalent to a maximum 'volumetric error' of <0.06 ppmv of CO_2 or <0.3 ppbv of CH_4 or <0.05 ppbv N_2O. A schematic overview of the sample flow set-up is shown in Figure 3.

Gas Chromatograph Agilent 6890N (S/N US10701038*)*

For continuous monitoring at a 6 minute time resolution of CO_2, CH_4, N_2O, and SF_6 we apply an Agilent 6890N gas chromatograph equipped with a Flame Ionization Detector and micro-Electron Capture Detector based on the set-up described by Worthy el al. (1998). The calibration strategy has been adopted from Pépin et al. (2001) and is based on applying a Working High (WH) and Working Low (WL) standards (bracketing standards), which are calibrated regularly using NOAA primary standards. The WH and WL are both measured 2 times per hour for calculating ambient mixing ratios and a Target (TG) sample is measured every 6 hours for quality control (purchased from Deuste Steininger GmbH, Germany). The GHG measurements are reported as dry air mole fractions (mixing ratios) using the WMO NOAA2004 scale for CO_2 and CH_4, the NOAA2006 scale for N_2O and SF_6. We apply a suite of five NOAA tanks ranging from 369-523 ppm for CO_2, 1782-2397 ppb for CH_4, 318-341 ppb for N_2O, and 6.1-14.3 ppt for SF as primary standards. The GC control and peak integration runs on *ChemStation* commercial software. Further processing of the raw data is based on custom built software developed in C language and named GC_6890N_Pro. A schematic of the GC-system set-up and typical chromatograms are shown in Figure 4, while Figure 5 shows the graphical user interface of the GC_6890N_Pro software.

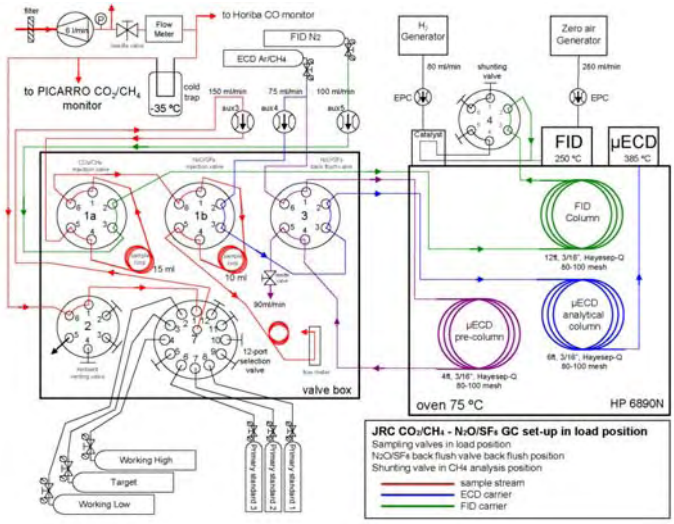

Fig.4: Schematic of the GC-system set-up for greenhouse gas concentration measurements

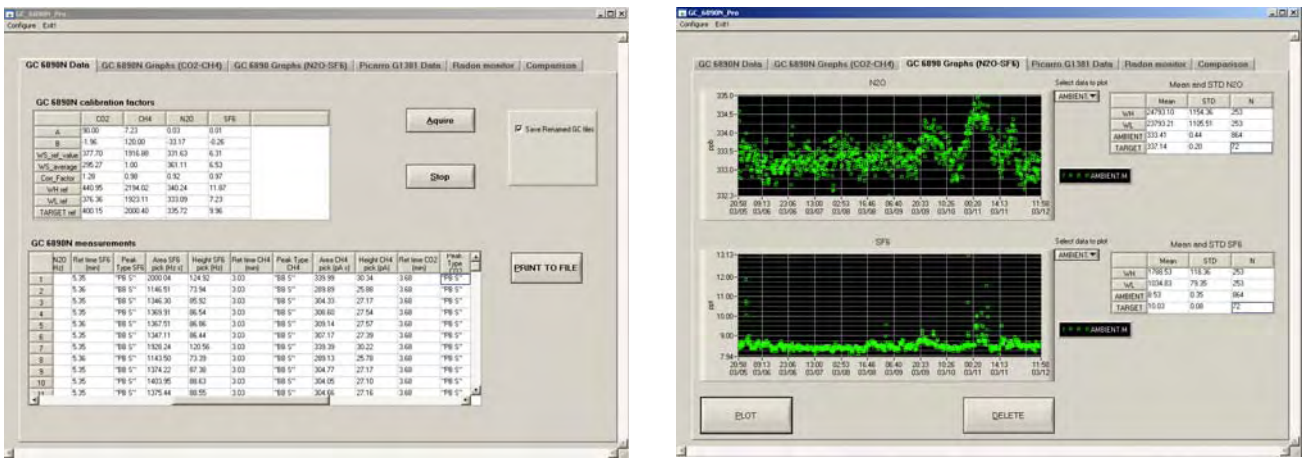

Fig. 5: *Graphical User Interface of GC_6890N_Pro software, developed for data processing of GC raw data*

Cavity Ring-Down Spectrometer (Picarro G1301) (S/N CFDAS-42*)*

In addition to the low time resolution GC-system we have been operating a fast Picarro G1301 Cavity Ring-Down Spectrometer (Picarro CRDS) for CO_2 and CH_4 since February 2009. The Picarro instrument collects air samples from the same inlet used for the GC at a 12 second time resolution. From March 24, 2009 onwards we applied a commercial M&C Products Compressor gas Peltier cooler type EC30/FD for drying of the sampling air to below 0.02%v. This corresponds to a maximum 'volumetric error' of about 0.08 ppm CO_2 and 0.4 ppb CH_4. To compensate for the remaining water vapor fraction we apply an empirically determined instrument specific water vapor correction factor. From May 27, 2009 onwards, the monitor received a WL and WH standard for 10 minutes each once every two days which was reduced to once every 4 days from September 2011 onwards, to serve as a Target control sample and to allow for correction of potential instrumental drift. A full scale calibration with 5 NOAA standards is performed 2 to 3 times per year. The monitor response has shown to be highly linear and the calibration factors obtained with the 5-point calibration have shown negligible changes within the precision of the monitor over the course of a year. The monitor calibration factors to calculate raw concentration values have been set to provide near real-time raw data with an accuracy of <0.5 ppm for CO_2 and <2 ppb for CH_4.

Radon analyser ANSTO (custom built)

^{222}Radon activity concentrations in Bq m^{-3} have been semi-continuously monitored (30 minute time integration) applying an ANSTO dual-flow loop two-filter detector (Zahorowski et al., 2004) since October of 2008. The monitor is positioned close to the GHG-sampling mast and used a separate inlet positioned at 3.5 m above the ground. A 500 L decay tank was placed in the inlet line to allow for the decay of Thoron (^{220}Rn with a half-life of 55.6 s) before reaching the ^{222}Radon monitor. The ANSTO ^{222}Radon monitor is calibrated once a month using a commercial passive ^{226}Radium source from Pylon Electronic Inc. (Canada) inside the calibration unit with an activity of 21.99 kBq, which corresponds to a ^{222}Radon delivery rate of 2.77 Bq min^{-1}. The lower limit of detection is 0.02 Bq m^{-3} for a 30% precision (relative counting error). The total measurement uncertainty is estimated to be <5% for ambient ^{222}Radon activities at Ispra.

Measurement uncertainties

The different types of uncertainties affecting the GHG measurements have been estimated using the algorithms developed in the Integrated non-CO2 Greenhouse gas Observing System (InGOS) project (http://www.ingos-infrastructure.eu/). These uncertainties are defined as follows:

- Statistical uncertainty (repeatability) is calculated as the 24-hours centered moving, 1σ standard deviation of the bracketing standards.
- Laboratory internal scale consistency uncertainty is the median of the difference between measured and assigned target value. The median is calculated for different time periods.
- Reproducibility represents the absolute values of the smoothed target residuals. Smoothing is performed with a centered running median with a window length of 30 days.
- Scale transfer and non-linearity uncertainty is calculated as the root mean square difference of the externally assigned and measured values of the laboratory reference NOAA standards.

For the PICARRO G1301 we define the precision by the 1σ standard deviation of the average of a 10 minutes dry standard measurement. To determine the long-term reproducibility we evaluated the deviations of the Target from the assigned value over a period of about 7 months. We found that the reproducibility over this period was <0.04 ppm for CO_2 and <0.3 ppb for CH_4. The precision and reproducibility for the PICARRO measurements are presented in Table 1.

Table 1: *Precision and reproducibility for the different gas species measured by PICARRO G1301.*

Species-method	Precision	Reproducibility Long-term	WMO (1) compatibility goal
CO_2-CRDS	0.03 ppm	0.04 ppm	
CH_4-CRDS	0.2 ppb	0.3 ppb	

(1) *WMO-GAW Report No. 194, 2010.*

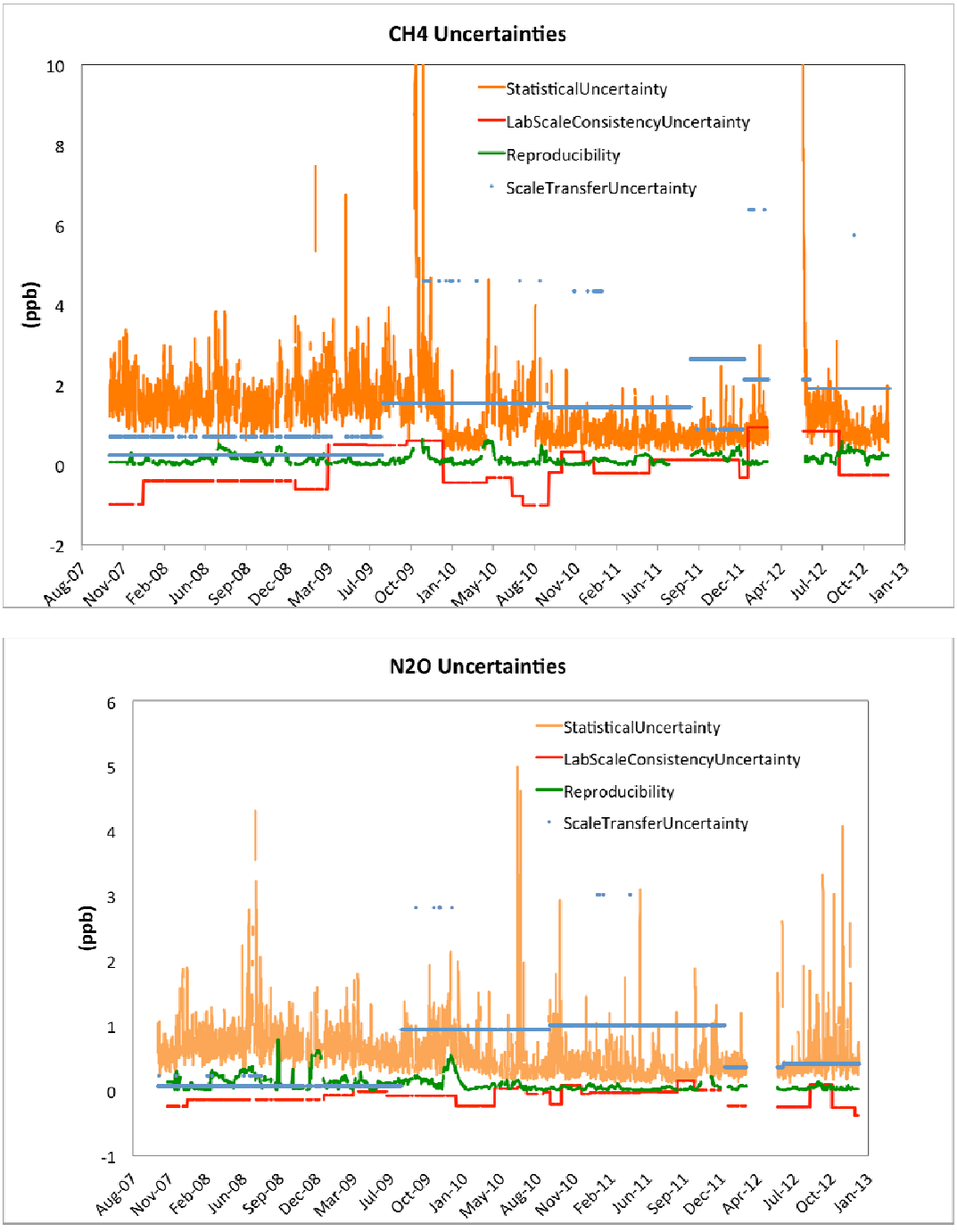

Figure 7: *Uncertainties affecting CH_4 and N_2O measurements performed by the GC system.*

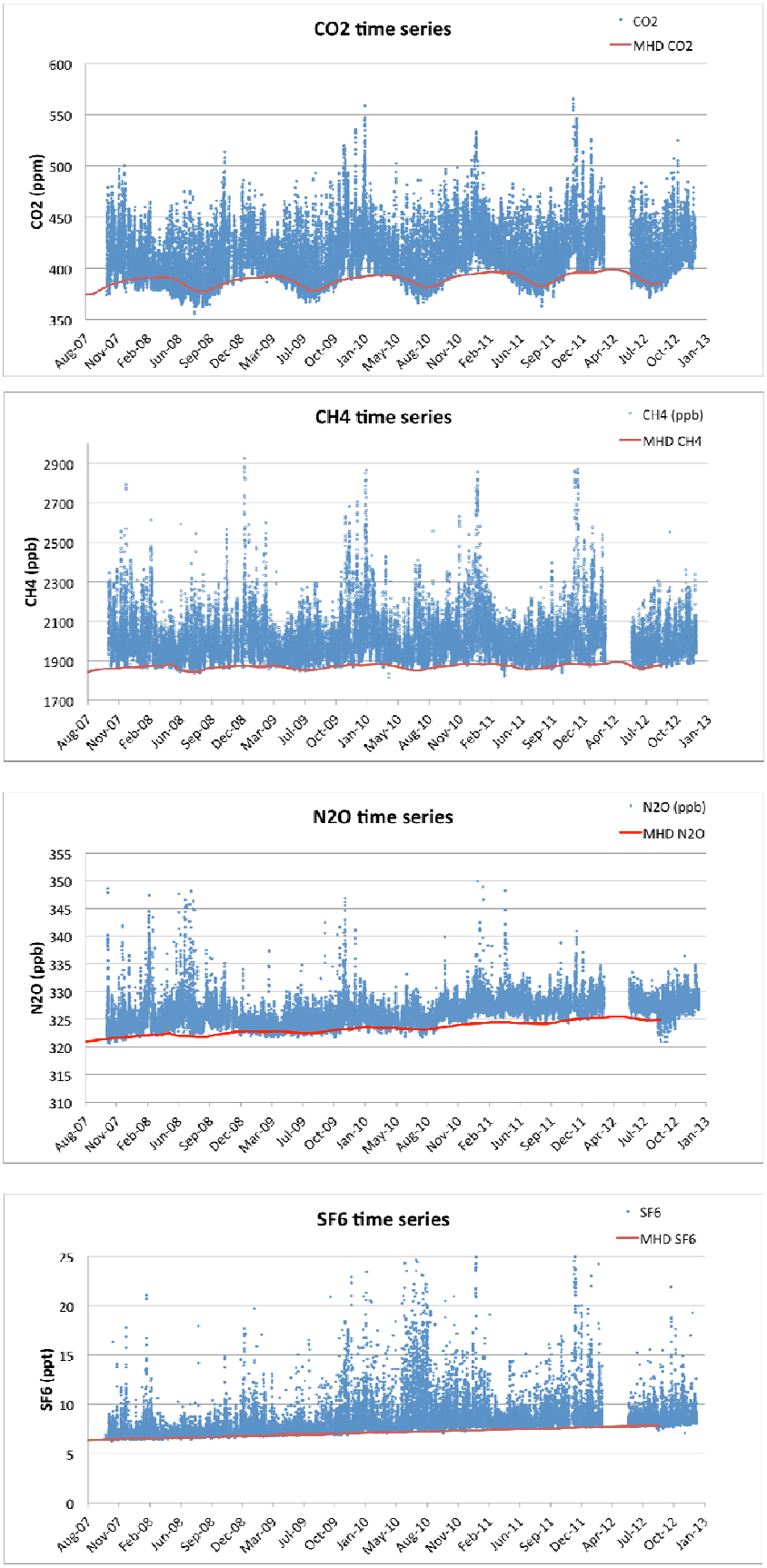

Fig. 6 *Time series of continuous CO_2, CH_4, N_2O, SF_6, measurements at Ispra between October 2007 and December 2012. The figure shows hourly mean values of dry air mole fractions (blue points). Monthly mean concentrations from the background station Mace Head on the West coast of Ireland are also included (red points).*

Overview of measurement results

Figure 6 gives an overview of the GC greenhouse gas measurements since the start of the measurements in October of 2007 until December of 2012. The figure shows hourly averages concentrations. Furthermore, continuous measurements from the Mace Head (Ireland) station are included in the Figure to illustrate the Atlantic background mixing ratios. Mace Head data are from the WMO World Data Centre for Greenhouse gases: CO_2 from Michel Ramonet, LSCE, Paris; CH_4 and N_2O from Ed Dlugokencky, NOAA/ESRL, and SF_6 from Ray Wang, Georgia Institute of Technology.
At the end of February 2012 GC measurement were stopped because of the end of the working contract of Bert Scheeren. Measures restarted at the end of May 2012 when Giovanni Manca took over from B. Scheeren.
Figure 7 shows the four types of uncertainties as defined in the InGOS project for CH_4 and N_2O. Statistical uncertainty (repeatability) is the major contributor to the overall uncertainty affecting the GC.
Figure 8 shows hourly mean ^{222}Radon activities since October 2008.

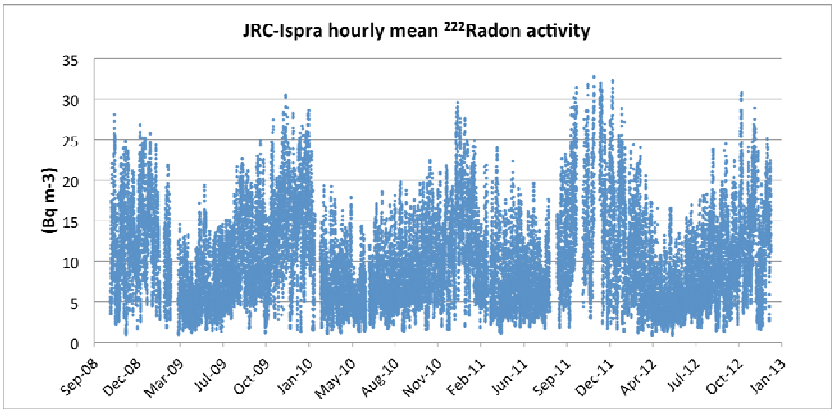

Fig. 8**:** *Time series of hourly mean ^{222}Radon activity from Oct. 2008 to Dec. 2012.*

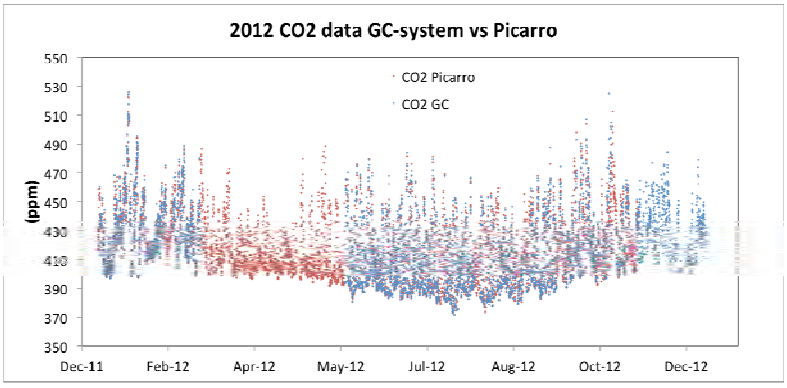

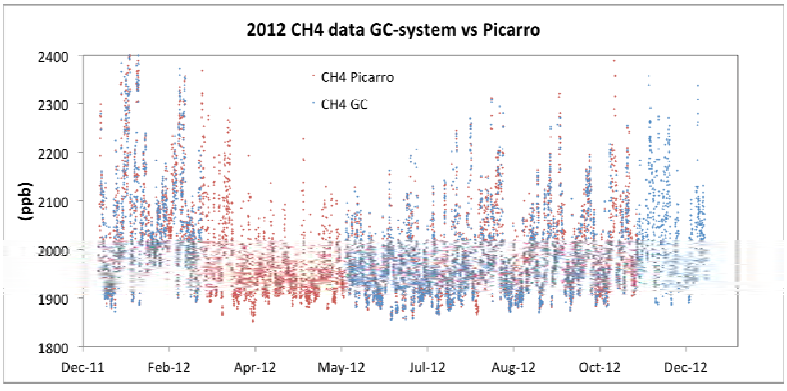

Fig. 9a: *Time series of hourly mean CH_4 and CO_2 dry air mole fractions at Ispra during 2012 from the GC-system and the Picarro CRDS.*

Focus on 2012 data

In Figure 9a we show the CO_2 and CH_4 hourly mean time series from both the GC-system and the Picarro CRDS for 2012. In Figure 9b the excellent agreement between both measurements system is illustrated by the fact that the absolute difference between the hourly mean values of the Picarro and the GC-system is usually well within the variability (depicted as the 1-σ standard deviation) of the hourly mean data from the Picarro instrument.

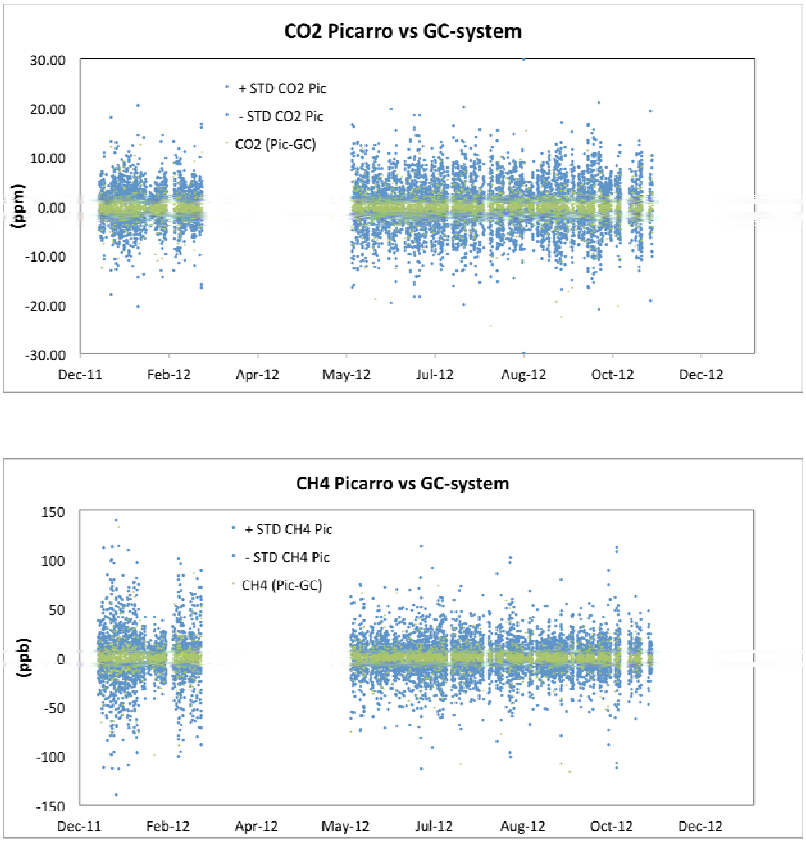

Fig. 9b: *Comparison between the absolute difference of the hourly mean values of the Picarro and the GC-system and the variability (depicted as the 1-σ standard deviation) of the hourly mean data from the Picarro instrument*.

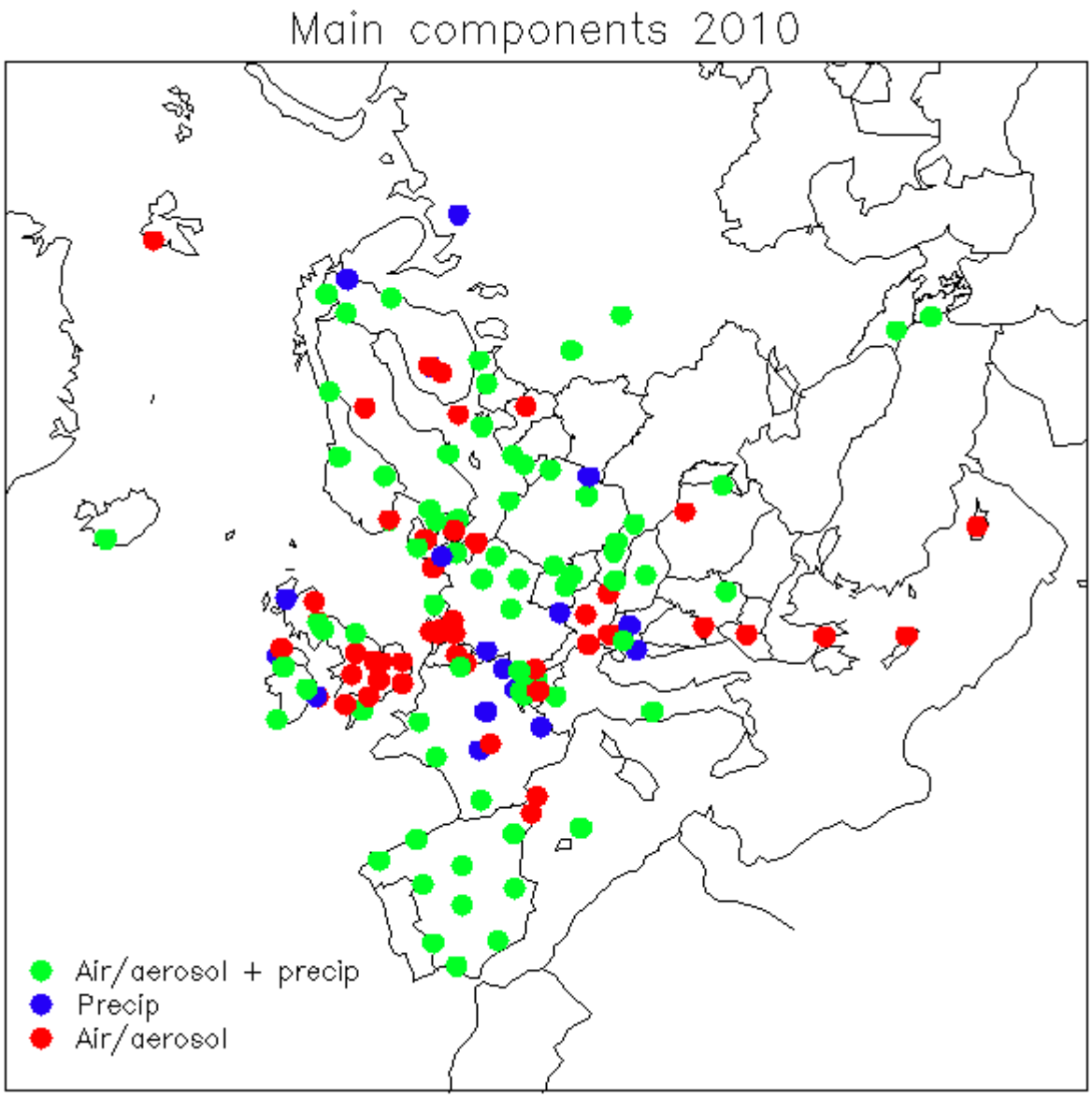

Fig 10: *most recent available map of the EMEP stations across Europe.*

Atmosphere watch at the JRC-Ispra site

Introduction

Location

Air pollution has been monitored since 1985 at the EMEP and regional GAW station for atmospheric research (45°48.881'N, 8°38.165'E, 209 m a.s.l.) located by the Northern fence of the JRC-Ispra site (see Fig. 1), situated in a semi-rural area at the NW edge of the Po valley in Italy. The main cities around are Varese (20 km east), Novara (40 km south), Gallarate - Busto Arsizio (about 20 km south-east) and the Milan conurbation (60 km to the south-east). Busy roads and highways link these urban centers. Emissions of pollutants reported for the four industrial large point sources (CO_2 emissions > 1500 tons d^{-1}) located between 5 and 45 km NE to SE from Ispra also include 2 and 3 tons of CO per day, plus 3 and 5 tons of NOx (as NO_2) per day for the 2 closest ones (PRTR emissions, 2010).

Underpinning programs

The EMEP program (*http://www.emep.int/*)

Currently, about 50 countries and the European Community have ratified the CLRTAP. Lists of participating institutions and monitoring stations (Fig. 10) can be found at: *http://www.nilu.no/projects/ccc/network/index.html*

The set-up and running of the JRC-Ispra EMEP station resulted from a proposal of the Directorate General for Environment of the European Commission in Brussels, in agreement with the Joint Research Centre, following the Council Resolution N° 81/462/EEC, article 9, to support the implementation of the EMEP programme.

The JRC-Ispra station operates on a regular basis in the extended EMEP measurement program since November 1985. Data are transmitted yearly to the EMEP Chemical Coordinating Centre (CCC) for data control and statistical evaluation, and available from the EBAS data bank (Emep dataBASe, *http://ebas.nilu.no/*).

The GAW program (*http://www.wmo.int/web/arep/gaw/gaw_home.html*)

WMO's Global Atmosphere Watch (GAW) system was established in 1989 with the scope of providing information on the physico-chemical composition of the atmosphere. These data provide a basis to improve our understanding of both atmospheric changes and atmosphere-biosphere interactions. GAW is one of WMO's most important contributions to atmosphere-biosphere the study of environmental issues, with about 80 member countries participating in GAW's measurement program. Since December 1999, the JRC-Ispra station is also part of the GAW coordinated network of regional stations. Aerosol data submitted to EMEP and GAW are available from the World Data Centre for Aerosol (WDCA).

Fig. 11. *Measurements performed at the JRC-Ispra station for atmospheric research since 1985.*

The institutional program (***http://ccaqu.jrc.ec.europa.eu***)

Since 2002, the measurement program of the air pollution monitoring station of JRC-Ispra has gradually been focused on short-lived climate forcers such as tropospheric ozone and aerosols, and their precursors (Fig. 11). Concretely, more sensitive gas monitors were introduced, as well as a set of new measurements providing aerosol characteristics that are linked to radiative forcing. In 2012, the station's duty as listed in the Airclim action work plan was to deliver "data on regulated and non-regulated pollutants delivered to EMEP and the World Data Centre for Aerosols international databases"

The site is also being used for research and development purposes. Regarding particulate organic and elemental carbon, techniques developed in Ispra are implemented and validated by international research station networks (EUSAAR, ACTRIS), recommended in the EMEP sampling and analytical procedure manual, and considered by the European Committee for Standardisation (CEN) as possible future standard methods.

Additional information about the JRC-Ispra air monitoring station and other stations from the EMEP network can also be found in the following papers: Van Dingenen et al., 2004; Putaud et al., 2004; Mira-Salama et al., 2008; Putaud et al., 2010). Nowadays, all validated monitoring data obtained at the JRC-Ispra station within the EMEP and the GAW program and other international projects (EUSAAR, ACTRIS) can be retrieved from the EBAS database (*http://ebas.nilu.no/*), selecting Ispra as the station of interest.

Table 2. Parameters measured during 2012

METEOROLOGICAL PARAMETERS	Pressure, temperature, humidity, wind, solar radiation
GAS PHASE	SO_2, NO, NO_X, O_3, CO
PARTICULATE PHASE	For $PM_{2.5}$: PM mass and Cl^-, NO_3^-, SO_4^{2-}, $C_2O_4^{2-}$, Na^+, NH_4^+, K^+, Mg^{2+}, Ca^{2+}, OC, and EC For PM_{10}: PM mass and Cl^-, NO_3^-, SO_4^{2-}, $C_2O_4^{2-}$, Na^+, NH_4^+, K^+, Mg^{2+}, Ca^{2+}, OC, and EC + 31 trace elements (till June) Number size distribution (10 nm - 10 µm) Aerosol absorption, scattering and back-scattering coefficient Altitude-resolved aerosol back-scattering
PRECIPITATION	Cl^-, NO_3^-, SO_4^{2-}, $C_2O_4^{2-}$, Na^+, NH_4^+, K^+, Mg^{2+}, Ca^{2+} pH, conductivity

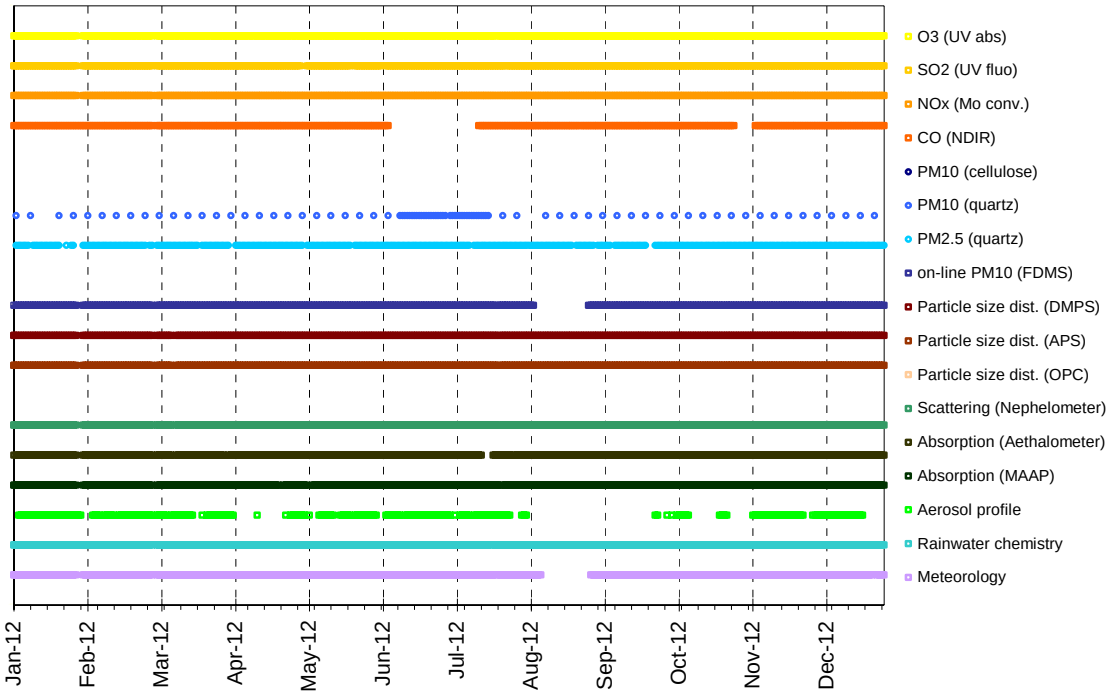

Fig. 12. *The year 2012 data coverage at the JRC EMEP-GAW station.*

Measurements and data processing

The air pollution monitoring program at the JRC- Ispra station in 2012

Since 1985, the JRC-Ispra air monitoring station program evolved significantly (Fig. 11). The variables measured at the JRC-Ispra station in 2012 are listed in Table 2. Fig. 12 shows the data coverage for 2012.

Meteorological parameters were measured during the whole year 2012, except for a gap from Aug. 9th to 28th, for which data measured at the JRC building 51 were used.

SO_2, O_3 and NOx were measured almost continuously during the year 2012. The measurement of CO was performed almost continuously from July 13th. CO measurements were also performed till June 7th to from the complementary JRC greenhouse gas monitoring station located about 900 m away from the EMEP-GAW station.

Particulate matter (PM2.5) samples were collected daily and analyzed for PM2.5 mass (at 20% RH), main ions, OC (organic carbon) and EC (elemental carbon). PM10 24-hour filter samples were generally collected every 6th day on average, except during the EMEP intensive observation period (daily) from June 11th to July 18th. PM10 samples were analyzed in the same way as the daily PM2.5 samples, and also for 31 trace elements from until July 2012. On-line PM10 measurements (FDMS-TEOM, Filter Dynamics Measurement System - Tapered Element Oscillating Microbalance) were carried out continuously, except from August 7th to 28th.

Particle number size distribution (10 nm < Dp < 10 µm), aerosol absorption coefficient and scattering coefficient were measured continuously over the whole year 2012.

The CIMEL LiDAR (Light Detection and Ranging) provided altitude resolved aerosol backscattering profiles during favourable weather conditions for all months but August, with several other significant gaps during to various breakdowns. The Raymetrics LiDAR started to measure in November. All data have been processed till October 2012.

Precipitation was collected throughout the year and analyzed for pH, conductivity, and main ions (collected water volume permitting).

Measurement techniques

On-line Monitoring

Meteorological Parameters

Meteorological data and solar radiation were measured directly at the EMEP station with the instrumentation described below.

WXT510 (S/N: A1410009 & A1410011)

Two WXT510 weather transmitters from Vaisala recorded simultaneously the six weather parameters temperature, pressure, relative humidity, precipitation and wind speed and direction from the top of a 10 m high mast.
The wind data measurements utilise three equally spaced ultrasonic transducers that determine the wind speed and direction from the time it takes for ultrasound to travel from one transducer to the two others. The precipitation is measured with a piezoelectrical sensor that detects the impact of individual raindrops and thus infers the accumulated rainfall. For the pressure, temperature and humidity measurements, separate sensors employing high precision RC oscillators are used.

CM11 (S/N: 058911) & CMP 11 (S/N: 070289)

To determine the solar radiation, a Kipp and Zonen CM11 was used. From 23.06.2008 and onwards an additional CMP11 Pyranometer have been installed that measures the irradiance (in W/m^2) on a plane surface from direct solar radiation and diffuse radiation incident from the hemisphere above the device. Both devices are ca. 1.5 m above the ground. The measurement principle is based on a thermal detector. The radiant energy is absorbed by a black disc and the heat generated flows through a thermal resistance to a heat sink. The temperature difference across the thermal resistance is then converted into a voltage and precisely measured. Both the CM11 & CMP11 feature a fast response time of 12 s, a small non stability of +/-0.5 % and a small non linearity of +/-0.2 %.

Gas Phase Air Pollutants

Sampling

SO_2, NO, NO_x and O_3 are sampled from a common inlet situated at about 3.5 m above the ground on the roof of the gas phase monitors' container (Fig. 13). The sampling line consists in an inlet made of a PVC semi-spherical cap (to prevent rain and bugs to enter the line), a PTFE tube (inner diameter = 2.7 cm, height = 150 cm), and a "multi-channel distributor" glass tube, with nine 14 mm glass connectors. This inlet is flushed by an about 60 L min^{-1} flow with a fan-coil (*measured with RITTER 11456*). Each instrument samples from the glass tube with its own pump through a 0.25 inch Teflon line and a 5 µm pore size 47 mm diameter Teflon filter (to eliminate particles from the sampled air).
CO was sampled as above during July-Dec. 2012, and from a 15 meter high mast located about 900 meter from the EMEP-GAW station at the JRC-Ispra greenhouse gas monitoring station (45.807°N, 8.631°E, 223 m asl) during Jan.-June 2012.

SO_2: UV Fluorescent SO_2 Analyser

Thermo 43C TL (S/N 0401904668)

At first, the air flow is scrubbed to eliminate aromatic hydrocarbons. The sample is then directed to a chamber where it is irradiated at 214 nm (UV), a wavelength where SO_2 molecules absorb. The fluorescence signal emitted by the excited SO_2 molecules going back to the ground state is filtered between 300 and 400 nm (specific of SO_2) and amplified by a photomultiplier tube. A microprocessor receives the electrical zero and fluorescence reaction intensity signals and calculates SO_2 based on a linear calibration curve.
Calibration was performed with a certified SO_2 standard at a known concentration in N_2. Zero check was done, using a zero air gas cylinder from Air Liquide, Alphagaz 1, CnHm < 0.5 ppm).
The specificity of the trace level instrument (TEI 43C-TL) is that it uses a pulsed lamp. The 43C-TL's detection limit is 0.2 ppb (about 0.5 µg m^{-3}) according to the technical specifications.

For more details about the instrument, the manual for the instrument is available on \\Ccunas3\largefacilities\ABC-IS\Quality_management\Manuals

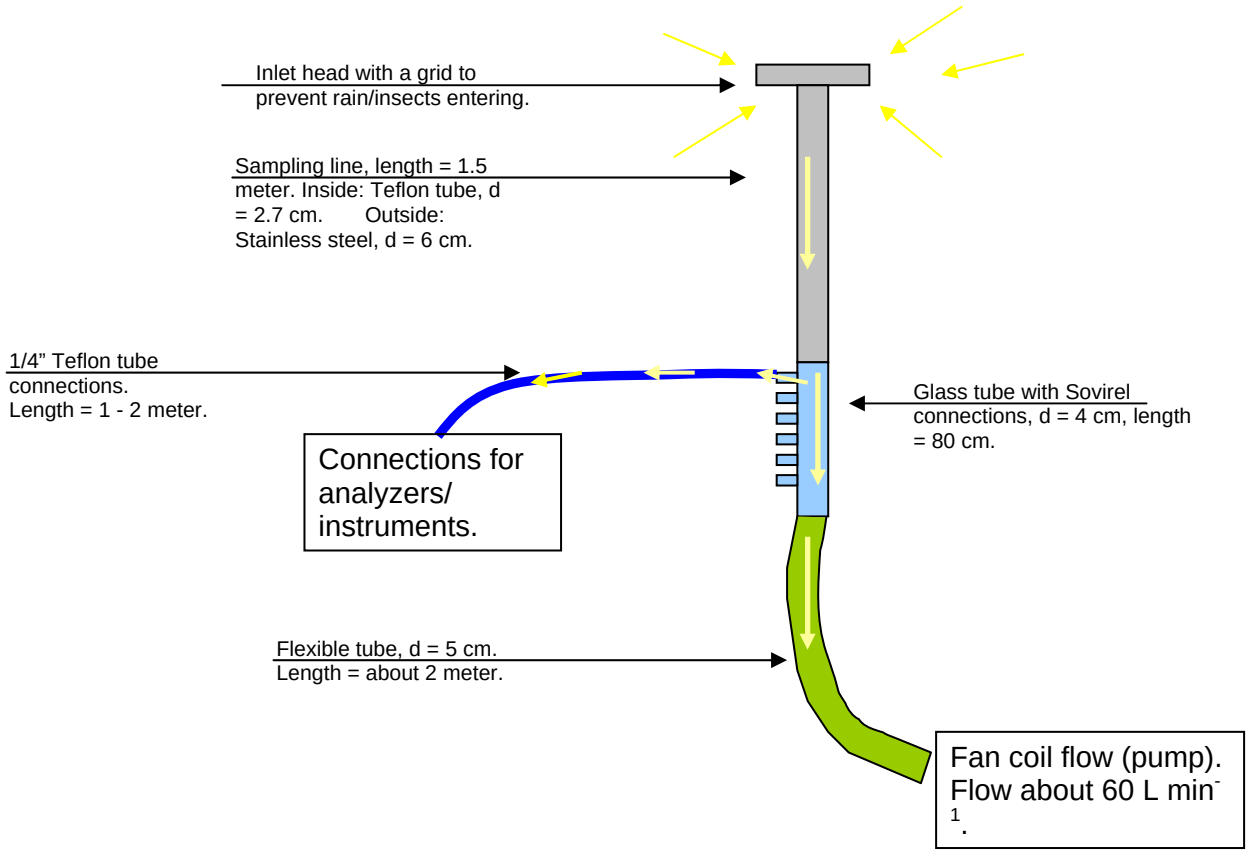

Fig. 13. *Sampling inlet system for the gases SO_2, NO,, NO_x and O_3.*

In 2012, the gas phase monitors were calibrated about every month with suitable span gas cylinders and zero air (see below for more details). Sampling flow rates are as follow:

Compounds	Flow rates (L min^{-1})
SO_2	0.5
NO, NO_x	0.6
O_3	0.7
CO	1.5

NO + NO_X: Chemiluminescent Nitrogen Oxides Analyzer (NO_2=NO_x-NO)

Thermo 42C (S/N 62581-336 and S/N 0401304317) and
Thermo 42iTL (S/N 936539473)

This nitrogen oxide analyser is based on the principle that nitric oxide (NO) and ozone react to produce excited NO_2 molecules, which emit infrared photons when going back to lower energy states:

$$NO + O_3 \rightarrow [NO_2]^* + O_2 \rightarrow NO_2 + O_2 + h\nu$$

A stream of purified air (dried with a Nafion Dryer) passing through a silent discharge ozonator generates the ozone concentration needed for the chemiluminescent reaction. The specific luminescence signal intensity is therefore proportional to the NO concentration. A photomultiplier tube amplifies this signal.
NO_2 is detected as NO after reduction in a Mo converter heated at about 325 °C.
The ambient air sample is drawn into the analyzer, flows through a capillary, and then to a valve, which routes the sample either straight to the reaction chamber (NO detection), or through the converter and then to the reaction chamber (NO_X

detection). The calculated NO and NO_X concentrations are stored and used to calculate NO_2 concentrations (NO_2 = NO_x - NO), assuming that only NO_2 is reduced in the Mo converter.
Calibration was performed using a zero air gas cylinder (Air Liquide, Alphagaz 1, CnHm<0.5 ppm) and a NO span gas. Calibration with a span gas was performed with a certified NO standard at a known concentration in N_2.
For more details about the instrument, the manual for the instrument is available on \\Ccunas3\largefacilities\ABC-IS\Quality_management\Manuals

O_3: *UV Photometric Ambient Analyzer*

Thermo 49C (S/N 55912-305 and S/N 0503110499)

The UV photometer determines ozone concentrations by measuring the absorption of O_3 molecules at a wavelength of 254 nm (UV light) in the absorption cell, followed by the use of Bert-Lambert law. The concentration of ozone is related to the magnitude of the absorption. The reference gas, generated by scrubbing ambient air, passes into one of the two absorption cells to establish a zero light intensity reading, I_0. Then the sample passes through the other absorption cell to establish a sample light intensity reading, I. This cycle is reproduced with inverted cells. The average ratio $R=I/I_0$ between 4 consecutive readings is directly related to the ozone concentration in the air sample through the Beer-Lambert law. Calibration is performed using externally generated zero air and external span gas. Zero air is taken from a gas cylinder (Air Liquide, Alphagaz 1, CnHm < 0.5 ppm). Span gas normally in the range 50 - 100 ppb is generated by a TEI 49C-PS transportable primary standard ozone generator (S/N 0503110396) calibrated/check by ERLAP (European Reference Laboratory of Air Pollution) and/or TESCOM annually.

For more details about the instrument, the manual for the instrument is available on \\Ccunas3\largefacilities\ABC-IS\Quality_management\Manuals
A Nafion Dryer system is connected to the O_3 instruments.

CO: *Non-Dispersive Infrared Absorption CO Analyzer*

Horiba AMPA-370 (S/N WYHEOKSN)

In 2012, carbon monoxide (CO) has been continuously monitored using a commercial Horiba AMPA-370 CO monitor based on the principle of non-dispersive infrared absorption (NDIR). The Horiba APMA-370 uses solenoid valve cross flow modulation applying the same air for both the sample and the reference, instead of the conventional technique to apply an optical chopper to obtain modulation signals. With this method the reference air is generated by passing the sample air over a heated oxidation catalyst to selectively remove CO which is then directly compared to the signal of the untreated sample air at a 1 Hz frequency. The result is a very low zero-drift and stable signal over long periods of time.
To reduce the interference from water vapor to about 1% the sample air was dried to a constant low relative humidity level of around 30% applying a Nafion dryer (Permapure MD-070-24P) tube in the inlet stream. The instrument was calibrated every 2-3 months against two primary NOAA standards based on the NOAA/WMO-2004 scale of 500 and 750 ppbv CO in dry air with an uncertainty of 0.7% (29 L Luxfer aluminum cylinders). In addition we applied a working standard at regular time intervals calibrated against the WMO/NOAA tanks with an initial CO concentration of 1030 ±10 ppbv in dry air in (30 L Luxfur aluminum cylinder). Automatic instrument zero checks were performed every 72 h feeding dry zero air (lab. air treated with Silica Gel, Molecular Sieve 4 A°, Sofnocat 514 (platinum, palladium and tin oxide coated spheres) at room temperature) to the zero air inlet of the monitor, which is further treated by an internal Horiba CO-scrubber containing Hopcalite (copper manganese oxide coated spheres) capable of removing CO from under dry conditions at room temperature. The detection limit of the Horiba AMPA-370 is ~20 ppbv for a one minute sampling interval, and the overall measurement uncertainty is estimated to be ±5%, which includes the uncertainty of the calibration standards, the H_2O interference, and the instrument precision (~2%).
Additional information (e.g. “manuals”, calibrations and standards, etc.) can be found at \\Pb2\NEWLabData\LabData\Quality_Management\GHG-Station_equipment_manuals, and \\Pb2\NEWLabData\LabData\Quality_Management\GHG-Station_calibration_maintenance

Atmospheric Particles

Sampling conditions

Since 2008, all instruments for the physical characterization of aerosols (Aethalometer, Nephelometer, Aerodynamic Particle Sizer, Differential Mobility Particle Sizer) sample isokinetically from nn inlet pipe (Aluminium), diameter = 15 cm, length of horizontal part ~280 cm and vertical part ~220 cm (see Jensen et al., 2010) The Tapered Element Oscillating Mass balance (FDMS-TEOMs) and the Multi-Angle Absorption Photometer (MAAP) use their own inlet systems.
The size dependent particle losses along the pipe radius were determined by measuring the ambient aerosol size distribution with two DMPS at the sampling points P0 and P2 for different radial positions relative to the tube centre (0, 40 and 52 mm) at P2 (Gruening et al., 2009). Data show a small loss of particles towards the rim of the tube can be observed, but it stays below 15 %. The bigger deviation for particles smaller than 20 nm is again a result of very small particle number concentrations in this diameter range and thus rather big counting errors.

PM10 mass concentration: Tapered Element Oscillating Mass balance (TEOM), Series 1400a

Thermo FDMS – TEOM (S/N 140AB233870012 & 140AB253620409)

The Series 1400a TEOM® monitor incorporates an inertial balance patented by Rupprecht & Patashnick, now Thermo. It measures the mass collected on an exchangeable filter cartridge by monitoring the frequency changes of a tapered element. The sample flow passes through the filter, where particulate matter is collected, and then continues through the hollow tapered element on its way to an electronic flow control system and vacuum pump. As more mass collects on the exchangeable filter, the tube's natural frequency of oscillation decreases. A *direct* relationship exists between the tube's change in frequency and mass on the filter. The TEOM mass transducer does not require recalibration because it is designed and constructed from non-fatiguing materials. However, calibration is yearly verified using a filter of known mass.
The instrument set-up includes a Sampling Equilibration System (SES) that allows a water strip-out without sample warm up by means of Nafion Dryers. In this way the air flow RH is reduced to < 30%, when TEOM® operates at 30 °C only. The Filter Dynamic Measurement System (FDMS) is based on measuring changes of the TEOM filter mass when sampling alternatively ambient and filtered air. The changes in the TEOM filter mass while sampling filtered air is attributed to sampling (positive or negative) artefacts, and is used to correct changes in the TEOM filter mass observed while sampling ambient air.

Particle number size distribution: Differential Mobility Particle Sizer (DMPS)

DMPS "B, DMA serial no. 158", CPC TSI 3010 (S/N 2051), CPC TSI 3772 (S/N 70847419), neutraliser ^{85}Kr 10 mCi (2007)

The Differential Mobility Particle Sizer consists in a home-made medium size (inner diameter 50 mm, outer diameter 67 mm and length 280 mm) Vienna-type Differential Mobility Analyser (DMA) and a Condensation Particle Counter (CPC), TSI 3010 (S/N 2051) or TSI 3772 (S/N 70847419). Its setup follows the EUSAAR specifications for DMPS systems.
DMA's use the fact that electrically charged particles move in an electric field according to their electrical mobility. Electrical mobility depends mainly on particle size and electrical charge. Atmospheric particles are brought in the bipolar charge equilibrium in the bipolar diffusion charger (Eckert & Ziegler neutralizer with 370 MBq): a radioactive source (^{85}Kr) ionizes the surrounding atmosphere into positive and negative ions. Particles carrying a high charge can discharge by capturing ions of opposite polarity. After a very short time, particles reach a charged equilibrium such that the aerosol carries the bipolar Fuchs-Boltzman charge distribution. A computer program sets stepwise the voltage between the 2 DMA's electrodes (from 10 to 11500 V). Negatively charged particles are so selected according to their mobility. After a certain waiting time, the CPC measures the number concentration for each mobility bin. The result is a particle mobility distribution. The number size distribution is calculated from the

mobility distribution by an inversion routine (from Stratmann and Wiedensohler, 1996) based on the bipolar charge distribution and the size dependent DMA transfer function. The DMPS measured aerosol particles in the range 10 – 600 nm during an 8 minute cycle until 12.06.2009 and afterwards in the range 10 to 800 nm with a 10 minute cycle. It records data using 45 size channels for high-resolution size information. This submicrometer particle sizer is capable of measuring concentrations in the range from 1 to 2.4 x 10^6 particles cm^{-3}. Instrumental parameters that are necessary for data evaluation such as flow rates, relative humidity, ambient pressure and temperature are measured and saved as well.
The CPC detection efficiency curve and the particle diffusion losses in the system are taken into account at the data processing stage.

Accessories include:
- FUG High voltage cassette power supplies Series HCN7E – 12500 Volts.
- Rotary vacuum pump vane-type (sampling aerosol at 1 LPM)
- Controlled blower (circulating dry sheath air)
- Sheath air dryer only using silica gel until 27.10.2009, thereafter sheath and sample air dryer using Nafion dryer; this mean that the DMPS started to sample in dry conditions from 27 October 2009 onwards.
- Mass flow meter and pressure transducer (to measure sheath air and sample flows).

Particle number size distribution: Aerodynamic Particle Sizer (APS)

APS TSI 3321 (S/N 70535014)

The APS 3321 is a time-of-flight spectrometer that measures the velocity of particles in an accelerating air flow through a nozzle.
Ambient air is sampled at 1 L min^{-1}, sheath air (from the room) at 4 L min^{-1}. In the instrument, particles are confined to the center-line of an accelerating flow by sheath air. They then pass through two broadly focused laser beams, scattering light as they do so. Side-scattered light is collected by an elliptical mirror that focuses the collected light onto a solid-state photodetector, which converts the light pulses to electrical pulses. By electronically timing between the peaks of the pulses, the velocity can be calculated for each individual particle.
Velocity information is stored in 1024 time-of-flight bins. Using a polystyrene latex (PSL) sphere calibration, which is stored in non-volatile memory, the APS Model 3321 converts each time-of-flight measurement to an aerodynamic particle diameter. For convenience, this particle size is binned into 52 channels (on a logarithmic scale).
The particle range spanned by the APS is from 0.5 to 20 µm in both aerodynamic size and light-scattering signal. Particles are also detected in the 0.3 to 0.5 µm range using light-scattering alone, and are binned together in one channel. The APS is also capable of storing correlated light-scattering-signal. *dN/dLogDp* data are averaged over 10 min.

Particle scattering and back-scattering coefficient

Nephelometer TSI 3563 (S/N 1081)

The integrating nephelometer is a high-sensitivity device capable of measuring the scattering properties of aerosol particles. The nephelometer measures the light scattered by the aerosol and then subtracting light scattered by the walls of the measurement chamber, light scattered by the gas, and electronic noise inherent in the detectors.
Dried ambient air is sampled at 5.3 L min^{-1} since 18.11.2009 from a PM10 inlet. .
The three-color detection version of TSI nephelometer detects scattered light intensity at three wavelengths (450, 550, and 700 nm). Normally the scattered light is integrated over an angular range of 7–170° from the forward direction, but with the addition of the backscatter shutter feature to the Nephelometer, this range can be adjusted to either 7–170° or 90–170° to give total scatter and backscatter signals. A 75 Watt quartz-halogen white lamp, with a built-in elliptical reflector, provides illumination for the aerosol. The reflector focuses the light onto one end of an optical pipe where the light is carried into the internal cavity of the instrument. The optical pipe is used to thermally isolate the lamp from the sensing volume. The output end of the optical light pipe is an opal glass diffuser that acts as a *quasi*-cosine (Lambertian) light source. Within the measuring volume, the first aperture on the detection side of the instrument limits the light integration to angles greater than 7°, measured from the horizontal at the opal glass. On the other side, a shadow plate limits the light to

angles less than 170°. The measurement volume is defined by the intersection of this light with a viewing volume cone defined by the second and fourth aperture plates on the detection side of the instrument. The fourth aperture plate incorporates a lens to collimate the light scattered by aerosol particles so that it can be split into separate wavelengths. The nephelometer uses a reference chopper to calibrate scattered signals. The chopper makes a full rotation 23 times per second. The chopper consists of three separate areas labelled: signal, dark, and calibrate.
The signal section simply allows all light to pass through unaltered. The dark section is a very black background that blocks all light. This section provides a measurement of the photomultiplier tube (PMT) background noise. The third section is directly illuminated this section to provide a measure of lamp stability over time. To reduce the lamp intensity to a level that will not saturate the photomultiplier tubes, the calibrate section incorporates a neutral density filter that blocks approximately 99.9 % of the incident light. To subtract the light scattered by the gas portion of the aerosol, a high-efficiency particulate air (HEPA) filter is switched in line with the inlet for 300 s every hour. This allows compensation for changes in the background scattering of the nephelometer, and in gas composition that will affect Rayleigh scattering of air molecules with time. When the HEPA filter is not in line with the inlet, a small amount of filtered air leaks through the light trap to keep the apertures and light trap free of particles. A smaller HEPA filter allows a small amount of clean air to leak into the sensor end of the chamber between the lens and second aperture. This keeps the lens clean and confines the aerosol light scatter to the measurement volume only.
Nephelometer data are corrected for angular non idealities and truncation errors according to Anderson and Ogren, 1998. From 18.11.2009 onwards, a Nafion dryer has been installed at the inlet to measure dry aerosols. Internal RH ranged from 0 to 50 % (average 18%, 99th percentile 41%), with values > 40% occurring between June 30th and July 22nd. At 40% RH, aerosol scattering is on average increased by 20% compared to 0% RH in Ispra (Adam et al., 2012). However, aerosol particle scattering coefficients presented in this report are **not** corrected for RH effects, except when specified.

Particle absorption coefficient

Aethalometer Magee AE-31 ('A' S/N 408: 0303 & 'B' S/N 740:0609)

The principle of the Aethalometer is to measure the attenuation of a beam of light transmitted through a filter, while the filter is continuously collecting an aerosol sample. Suction is provided by an internally-mounted pump. Attenuation measurements are made at successive regular intervals of a time-base period. The objectives of the Aethalometer hardware and software systems are as follows:
(a) to collect the aerosol sample with as few losses as possible on a suitable filter material;
(b) to measure the optical attenuation of the collected aerosol deposit as accurately as possible;
(c) to calculate the rate of increase of the equivalent black carbon (EBC) component of the aerosol deposit and to interpret this as an EBC concentration in the air stream;
(d) to display and record the data, and to perform necessary instrument control and diagnostic functions.

The optical attenuation of the aerosol deposit on the filter is measured by detecting the intensity of light transmitted through the spot on the filter. In the AE-31, light sources emitting at different wavelengths (370, 470, 520, 590, 660, 880 and 950 nm) are also installed in the source assembly. The light shines through the lucite aerosol inlet onto the aerosol deposit spot on the filter. The filter rests on a stainless steel mesh grid, through which the pumping suction is applied. Light penetrating the diffuse mat of filter fibers can also pass through the spaces in the support mesh. This light is then detected by a photodiode placed directly underneath the filter support mesh. As the EBC content of the aerosol spot increases, the amount of light detected by the photodiode will diminish.
For better accuracy, further measurements are necessary: the amount of light penetrating the combination of filter and support mesh is relatively small, and a correction is needed for the 'dark response signal' of the overall system. This is the electronics' output when the lamps are off: typically, it may be a fraction of a percent of the response when the lamps are on. To eliminate the effect of the dark response, we take 'zero' readings of the system response with the lamps turned off, and subtract this 'zero' level from the response when the lamps are on.

The other measurement necessary is a 'reference beam' measurement to correct for any small changes in the light intensity output of the source. This is achieved by a second photodiode placed under a different portion of the filter that is not collecting the aerosol, on the left-hand side where the fresh tape enters. This area is illuminated by the same lamps. If the light intensity output of the lamps changes slightly, the response of this detector is used to mathematically correct the 'sensing' signal. The reference signal is also corrected for dark response 'zero' as described above.
The algorithm in the computer program (see below) can account for changes in the lamp intensity output by always using the ratio quantity [Sensing]/[Reference]. As the filter deposit accumulates EBC, this ratio will diminish.
In practice, the algorithm can account for lamp intensity fluctuations to first order, but we find a residual effect when operating at the highest sensitivities. To minimize this effect and to realize the full potential of the instrument, it is desirable for the lamps' light output intensity to remain as constant as possible from one cycle to the next, even though the lamps are turned on and off again. The computer program monitors the repeatability of the reference signal, and issues a warning message if the fluctuations are considered unacceptable. When operating properly, the system can achieve a reference beam repeatability of better than 1 part in 10000 from one cycle to the next. The electronics circuit board converts the optical signals directly from small photocurrents into digital data, and passes it to the computer for calculation. A mass flow meter monitors the sampled air flow rate. These data and the result of the EBC calculation are written to disk and displayed on the front panel of the instrument.
Aethalometer data are corrected for the shadowing effect and for multiple-scattering in the filter to derive the aerosol absorption coefficient (Arnott et al., 2005) with a correction factor C = 3.60, 3.65, and 3.95 for green 450, 550 and 660 nm, respectively.

Multi Angle Absorption Photometer (S/N 4254515)

A new Multi Angle Absorption Photometer (MAAP) model 5012 from Thermo Scientific has been installed at the EMEP station in September 2008 and provides equivalent black carbon concentrations (EBC) and aerosol absorption (α) data at a nominal wavelength of 670 nm. Note that during a EUSSAR workshop (www.eusaar.org) in 2007 it has been observed that the operating wavelength of all MAAP instruments present at that workshop was 637 nm with a line width of 18 nm fwhm. The operating wavelength of this MAAP instrument has not been measured yet, therefore it is assumed to work at 670 nm as stated by the manufacturer.

The MAAP is based on the principle of aerosol-related light absorption and the corresponding atmospheric equivalent black carbon (EBC) mass concentration. The Model 5012 uses a multi angle absorption photometer to analyze the modification of scattering and absorption in the forward and backward hemisphere of a glass-fibre filter caused by deposited particles. The internal data inversion algorithm of the instrument is based on a radiation transfer model and takes multiple scattering processes inside the deposited aerosol and between the aerosol layer and the filter matrix explicitly into account (see Petzold et al., 2004).
The sample air is drawn into the MAAP and aerosols are deposited onto the glass fibre filter tape. The filter tape accumulates the aerosol sample until a threshold value is reached, then the tape is automatically advanced. Inside the detection chamber (Fig. 14), a 670-nanometer light emitting diode is aimed towards the deposited aerosol and filter tape matrix. The light transmitted into the forward hemisphere and reflected into the back hemisphere is measured by a total of five photo-detectors. During sample accumulation, the light intensities at the different photo-detectors change compared to a clean filter spot. The reduction of light transmission, change in reflection intensities under different angles and the air sample volume are continuously measured during the sample period. With these data and using its proprietary radiation transfer scheme, the MAAP calculates the equivalent black carbon concentration (EBC) as the instruments measurement result.
Using the specific absorption cross section σ_{BC} = 6.6 m^2/g of equivalent black carbon at the operation wavelength of 670 nm, the aerosol absorption (α) at that wavelength can be readily calculated as:

$$\alpha = EBC \times \sigma_{BC} \qquad \textit{Eq. 1}$$

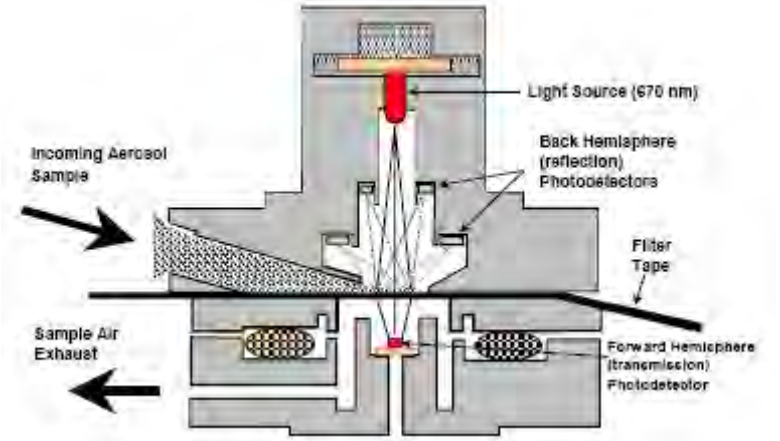

Fig. 14. MAAP detection chamber (sketch from the manual of the instrument).

Range-resolved aerosol backscattering, extinction and aerosol optical thickness

LIDAR measurements are based on the time resolved detection of the backscattered signal of a short laser pulse that is sent into the atmosphere (for an introduction see Weitkamp , 2005). Using the speed of light, time is converted to the altitude where the backscattering takes place. Utilising some assumptions about the atmospheric composition, aerosol backscattering and extinction coefficients as well as aerosol optical thickness can be derived using the LIDAR equation. The received power P of the detector is therein given as a function of distance and wavelength by *Eq. 2*:

$$P(R,\lambda) = P_0 \, {}^{c\tau}\!/_{2} \, A\eta \frac{O(R)}{R^2} \beta(R,\lambda) \exp\left(-2 \int_0^R \alpha(r,\lambda) dr \right)$$

Eq. 2: P_0: Power of the laser pulse, c: speed of light, τ: laser pulse length, A: area of the telescope, η: system efficiency, R: distance, O: overlap function (between laser beam and receiving optics field of view), λ: wavelength, β: backscatter coefficient, α: absorption coefficient

Cimel Aerosol Micro Lidar (CAML) CE 370-2 (laser & electronics: S/N 0507-846 and telescope: S/N 0507- 847)

The aerosol backscatter LIDAR instrument (LIght Detection And Ranging) from CIMEL (CAML) was installed in 2006 at the EMEP-GAW station for the range-resolved optical remote sensing of aerosols. It serves to bridge the gap between local, in-situ measurements of aerosols at the ground and satellite based characterizations of the aerosol column above ground. To reach this, altitude resolved aerosol backscattering, and estimated aerosol extinction are derived from the LIDAR data with high time resolution.

CAML is an eye-safe, single-wavelength, monostatic aerosol backscatter lidar. The lidar emitter is a diode pumped, frequency doubled Nd:YAG laser operating at a wavelength of 532 nm, with a repetition rate of 4.7 kHz, pulse energy of 8 μJ/pulse and a width of the laser pulse of less than 15 ns. The short integration time of the detector of 100 ns allows for a vertical resolution of 15 m. With 2048 time bins of the detector, the maximum altitude is ~30 km. However, depending on the actual atmospheric conditions and the quality of signal to noise ratio (SNR), the vertical limit for probing the atmosphere usually goes up to 15 km. Eye-safety of the system is reached by expanding the laser beam trough a 20 cm diameter, 1 m focal length refractive telescope. The emission and reception optical paths coincide through a single, 10 m long optical fibre that connects both the laser output and receiving detector with the telescope. The telescope field of view is approximately 50 µrad. The backscatter signal is sent to the receiver passing through a narrow band-pass interference filter (0.2 nm fwhm, centred at 532 nm) to reduce the background level. To avoid saturation of the detector immediately after the laser pulse is emitted and thus reduce the afterpulse signal, an acousto-optical modulator is placed before the detector that blocks the light from the detector that is directly backscattered from optical components in the light

path. The detector is an avalanche photodiode photon-counting module with a high quantum efficiency approaching 55 % with maximum count rates near 20 MHz.

Data evaluation is done with an inversion algorithm based on an iteration-convergence method for the LIDAR equation (see *Eq. 2*) that has been implemented in-house using the MATLAB programming environment. Starting with the CAML raw data, the 10 minutes time averages of the backscatter profiles are space–averaged over 60 m. Then the background signal (including afterpulse component) is subtracted. The afterpulse component originates from light that is scattered back to the detector from all surfaces on the optical path to the telescope. As its intensity is rather high compared to the atmospheric backscatter, it influences the raw detector signal. Furthermore, the overlap function O(R) (see *Eq. 2*) is applied to the data before it is range corrected, i.e. multiplied by R^2. The shape of this overlap function varied significantly and thus gives rise to a potentially large error in the evaluation of the lidar data. The range corrected signal constitutes the level 0 data.
Usually, the US standard atmosphere is used to calibrate the molecular backscattering in an aerosol free region and an assumed LIDAR ratio (i.e. extinction-to-backscatter ratio) that is constant with height is used to retrieve the aerosol backscatter, extinction and optical thickness (AOT) profiles (provided as level 1 data). During 2011, the molecular extinction and backscatter profiles are computed using radiosonde measurements (launched at Linate airport) for air number of molecules. The Lidar Ratio (LR) is determined using as a constraint the AOT measured by sun photometer.
The mean (median) estimate of the LIDAR ratios (LR = Lidar Ratios) that have been used for the data inversion was LR = 29.73 sr (with median = 22).

In 2012, LIDAR measurements were performed with CAML in automatic mode following the program “running for 20 min, and off for 10 min”. This 30 min-cycle was repeated continuously during favourable weather conditions, i.e. no precipitation and no cloud coverage that would absorb the laser pulse and thus prevent meaningful aerosol LIDAR measurements above clouds.

Raymetrics Aerosol Raman Lidar (S/N 400-1-12, QUANTEL Brilliiant B Laser and cooler S/N 120059004 and S/N 120034401, LICEL Transient Recorder & Hi Voltage Supply S/N BS3245 and BS3245b, industrial PC S/N TPL-1571H-D3AE, Radar LS150-24)

The instrument itself was installed on October 8-11th, 2012, and indispensable accessories (including radar) on December 11-13, 2012. This lidar emits at 3 wavelengths from IR to UV (1064 nm, 532 nm, 355 nm) and records at 5 wavelengths, namely the emission wavelengths and two Raman channels 387 and 607 nm. Measurements at 1064 nm, 532 nm, and 355 nm provide aerosol backscatter profiles, while measurements at 687 nm, and 387 nm provide aerosol extinction profiles during the dark hours of the day. Light depolarisation is also measured. As very little data were acquired with this instrument in 2012, it will be further described in the 2013 ABC-IS annual report.

Sampling and off-line analyses

Particulate Matter

PM2.5 from quartz fibre filters

PM2.5 was continuously sampled at 16.7 L min^{-1} on quartz fibre filters with a Partisol sampler equipped with carbon honeycomb denuder. The sampled area is 42 mm. Filters were from PALL Life Sciences (type TISSUEQUARTZ 2500QAT-UP). Filter changes occurred daily at 08:00 UTC.
Filters were weighed at 20 % RH before and after exposure with a microbalance Sartorius MC5 placed in a controlled (dried or moisture added and scrubbed) atmosphere glove box. They were stored at 4 °C until analysis.
Main ions (Cl^-, NO_3^-, SO_4^{2-}, $C_2O_4^{2-}$, Na^+, NH_4^+, K^+, Mg^{2+}, Ca^{2+}) were analysed by ion chromatography (Dionex DX 120 with electrochemical eluent suppression) after extraction of the soluble species in an aliquot of 16 mm Ø in 20 ml 18.2 MOhm cm resistivity water (Millipore mQ).
Organic and elemental carbon (OC+EC) were analysed using a Sunset Dual-optical Lab Thermal-Optical Carbon Aerosol Analyser (S/N 173-5). PM2.5 samples were analysed using the EUSAAR-2 thermal protocol that has been developed to minimize biases inherent to thermo-optical analysis of OC and EC (Cavalli et al., 2010):

Fraction Name Sunset Lab.	Plateau Temperature (°C)	Duration (s)	Carrier Gas
OC 1	200	120	He 100%
OC 2	300	150	He 100%
OC 3	450	180	He 100%
OC 4	650	180	He 100%
cool down		30	He 100%
EC1	500	120	He:O_2 98:2
EC2	550	120	He:O_2 98:2
EC3	700	70	He:O_2 98:2
EC4	850	80	He:O_2 98:2

PM10 from quartz fibre filters

PM10 was usually sampled every 6th day for a 24 h period at 16.7 L min^{-1} on quartz fibre filters (TISSUEQUARTZ 2500QAT-UP) with a Partisol Plus 2025 sampler using a PM10 sampling head (59 filters in 2012) without denuder. Intensive sampling was performed during the EMEP intensive campaign from June 11th to July 18th (48 filters). Filter preparation and analysis has been performed exactly as described above for PM2.5 samples to check for differences in the chemical composition of coarse particles compare to PM2.5.

PM10 samples collected from 18 June 2011 to 30 June 2012 were also analysed for 26 trace elements. Samples were prepared in a class 100clean room. Filters were mineralised (Milestone Ethos microwave with unpulsed power assisted digestion) for 36 min [digestion process steps: i) power from 100W to 1000W in 20 min; ii) constant power at 800 for 1 min and iii) cooling for 15 min by air ventilation] with an acidic mixture consisting of 8 ml of HNO_3 69%, 2 ml of H_2O_2 30% and 0.5 ml of HF 51%. [The European standard method, EN 14902, describes a digestion method for As, Cd, Ni and Pb using a mixture of 8 ml HNO_3 and 2 ml H_2O_2, only. However, several studies have demonstrated that this acidic mixture leads to a poor recovery for elements such as Cr, Al, K and Fe and that, instead, adequate recoveries (>80%) can be obtained by the addition of HF (e.g. Pekney et al., 2005 and Chang et al., 2009)].

The acid extracts were gravimetrically brought to a final mass of 100 g and diluted with pure deionized water to a final concentration of 5% HNO_3 acid. Trace elements were determined by inductively coupled plasma mass spectrometry (Agilent 7500ce equipped with high efficiency sample introduction Elemental Scientific Apex IR).

The 26 elements analysed were Na, Mg, Al, K, Ca, Ti, V, Cr, Mn, Fe, Co, Ni, Cu, Zn, As, Se, Rb, Sr, Ag, Cd, Sn, Sb, Cs, La, Ca, and Pb (K, Fe, As, Se were also analyzed with a He collision cell to minimize isobaric interferences).

Three internal standards, i.e. Sc, In, and Tl, were added on-line to all samples to correct analytical signal suppression (or enhancement) due to matrix effects or signal fluctuations.

Quantification was based on external standard calibration curves constructed from ten standard solutions containing known amounts of metals in the range of their expected concentrations in PM.

Good laboratory practices included analysis of filter blanks for about 10% of all samples, laboratory reagent blanks and quality control standards.

The urban particulate standard reference material 1648 and the European reference material CZ120 were employed to assess the analytical non-random uncertainty. The two reference materials cover different ranges of trace elements concentrations, i.e. lower for the CRM CZ120 and higher for SRM1648. The percentage deviations from the certified trace elements obtained from ten replicates are reported in Table 3 for both reference materials. The absolute deviations from the certified values are within the uncertainties of the certified values for Ni, As and Se for the SRM 1648 and for Ni, As, Cd and Pb for CRM CZ-120.

Table 3: Percentage deviations from the certified values for the two reference material employed, i.e. SRM 1648 and CRM CZ-120.

Reference material	Na	Al	K	V	Cr	Fe	Ni	Cu	Zn	As	Se	Cd	Pb
SRM 1648	-5	-7	-6	-14	-17	6	0.5	-8	-7	-8	-3	-16	-8
CRM CZ120							12			9		22	13

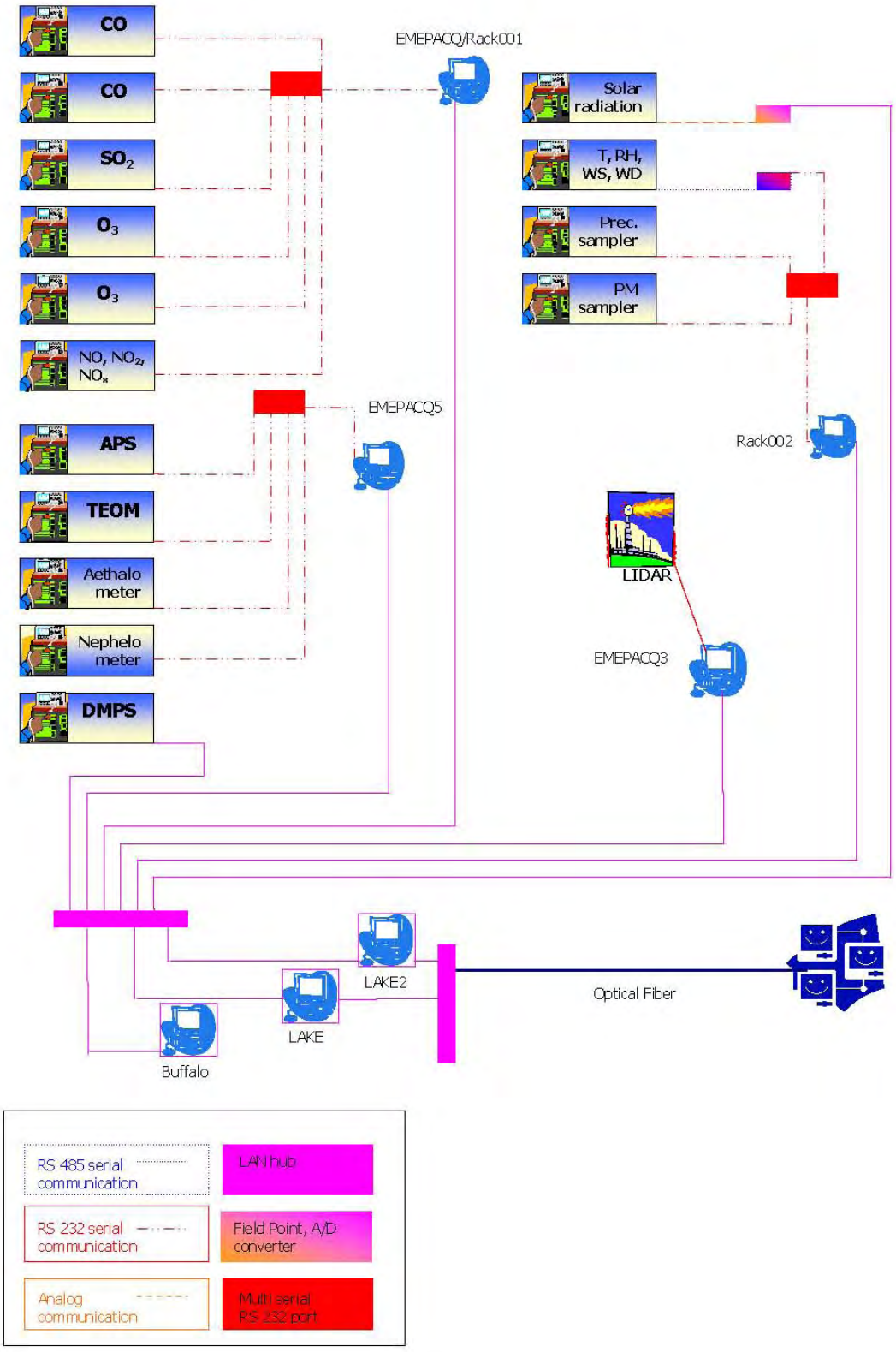

Fig. 14. *Set-up of the EMEP- GAW station Data Acquisition System.*

Wet-only deposition

For the precipitation collection, two Eigenbrodt wet-only samplers (S/N 3311 and 3312) were used that automatically collect the rainfall in a 1 L polyethylene container. The collection surface is 550 cm^2. 24-hr integrated precipitation samples (if any) are collected every day starting at 8:00 UTC. All collected precipitation samples were stored at 4 °C until analyses (ca. every 3 months).
Analyses include the determinations of pH and conductivity at 25 °C with a Sartorius Professional Meter PP-50 and principal ion concentrations (Cl^-, NO_3^-, SO_4^{2-}, $C_2O_4^{2-}$, Na^+, NH_4^+, K^+, Mg^{2+}, Ca^{2+}) by ion chromatography (Dionex DX 120 with electrochemical eluent suppression).

On-line data acquisition system / data management

The JRC EMEP-GAW station Data Acquisition System (DAS) is a specifically tailored set of hardware and software (implemented by NOS s.r.l), designed to operate instruments, acquire both analog and digital output from instruments and store pre-processed measurement data into a database for further off-line evaluation. The DAS operated and controlled the instrumentation during 2012. No updates were implemented.

The software environment of the DAS is Labview 7.1 from National Instruments and the database engine for data storage is Microsoft SQL Server 2008.

The DAS is designed to continuously run the following tasks:

- Start of the data acquisition at a defined time (must be full hour);
- Choose the instruments that have to be handled;
- Define the database path where data will be stored;
- Define the period (10 minutes currently used) for storing averaged data, this is the data acquisition cycle time;
- Obtain data (every 10 seconds currently set) for selected instruments within the data acquisition cycle:
  - For analog instruments (currently only the CM11 and CMP11 Pyranometers), apply the calibration constants to translate the readings (voltages or currents) into analytical values;
  - Send commands to query instruments for data or keep listening the ports for instruments that have self defined output timing;
  - Scan instruments outputs to pick out the necessary data;
- Calculate average values and standard deviations for the cycle period;
- Query instruments for diagnostic data (when available), once every 10 minutes;
- Store all data in a database
  - With a single timestamp for the gas analyzers, FDMS-TEOM and Nephelometer
  - With the timestamp of their respective measurement for all other instruments.

The following instruments are managed with the DAS, using two PCs (currently called emepacq2 and emepacq5):

Emepacq5:

- Number size distribution for particles diameter >0.500 µm, APS
- On-line FDMS-TEOMs
- Aerosol light absorption, Aethalometer
- Aerosol light absorption, MAAP
- Aerosol light scattering, Nephelometer

Rack001:

- Reactive gases: CO, SO2, NO, NO_2, NO_x, O_3

Rack002:

- Solar radiation

- Weather transmitter (temperature, pressure, relative humidity, wind speed and direction, precipitation)
- Precipitation data

The additional pc, **Buffalo**, set-up to manage the near real time data submission (hourly averages of MAAP raw data) to NILU in the frame of the competitive project EUSAAR and ACTRIS, was switched off, due to lack of staff to follow the topic.

Data acquired are stored on the central database e***mep_db*** hosted on the PC **Lake2**. The PC "**Lake**" connects the laboratory to the JRC network (*ies* domain) via optical line. The schematic setup of the data acquisition system is shown in Fig. 14.
The four containers at building 77p that make up the EMEP-GAW station are connected to each others by user configurable point-to-point lines (see Fig. 15).
Through these point-to-point connections, data are exchanged via TCP-IP and RS232 protocols, depending on the instruments connected to the lines.
The acquisition time is locally synchronized for all PCs via a network time server running on lake and is kept at UTC, without adjustment for summer/winter time. Data are collected in a Microsoft SQL Server 2008 database, called ***emep_db*** that runs on "**Lake2**".
On March, 2011, the database was moved to a new database server, called **Lake2**. Also with this computer, the back-up is automatically performed twice a day, at 8:00 and at 20:00.
Lake is the user gateway for the Station user, to allow granted staff remotely access acquisitions pc's. This pc is also used to share information (life cycle sheets, lidar data) between IES domain and bd.77p network.

During 2012 the ABC-IS web site http://abc-is.jrc.ec.europa.eu/ was not updated. The aim of this product is to have of the Station presented as whole on the Internet: measurements distributed over different points within the JRC site, also covering different branches of environmental sciences, long-lived greenhouse gases, short-lived pollutants, and biosphere-atmosphere fluxes. The various sets of preliminary data reported on 24 hours window plots, updated every 10 minutes, are publically available. In the web site the projects to which ABC-IS contributes and contact persons can also be retrieved.
The web site runs over two machines. The first is the web server, **ccuprod2**, in the DMZ (demilitarized zone), where the web page code runs and is managed by the Air and Climate Unit IT staff. The development environment was Python and Ajax. The second computer, **emeimag**, in the JRC network, queries the database for data, generate plots and store plots in a folder in ccuprod2, to make them available to the internet. This second machine is managed by ABC-IS data management team and the software has been developed in C-sharp.

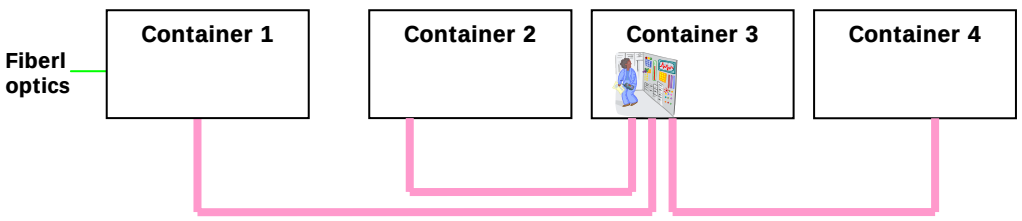

Fig. 15. *Interconnections of the laboratory container at the EMEP station.*

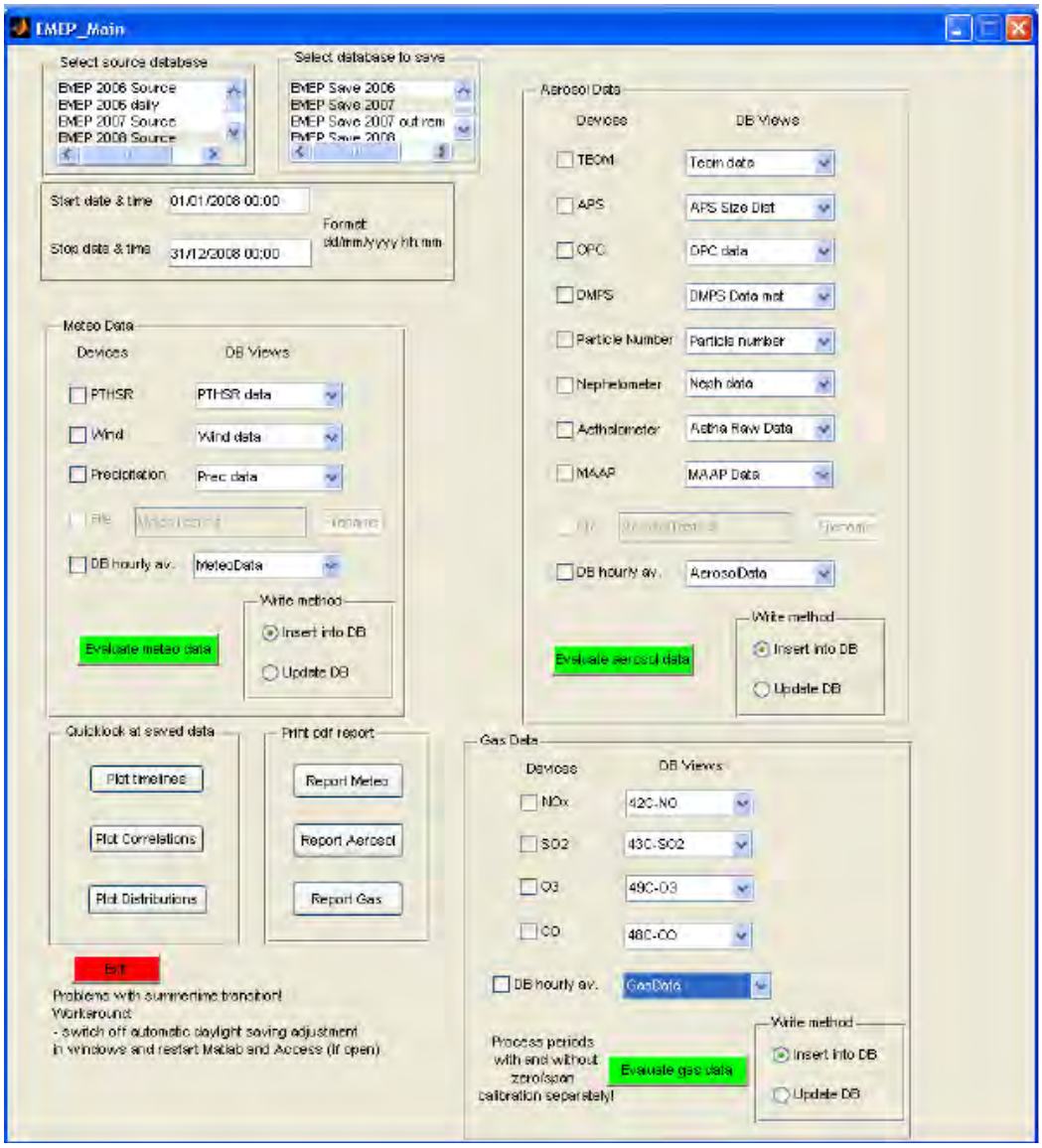

Fig. 16. *Graphic user interface of the EMEP data evaluation program.*

Data evaluation

The structured data evaluation system (EMEP_Main.m) with a graphic user interface (see Fig. 16) has been used with Matlab Release R2007b (www.mathworks.com) as the programming environment. The underlying strategy of the program is:

1) Load the necessary measurement data from all selected instruments from the data acquisition database as stored by the DAS (source database).
2) Apply the necessary individual correction factors, data analysis procedures, etc. specific to each instrument at the time base of the instrument.
3) Perform the calculation of hourly averages for all parameters.
4) Calculate results that require data from more than one instrument.
5) Store hourly averages of all results into a single Microsoft Access database, organized into different tables for gas phase, aerosol phase and meteorological data (save database).

Only the evaluation of gas phase data has an automatic removal algorithm for outliers / spikes implemented: d_i = 10 minute average value at time i, std_i = standard deviation for the 10 minute average (both saved in the raw data)

if $std_i > 100 \cdot \overline{std}$ and $|d_i - d_{i\pm1}| > 10 \cdot \overline{std}$

$\Rightarrow d_i = 1/2\left(d_{i-1} + d_{i+1}\right)$ for d_{i-1} **and** d_{i+1} **no** outliers,

otherwise $d_i = missig\ data$.

This algorithm corrects for single point outliers and removes double point outliers. All other situations are considered correct data. To check these data and to exclude outliers for all other measurements, a visual inspection of the hourly data needs to be performed.

In addition, quick looks of evaluated data for selected time periods can be produced as well as printed timelines in the pdf-format for the evaluated data. All database connections are implemented via ODBC calls (Open DataBase Connectivity) to the corresponding Microsoft (MS) Access database files.

With a second program (EMEP_DailyAverages.m), daily averages (8:00 < t ≤ 8:00 +1 day) of all parameters stored in the hourly averages database can be calculated and are subsequently stored in a separate MS Access database.

Station representativeness

The representativeness of the JRC EMEP-GAW station has been evaluated to check:

- what area are the data currently acquired at the EMEP-GAW station representative for?
- would a move from the actual location to building 51 (or to “Roccolo hill, nido blu” 150 m from building 51 on Rocolo hill) lead to a break in the data series collected during the past 2 decades?

Summarizing the comparisons which are discussed in details in Dell’Acqua et al. (2010): No relevant difference in the daily maximum concentration of the compared parameters was observed. However, daily minimum are generally lower at the current site compared to Bd. 51 on Rocolo hill. The fact that O_3 daytime maximum concentrations are very similar at the EMEP-GAW station compared to the top of JRC Bd. 51 located 50 m higher also indicates that there are no significant local sources of O_3 precursors at the current site. However, O_3 minima and SO_2 concentrations in general are lower at the EMEP-GAW station, suggesting stronger sinks at the EMEP site.

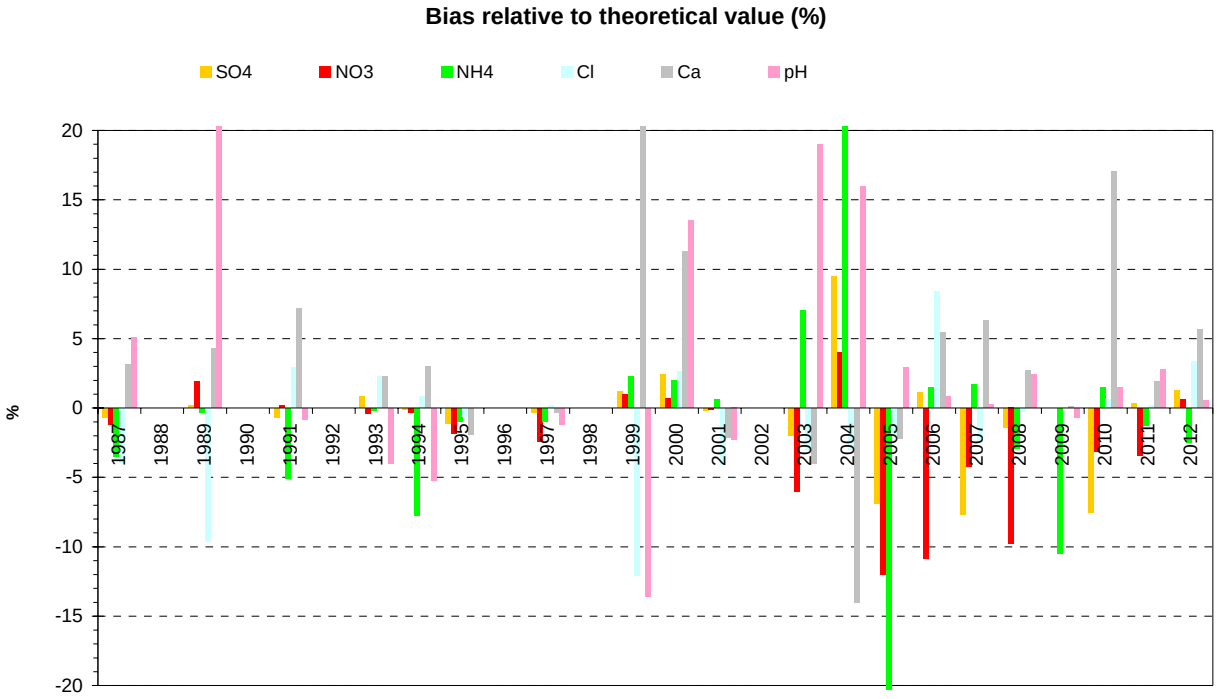

Fig. 17. *JRC-Ispra results of the EMEP intercomparison for rainwater analyses (1987-2012).*

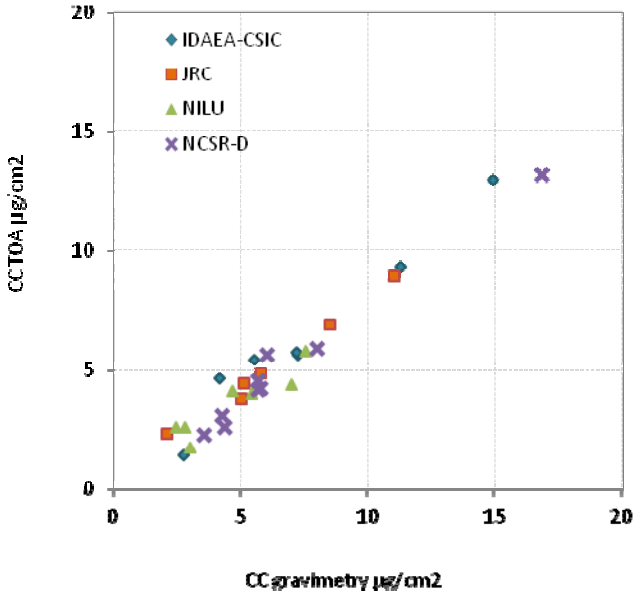

Fig. 18. *Comparison between thermal and gravimetric analyses of carbonate in synthetic samples.*

Quality assurance

At JRC level the quality system is based on the Total Quality Management philosophy the implementation of which started at the Environment Institute in December 1999. It should be mentioned that we now work under ISO 9001 and ISO 14001 (from 2010 and onwards), and more information about our QMS system can also be found in the chapter "Quality management system". Lacking personnel to specifically follow this business, the JRC-Ispra station for atmospheric research did not renew the accreditation for the monitoring of SO_2, NO, NO_2 and O_3 under EN 45001 obtained in 1999. However, most measurements and standardized operating procedures are based on recommendations of the EMEP manual (1995, revised 1996; 2001; 2002), WMO/GAW 153, ISO and CEN standards. Moreover, the JRC-Ispra gas monitors and standards are checked by the European Reference Laboratory for Air Pollution (ERLAP) regularly (see specific measurement description for details). For on-line aerosol instrumentation, intercomparisons took place in February 2013 (DMPS and CPC) and September 2013 (Nephelometer, Aethalometer, MAAP) at the world calibration center for aerosol physics (WCCAP) in Leipzig (D) in the frame of ACTRIS (www.actris.net). In addition, the EMEP-GAW station was audited on march 22-24.03, 2010, in the frame of EUSAAR (www.eusaar.net) by Dr. T. Tuch, World Calibration Centre for Aerosol Physics (WCCAP). The audit went very well and a report is available within the frame of EUSAAR.

Ion analysis quality was checked through the 30th annual EMEP intercomparison (Fig. 17). In the 2012 exercise, all ions measured in the rain water synthetic samples provided by NILU were determined with an error <3%, except Ca^{2+}, Mg^{2+}, and K^{+} (+6%, +8%, and -13%, respectively). The mean error for pH measurements was 0.6%.

There was no OC& EC intercomparison in 2012 because focus was set on carbonate analyses (Fig. 18).

Data quality for other measurements is also checked whenever possible through comparison among different instruments (for gases), mass closure (for PM) and ion balance (for precipitation) exercises. In addition, some instruments are regularly calibrated through maintenance contracts.

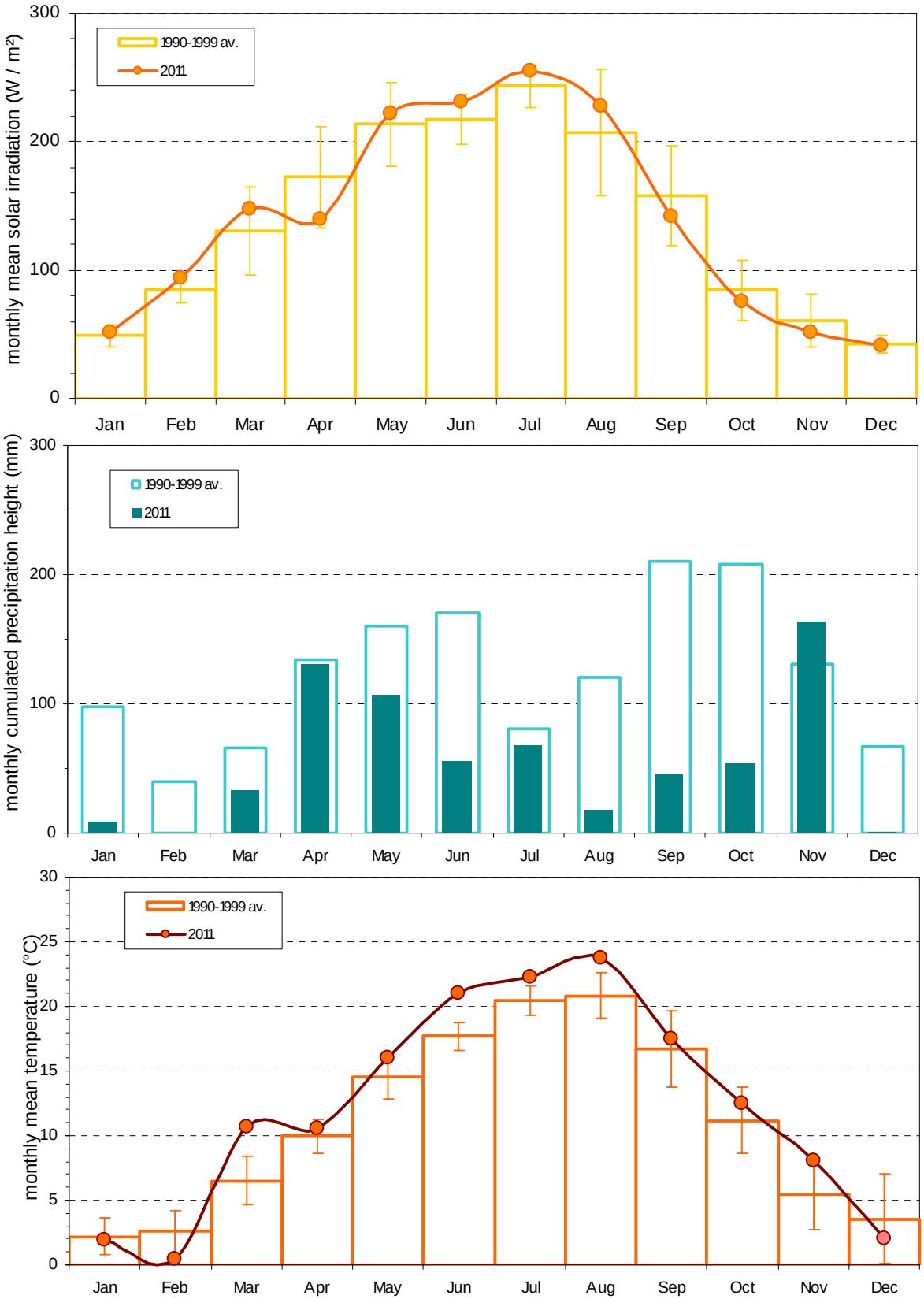

Fig. 14. Solar global irradiation, precipitation amount, and temperature monthly means observed at the EMEP station in the JRC-Ispra in 2012, compared to the 1990-1999 period ± standard deviations.

Results of the year 2012

Meteorology

Meteorological data were acquired directly at the EMEP site using the weather transmitter (T, P, RH, precipitation) and a pyranometer (solar radiation) at 10 m and 1.5 m above the ground, respectively. For February (solar radiation) and August (all variables), data were obtained from Malpensa, and the forest flux tower of ABC-IS, respectively. Fig. 14 shows monthly values of meteorological variables for 2012 compared to the 1990-1999 average used as reference period.

The monthly averaged solar radiation for 2012 shows that Mars and April sun radiation were inverted (although within 1 standard deviation) compared to the reference period "1990-1999 average".

The total yearly rainfall was accumulated to 1141 mm, i.e. very close to the 2011 rainfall, about 25 % lower compared to the 1990-1999 average (1484 mm). All months but April and November were dryer than during the "1990-1999" reference period. December, January, February and August were particularly dry.

Regarding temperature, March, June, July and August were significantly warmer than during the reference period "1990-1999". The temperature average in 2012 was 11.6°C, to be compared to 12.2 °C in 2011, and 11.0 °C over 1990-1999.

Gas phase air pollutants

SO_2, CO, NOx and O_3 were measured almost continuously during the year 2012. An uncertainty of 15 % may be applied to these data in accordance with *European Directive 2008/50/EC.*

The measurement of CO was performed until June 5th 2012 from the complementary nearby JRC greenhouse gas monitoring station located about 900 m away from the EMEP-GAW station. Measurements were resumed at the station itself from July 11th (gap due to instrumental problems). An uncertainty of 5 % can be applied (see discussions in the chapter "Measurement techniques").

In 2012, seasonal variations in SO_2, NO, NO_2, NO_x and O_3 were similar to those observed over the 1990-1999 period (Fig. 20). Concentrations are generally highest during wintertime for primary pollutants (SO_2, CO, NOx), and in summertime for O_3. The higher concentrations of SO_2, CO, NOx in winter result from a least dispersion of pollutant during cold months (low boundary layer height and stagnant conditions), whereas the high concentration of O_3 during summer is due to enhanced photochemical production.

SO_2 concentrations (average = 0.85 µg/m³) were generally about 5 times less compared to the reference period (1990-1999) but on average 30% lower than in 2011.

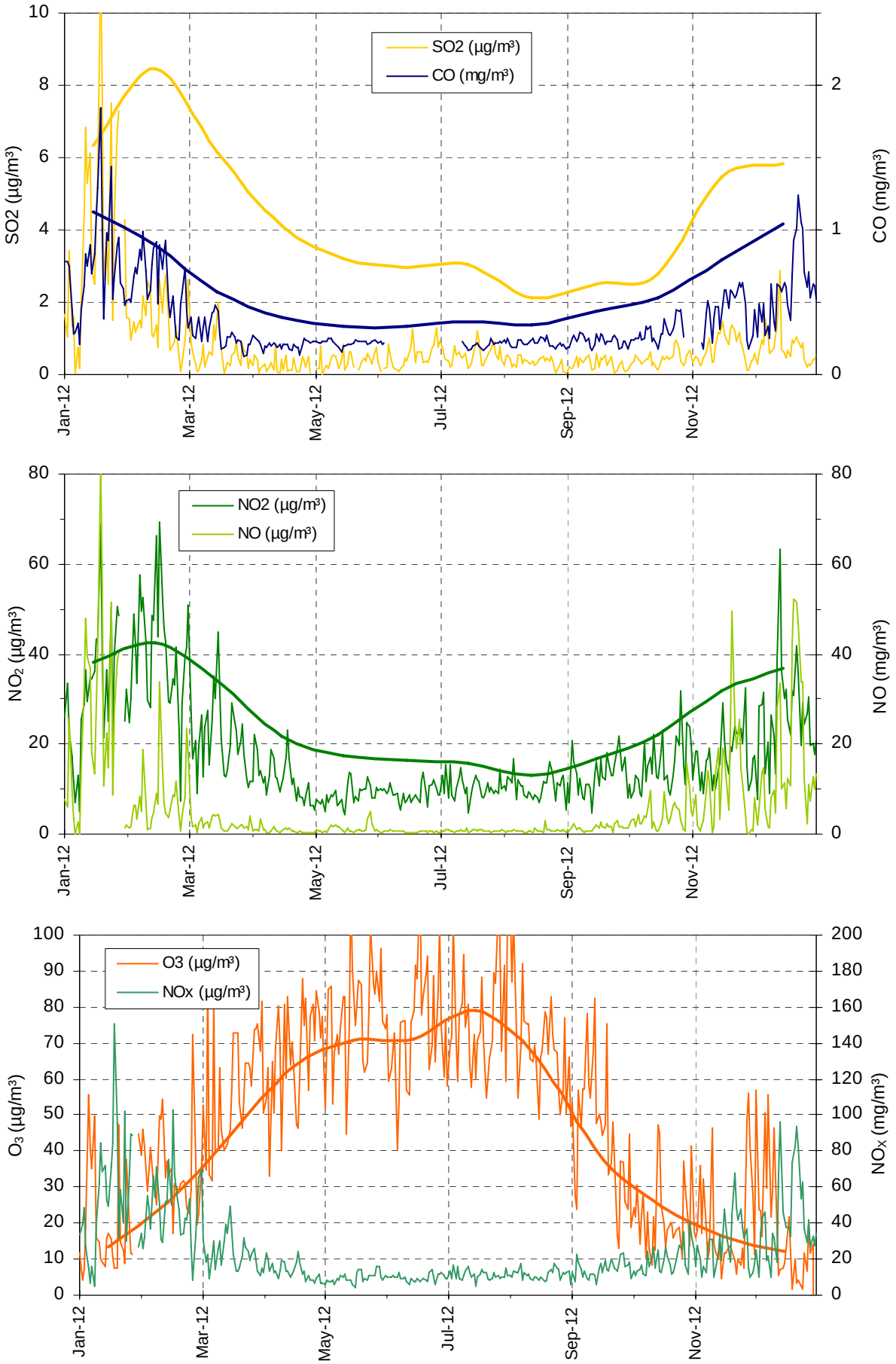

Fig. 20. *Seasonal variations of the 24 hr averaged concentrations of SO_2, CO, NO_2, NO, O_3 and NO_x in 2012 (thin lines) and 1990-1999 monthly averages (thick lines: yellow=SO_2, blue=CO, green=NO_2, orange=O_3).*

Daily mean CO concentrations ranged from 0.13 to 1.84 µg m^{-3} (~0.1 – 1.6 ppmv), which are typical values in a regional background station like the ABC-IS station in Ispra. The lowest values were observed in very clean air masses during Föhn events and also during summer, and the highest values during winter night time conditions.

NO_2 concentrations (annual average = 18 µg m^{-3}) were on average 30% lower than during 1990-1999 but about 10% higher than the 2011 levels. In contrast NO concentrations from 2012 (annual average = 5.9 µg m^{-3}) were equal to those of 2011.

The mean O_3 concentration in 2012 (48 µg m^{-3}, 24 ppb) was 30% higher than in 2011, and back to values observed during the period 1990-1999. Furthermore, several ozone indicators (Fig. 21) did not improve compared to previous years, as further illustrated by Figure 46.

The vegetation exposure to above the ozone threshold of 40 ppb (AOT 40 = Accumulated dose of ozone Over a Threshold of 40 ppb, normally uses for "crops exposure to ozone") was 28100 ppb h in 2012 (with a data coverage for O_3 of 92 % for the whole year), i.e. almost 3 times as much as much as in 2011, and close to the 34000 ppb h yr^{-1} observed over the 1990-1999 decade (Fig. 21).

For quantification of the health impacts (population exposure), the World Health Organisation uses the SOMO35 indicator (Sum of Ozone Means Over 35 ppb, where means stands for maximum 8-hour mean over day), i.e. the accumulated ozone concentrations dose over a threshold of 35 ppb (WHO, 2008). In 2012, SOMO35 was 4648 ppb day (Fig. 21), i.e. twice as much as in 2011. Eight (8) extreme O_3 concentrations (>180 µg m^{-3} over 1 hour) were also observed in 2012. This value corresponds to the threshold above which authorities have to inform the public (European Directive 2008/50/EC on ambient air quality and cleaner air for Europe).

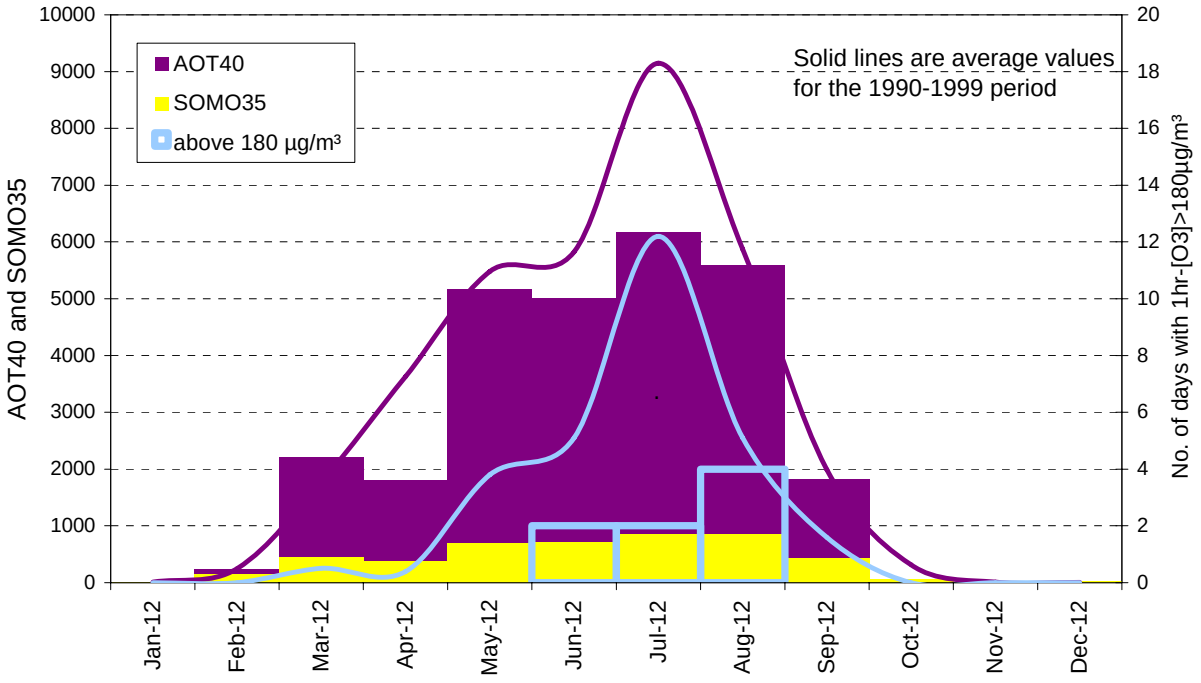

Fig.21.*: AOT 40 (ppb h), SOMO35 (ppb day) and number of exceedances of the 1-hour averaged 180 µg/m³ threshold values in 2012 (bars), and reference period values 1990-1999 (lines).*

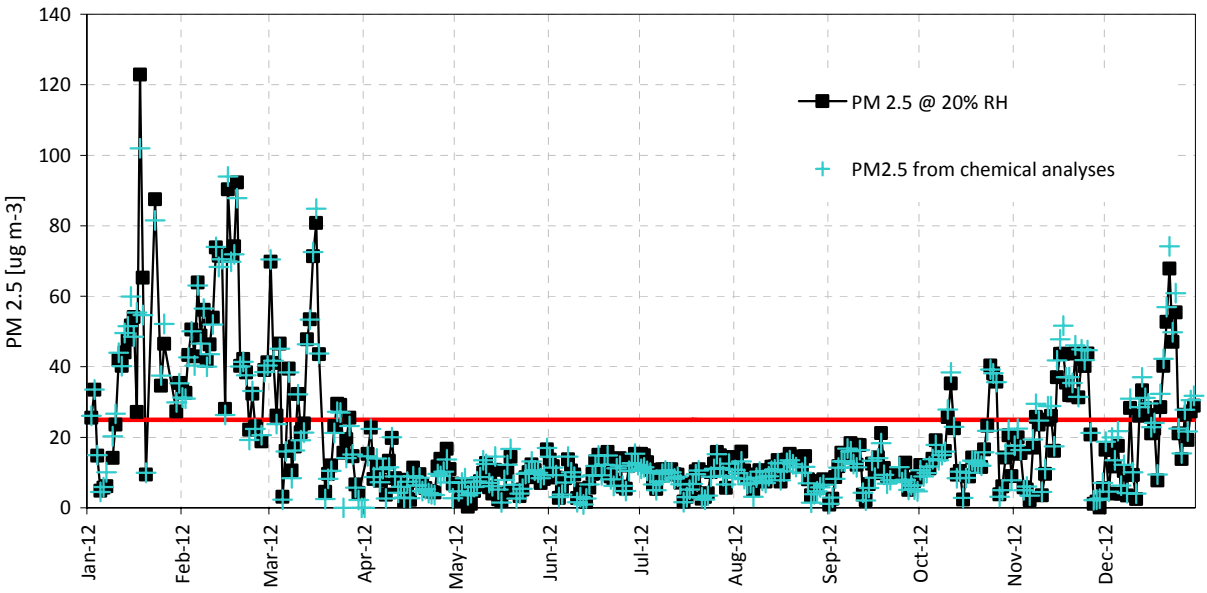

Fig. 22. *24hr-integrated PM2.5 mass concentrations from off-line gravimetric measurements at 20 % RH and chemical determination of main constituents in 2012.The red line indicates the annual limit value of 25 µg/m³ to be reached by 2015 (European directive 2008/50/EC)*

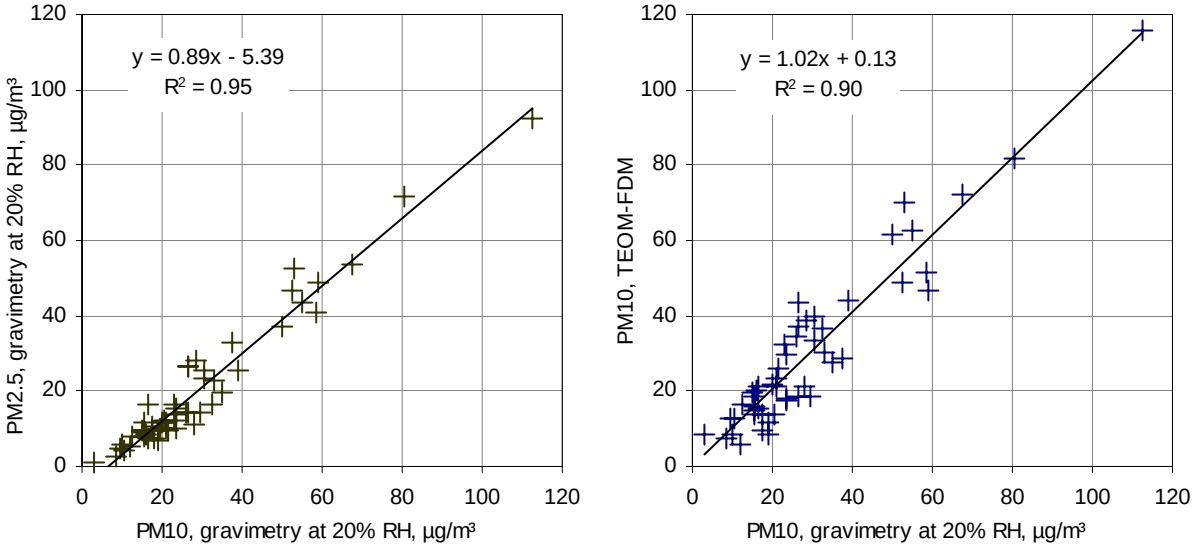

Fig. 23. *Regressions between gravimetric PM2.5 measurements at 20 % RH (right) and FDMS-TEOM PM10 (left) vs. gravimetric PM10 measurements at 20 % RH in 2012*

During the reference period 1990-1999, the information level of 180 µg m^{-3} has been exceeded 29 times per year on average. The other "protection of human health factor" mentioned by the European Directive 2008/50/EC (120 µg m^{-3} as maximum daily 8-hour average) was exceeded 65 times in 2012, i.e. well above the threshold of 25 exceedances per year (averaged over three years).

Particulate phase

Particulate matter mass concentrations

$PM_{2.5}$ concentrations (Fig. 22) measured gravimetrically at 20 % relative humidity (RH) averaged 19.2 µg m^{-3} over 2012. This value is lower than in 2011 (21.4 µg m^{-3}), but higher than in 2010 (17.5 µg m^{-3}), and still below the European annual limit value of 25 µg m^{-3} that has to be reached by 2015 (European directive 2008/50/EC). Over the PM_{10} samples collected every 6th day (n = 57) in 2012, PM_{10} averaged 27.6 µg m^{-3}. The correlation between $PM_{2.5}$ and PM_{10} concentrations measured simultaneously (Fig. 23, left hand) is good (R^2=0.95). $PM_{2.5}$ concentration was generally 10-15 % lower than PM_{10}. The intercept may be due to larger positive sampling artefacts in the PM_{10} filters (no denuder) and/or larger negative artefacts in the $PM_{2.5}$ filters (with denuder).

FDMS-TEOM_A (s/n 233870012) and FDMS-TEOM_B (s/n 253620409) were used to measure PM_{10} from 01 Jan. to 10 May, and 11 May. to 31 Dec. 2012, respectively. 51 exceedances of the 24-hr limit value for PM_{10} (50 µg/m³) were observed in 2012 (93% annual data coverage). The annual PM_{10} average (28.6 µg m^{-3}), very close to the average of PM_{10} mass measured by gravimetry over the 59 samples collected very 6th day, was far below the 40 µg m^{-3} annual average limit value though.

The regression between PM_{10} concentrations measured gravimetrically at 20 % RH and PM10-TEOM data averaged over the corresponding sampling periods (Fig. 23, right hand) shows a good agreement between these 2 methods (R^2= 0.90, slope = 1.02, n = 56).

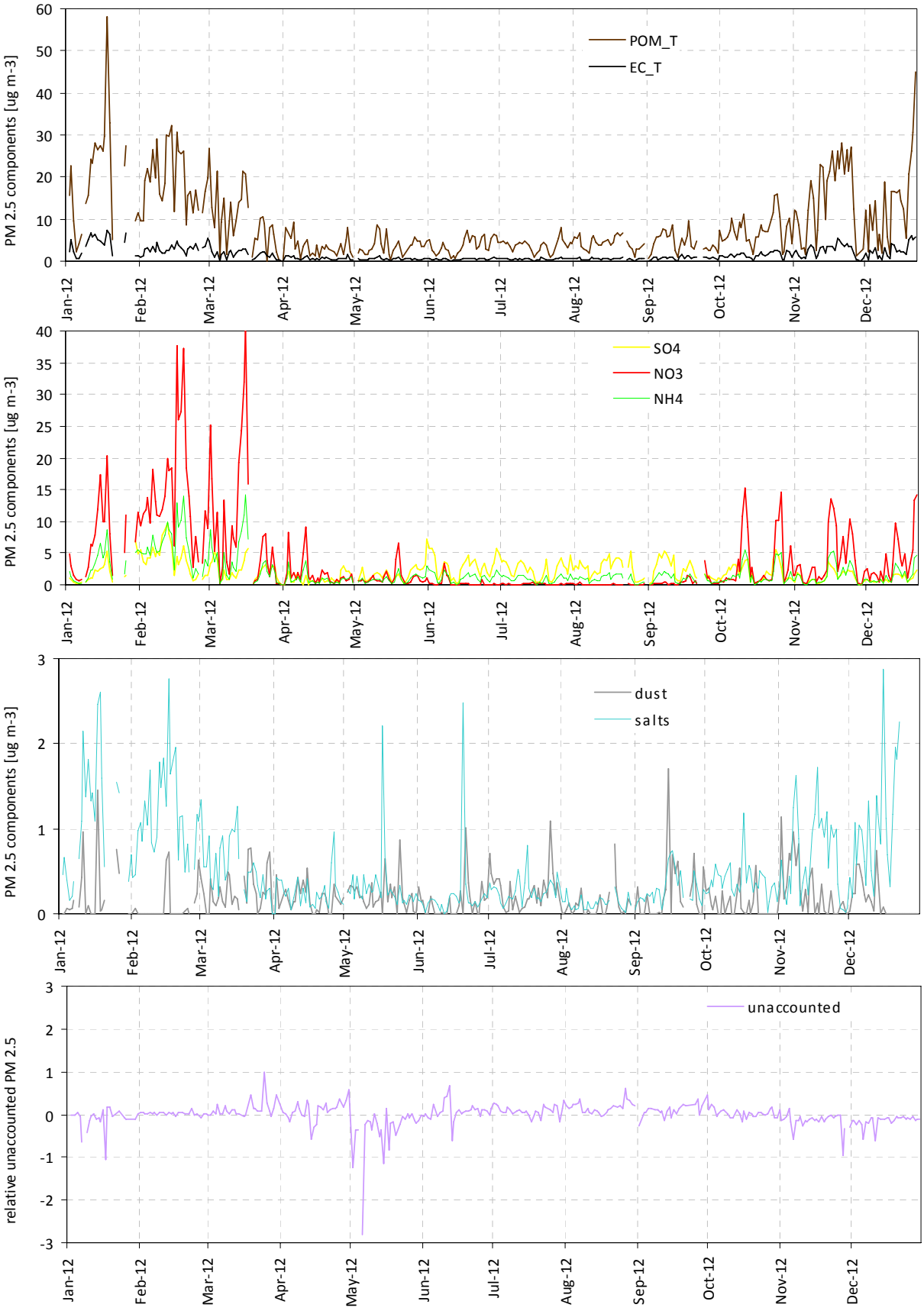

Fig. 24. 24-hr integrated concentrations of the main aerosol constituents of PM2.5 during 2012.

PM2.5 chemistry:

Main ions (Cl^-, NO_3^-, SO_4^{2-}, $C_2O_4^{2-}$, Na^+, NH_4^+, K^+, Mg^{2+}, and Ca^{2+}), OC and EC were determined from the quartz fibre filters (for the whole year) collected for PM mass concentration measurements.

Fig. 24 shows the temporal variations in the PM2.5 main components derived from these measurements. Particulate organic matter (POM) is calculated by multiplying OC (organic carbon) values by the 1.4 conversion factor to account for non-C atoms contained in POM (Russell et al., 2003). "Salts" include Na^+, K^+, Mg^{2+}, and Ca^{2+}. Dust is calculated from Ca^{2+} concentrations and the regression (slope = 4.5) found between ash and Ca^{2+} in the analyses of ash-less cellulose filters (Whatman 40) in previous years. Most components show seasonal variations with higher concentrations in winter and fall, and lower concentrations in summer, like $PM_{2.5}$ mass concentrations. This is mainly due to changes in pollutant horizontal and vertical dispersion, related to seasonal variations in meteorology (e.g. lower boundary layer in winter). The amplitude of the POM, NH_4^+ and NO_3^- seasonal cycles may be enhanced due to equilibrium shifts towards the gas phase, and/or to enhanced losses (negative artefact) from quartz fibre filters during warmer months.

NH_4^+ follows NO_3^- + SO_4^{2-} very well as indicated by the regression shown in Fig. 25. This correlation results from the atmospheric reaction between NH_3 and the secondary pollutants H_2SO_4 and HNO_3 produced from SO_2 and NO_x, respectively. The slope of this regression is smaller than 1, which means that NH_3 was sufficiently available in the atmosphere to neutralise both H_2SO_4 and HNO_3. This furthermore indicates that PM2.5 aerosol was generally not acidic in 2012.

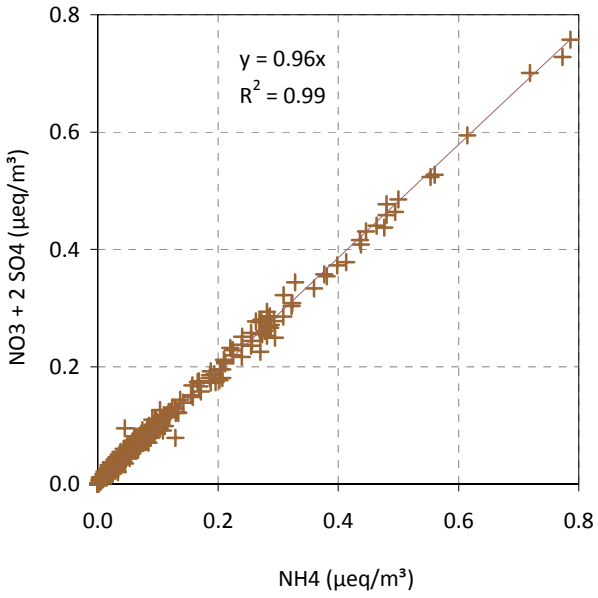

Fig. 25. SO_4^{2-} + NO_3^- vs. NH_4^+ (µeq/m³) in $PM_{2.5}$ for 2011

Table 4*: annual mean concentrations and contributions of major $PM_{2.5}$ constituents in 2011*

constituent	salts Cl^-, Na^+, K^+, Mg^{2+}, and Ca^{2+}	NH_4^+	NO_3^-	SO_4^{2-}	POM	EC	dust	unaccounted
Mean conc. (µg m^{-3})	0.53	1.90	3.77	2.13	9.03	1.55	0.27	0.10
Mean cont. (%)	3.5	9.3	13.2	15.4	48.4	8.8	3.1	-10.7

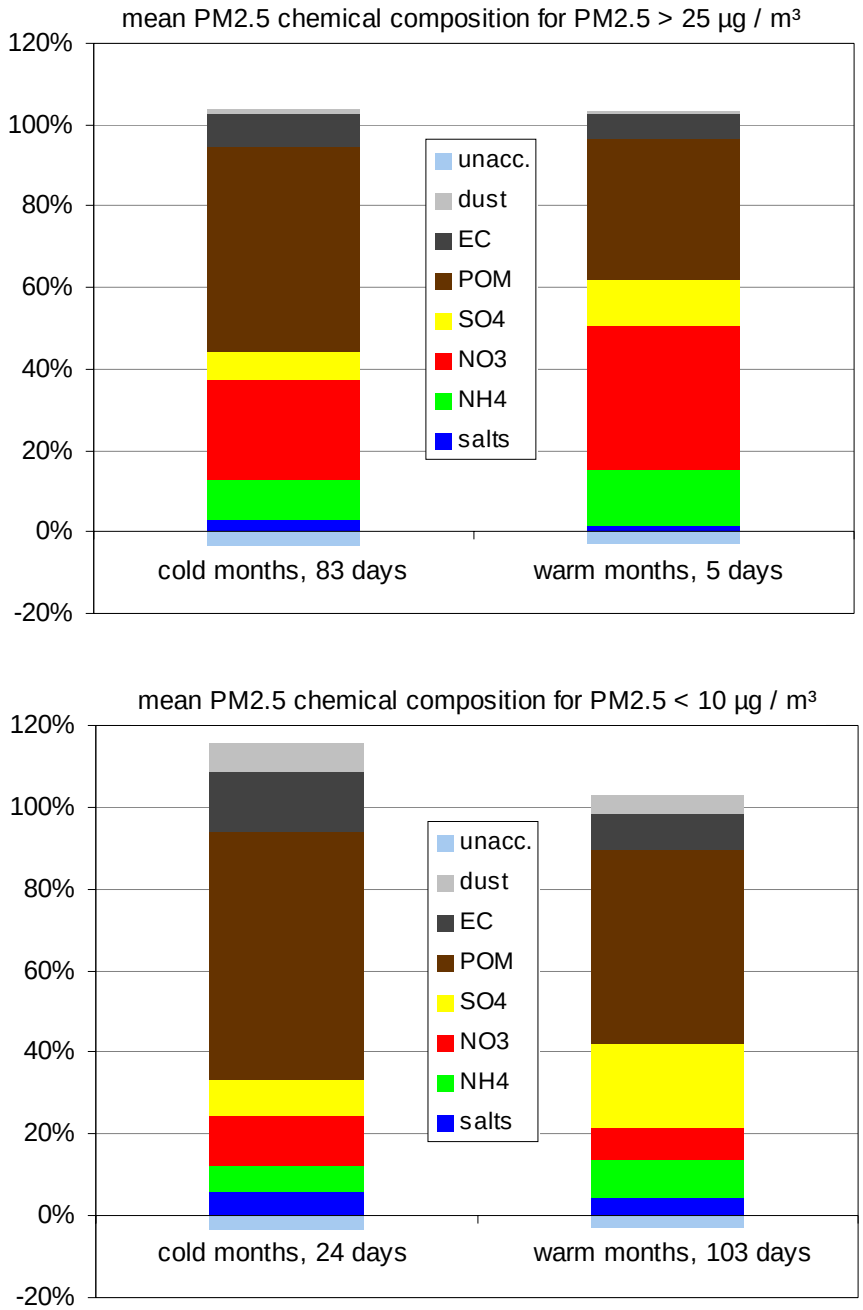

Fig. 26. *Average composition of PM2.5 in 2012 for days on which PM2.5 > 25 µg/m³(top) and PM2.5 < 10 µg/m³(bottom),over cold (Jan., Feb. ,Mar, Nov., Dec.) and warm (Apr. – Oct.) months*

Contribution of the main aerosol components in PM2.5

The contributions of the main aerosol components to PM2.5 are presented in Table 4 (annual averages) and in Fig. 26 (a) for days on which the "24-hr limit value for PM2.5 of >25 µg/m³ was exceeded" during cold months (Jan., Feb., March, Nov. and Dec., 83 cases) and the warm months (Apr. to Oct, 5 cases) and (b) for days on which 24-hr integrated $PM_{2.5}$ concentration was below 10 µg / m³ during cold (24 cases) and warm months (103 cases).

These $PM_{2.5}$ compositions may not always represent accurately the actual composition of particulate matter in the atmosphere (due to various sampling artefacts), but are suitable to assess which components contributed to the PM2.5 mass concentration when collected by a quartz fiber filter downstream of a 20 cm-long carbon monolith denuder.

Over the whole year 2012, carbonaceous species accounted for 57% of $PM_{2.5}$ (EC:9%, POM: 48%), and secondary inorganics for 38% (NH_4: 9 %, NO_3: 13%, and SO_4:16%). In both the cold and the warm seasons, particulate air pollution days are characterised by a strong increase in NO_3 contribution. Considering low $PM_{2.5}$ concentration days, summertime is characterised by higher SO_4^{2-} concentrations (faster SO_2 photochemical conversion) and lower NO_3^- concentrations ($HNO_3 + NH_3 \leftrightarrows NH_4NO_3$ equilibrium moves towards the gas phase, on the left side, as temperature increases). Dust and salts do not contribute significantly to the $PM_{2.5}$ mass (about 3 % each.). Their contribution is larger on cleanest days compared to most polluted days.

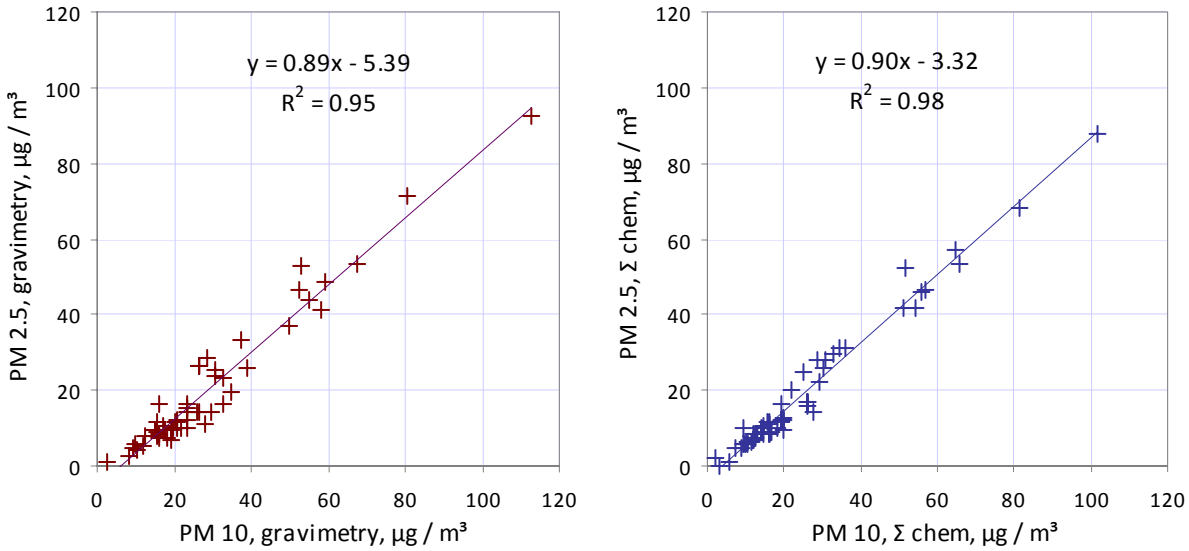

Fig. 27. *Regressions between PM_{10} and $PM_{2.5}$ determined gravimetrically at 20% RH and from chemical analyses.*

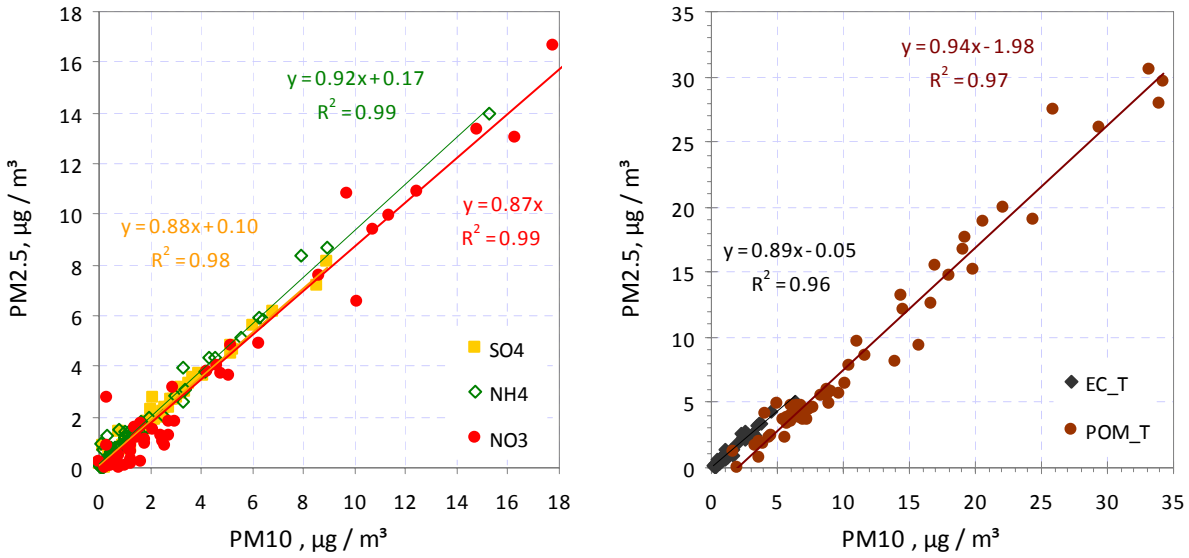

Fig. 28. *Correlations between chemical component concentrations (NH_4, SO_4 and NO_3 on the right hand and POM and EC on the left hand) in PM10 and $PM_{2.5}$ (2012).*

Table 5*: annual mean concentrations and contributions of major PM_{10} constituents in 2012*

constituent	salts (Cl^-, Na^+, K^+, Mg^{2+}, and Ca^{2+})	NH_4^+	NO_3^-	SO_4^{2-}	POM	EC	dust	unaccounted
Mean conc. (µg m^{-3})	1.3	2.0	4.8	2.4	11.1	1.6	1.5	2.6
Mean cont. (%)	5.1	5.7	12.7	9.3	42.1	6.0	6.8	12.2

PM10 chemistry

PM_{10} has been collected and analyzed for a total of 107 filters in 2012, of which 48 were collected during the intensive EMEP campaign in June - July. Concentrations and contributions of major PM_{10} constituents calculated from the 59 samples collected every 6th day, are listed in Table 5. Carbonaceous species account for almost 50% of PM_{10} mass, i.e. a bit less than in $PM_{2.5}$. NH_4NO_3 is the main inorganic constituent of PM_{10}. Comparing mass concentrations of $PM_{2.5}$ and PM_{10}, it appears that $PM_{2.5}$ makes up about 90 % of the total PM_{10} mass (Fig. 27).

Looking at single constituents of PM_{10} and $PM_{2.5}$, the regressions of Fig. 28 indicate that NO_3, NH_4, SO_4, POM and EC in $PM_{2.5}$ account for 80 – 90% of these same species in PM_{10} There is significantly less NH_4NO_3 in $PM_{2.5}$ compared to PM_{10} (ratio = 0.75). It is difficult to state if this difference is real or due to increased losses of semi-volatile inorganics (namely NH_4NO_3) due to the use of the OC denuder (PM2.5 filters were sampled with a denuder and PM_{10} filters were sampled without denuder).

Daily mass concentrations of PM10 and trace elements are reported in the file “trace elements 2011-2012.xlsx” under \\ccunas3.jrc.it\ABC-IS\Ispra_Station\2011\Off-line.

PM10 annual average concentration was 30.3±23.7 μg m^{-3} (min-max: 4.3-112 μg m^{-3}); and annual average concentration of the sum of all analysed elements was 1.5±0.9 μg m^{-3} (min-max: 0.1-4.2 μg m^{-3}). Among the elements determined, Fe and K were the most abundant, with annual average concentration of 347±216 and 346±239, respectively, accounting together for the 47±13%, on average, of the sum of all analysed elements. The atmospheric concentration of the remaining elements decreased as follows:

Ca>Na>Al>Mg>Zn>Cu>Ti>Pb>Mn>Sn>Sr>Sb>Ni>Cr>Rb>V>Se>As>Ce>Cd>La>Co>Ag>Cs.

Annual average concentrations of all evaluated elements are reported in Table 6.

Table 6: Annual average concentration ± standard deviation of trace elements (in ng m^{-3}).

Element	Concentration	Element	Concentration
Na	199±159	Zn	24.0±29.5
Mg	64.9±52.5	As	0.5±0.4
Al	204±179	Se	0.6±0.5
K	346±284	Rb	1.5±2.4
Ca	231±176	Sr	2.6±2.4
Ti	12.6±9.9	Ag	0.1±0.1
V	1.2±1.0	Cd	0.2±0.2
Cr	1.6±2.0	Sn	3.8±3.9
Mn	6.6±6.0	Sb	2.0±1.7
Fe	347±216	Cs	0.05±0.03
Co	0.1±0.1	La	0.2±0.2
Ni	1.8±1.7	Ce	0.3±0.2
Cu	14.1±11.6	Pb	10.5±10.8

The annual average concentration of Pb of 10.5±10.8 ng m^{-3} was far below the EU air quality limit value of 500 ng m^{-3} (EU, 2004). The annual average concentration of As = 0.5±0.4 ng m^{-3}, Cd = 0.2±0.2 ng m^{-3} and Ni = 1.8±1.7 ng m^{-3} were also significantly lower

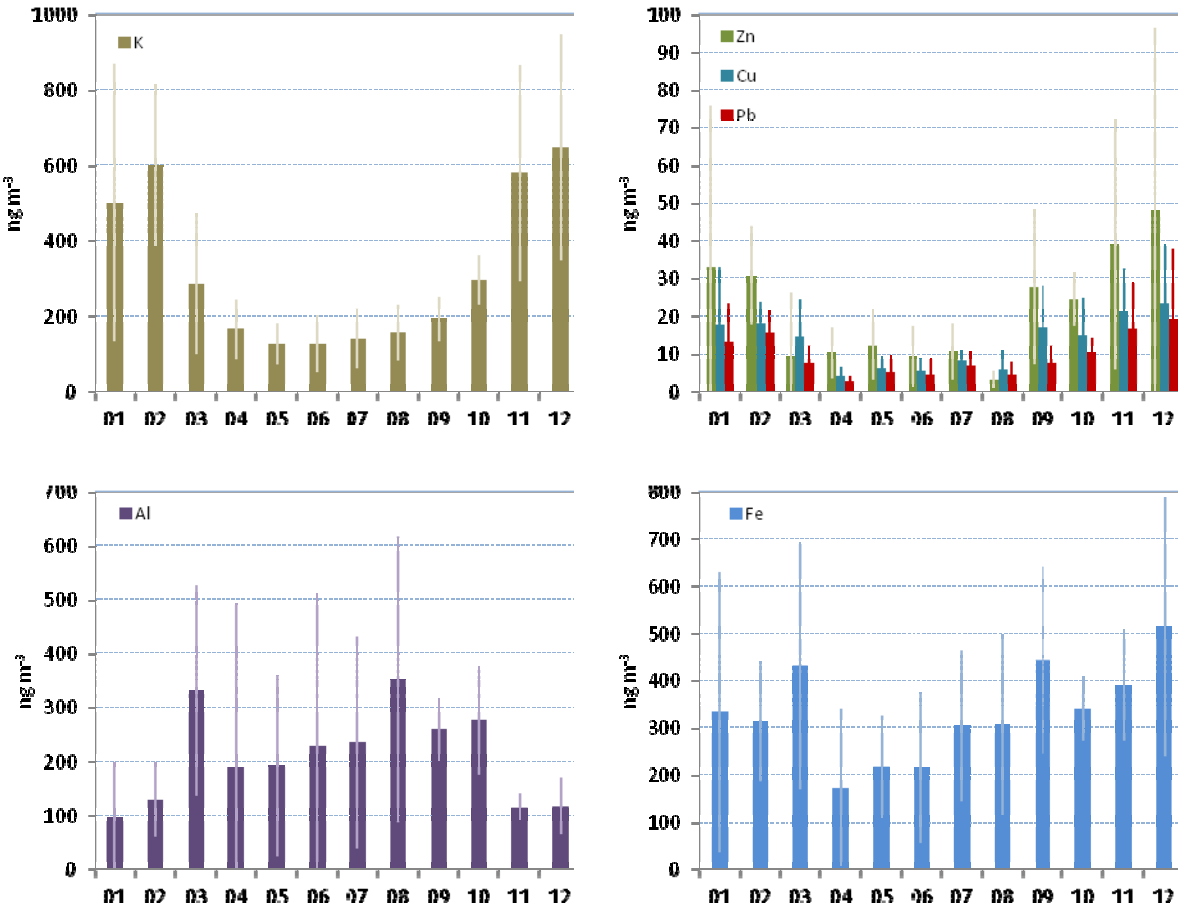

Fig. 29: *Monthly concentration of selected trace elements (in ng m^{-3}).*

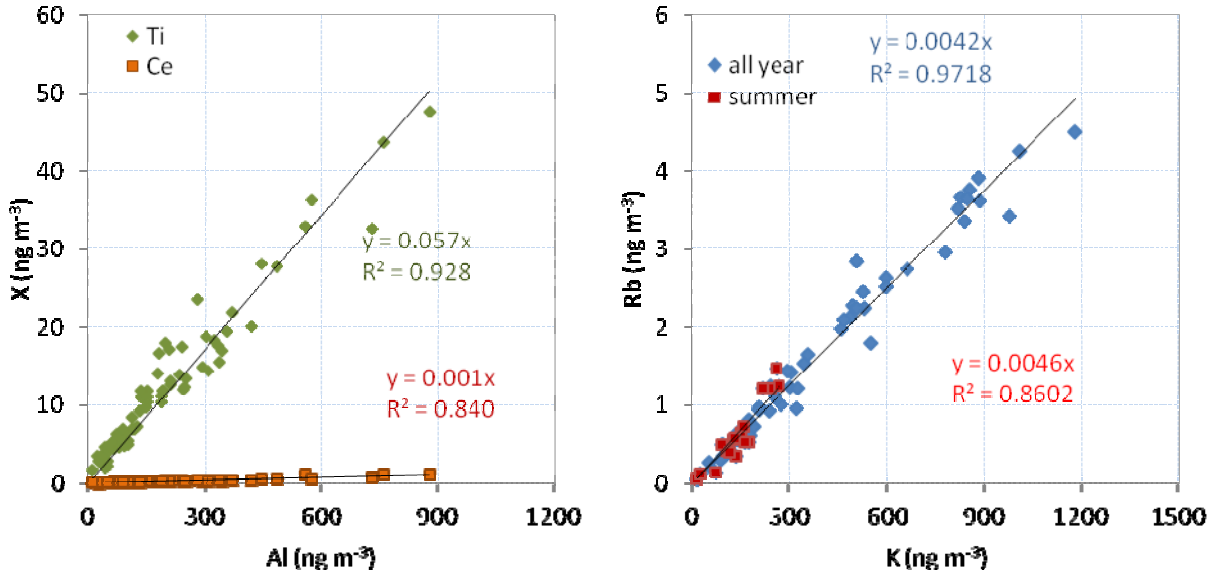

Fig. 30: Elemental ratio Ti/Al and Ce/Al and Rb/K.

than their EU target values, i.e. 6 ng m^{-3}, 5 ng m^{-3} and 20 ng m^{-3}, respectively (maximum annual average to be met by 2013). For Cd and Pb, the values represent also the WHO air

Pb, Cd, Hg, Cr, Zn, Ni, Cu and As became part of the EMEP monitoring programme in 1999, and particular attention has been paid to the first three elements. In comparison with the annual average concentrations reported by the EMEP sites (i.e. rural background locations) in 2010 (Aas et al., 2012), Pb, Cd and Zn levels in Ispra are among the highest ones reported in the network, i.e. in Slovakia and in the BeNeLux countries; similarly, Cr, Ni and As show annual concentrations comparable to the highest levels of Central Europe; finally, with the only exception of Niembro, in Spain, Cu in Ispra has the highest annual concentration.

The majority of the analysed metals (e.g. K, Pb, Cd, Rb, Sn, Sb, Cs, Se and Cu) show a similar trend as PM mass concentrations with maximum values in winter and minimum values in summer (Figure 29). A few remaining elements display, however, a different trend (e.g. Al and Fe, in Figure 29) indicating that, in addition to meteorology, other factors play a role in influencing their concentration throughout the year, e.g varying source strength.

A correlation matrix of trace element mass concentrations in air was calculated. Three groups were identified where trace elements correlated to each other with coefficients higher than 0.9:

- group 1 composed of Al, Ti, and Ce;
- group 2, composed of K and Rb;
- group 3 composed of Sn, Cr, Mn, Zn, Cd, Sb, and Pb.

Elemental ratios between elements of the same group were calculated as a linear regression slope and used as a diagnostic tool to estimate the profile of possible sources. In group 1 the measured ratio were Ti/Al 5.7 10^{-2} (R^2=0.93) and Ce/Al 1.3 10^{-3} (R^2=0.84), i.e. comparable to the average elemental concentration of the upper continental crust, i.e. Ti/Al 3.7-5.4 10^{-2} and Ce/Al 0.8 10^{-3} (Rudnick and Gao, 2003). The measured elemental ratio corroborates the hypothesis of a common crustal origin for the three elements.

The measured elemental ratio Rb/K of 4.2 10^{-3} (R^2= 0.97) is consistent with those measured in particles emitted from fireplace combustion tests of hard wood and softwood, i.e. 0.005-0.006, and 0.001-0.005 (values obtained as ratio of the average element concentrations) (Fine et al., 2001). This indicates that wood-burning is the single source for these two elements. Interestingly, a Rb/K ratio of 4.6 10^{-3} (R^2=0.86) was obtained also for summer (June-July-August) (Figure 30), where the average concentration of K is not zero but 141±72 compared to that of 603±304 in winter (November-December-January).

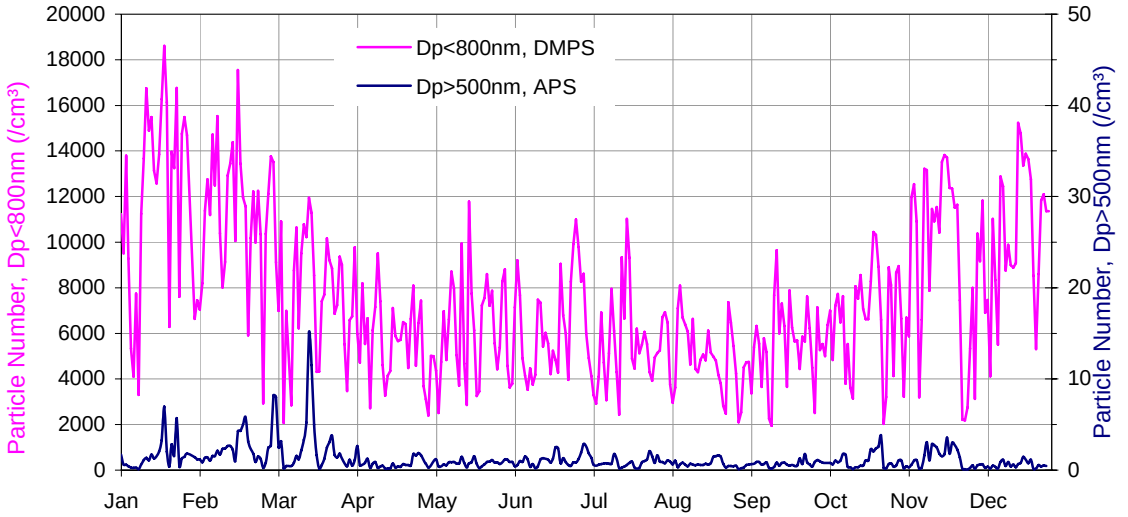

Fig. 31a. *24 hr – mean particle number concentrations for Dp > 500 nm and Dp< 600 nm.*

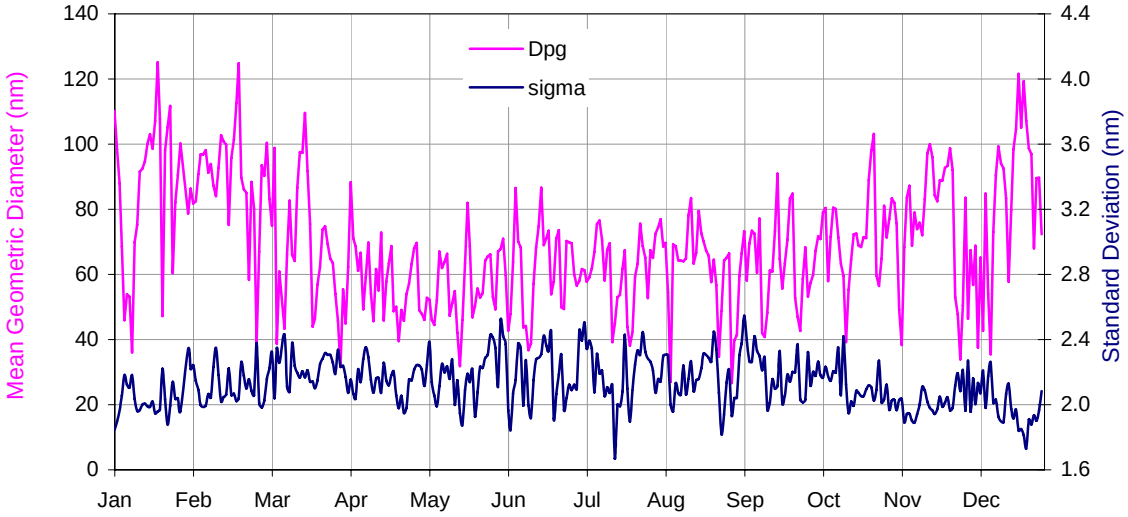

Fig. 31b. *24 hr - averaged particle geometric mean diameter (measured with DMPS) and standard deviation*

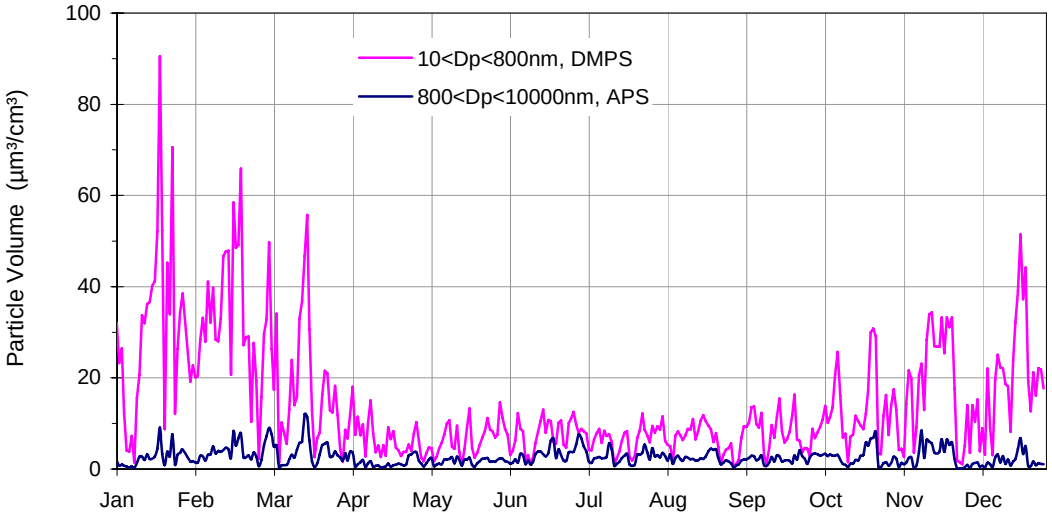

Fig. 31c. *24 hr - averaged particle volume concentrations for Dp< 800 nm and Dp > 800 nm.*

Aerosol physical properties

Measurements of the particle number size distributions smaller than 800 nm diameter were carried out using a Differential Mobility Particle Sizer almost continuously in 2012 (data coverage 99%). Major breaks occurred on Jan. 28-29th and March 7th.

Particle number concentrations averaged over 24 hr (from 08:00 to 08:00 UTC) ranged from 1950 to 18600 cm^{-3} (average: 7540 cm^{-3}) and followed a seasonal cycle comparable to that of PM mass concentrations, with maxima in winter and minima in summer (Fig. 31a). It should be mentioned, that the DMPS data presented here have not been corrected for inlet diffusion losses and CPC efficiency, but those normally account for only a few percent on particle number and have no impact on the other variables.

The mean mode diameter at RH < 30 % ranged 27 – 125 nm (average = 69 nm) in 2012. The variations in particle size distributions parameters (Fig. 31b) show seasonal patterns as well: the mean geometric diameter is generally larger in winter (around 80 nm) than in summer (around 60 nm), whereas the standard deviation of the distribution follows an opposite trend (larger in summer than in winter).

The size distribution of particles larger than 500 nm was measured using an Aerodynamic Particle Sizer almost continuously over 2012 too (data coverage: 99%). Aerodynamic diameters were converted to geometric diameter assuming a particle density of 1.50. As previously observed, particles larger that 500 nm generally (90th percentile) accounted for <<0.1% of the total particle number only (Fig. 31a), but for about 16 % of the total particle volume on average (Fig. 31c). The seasonal variations in particle volume concentration reflect the changes in particle number and mean geometric diameter, with larger volumes in winter than in summer.

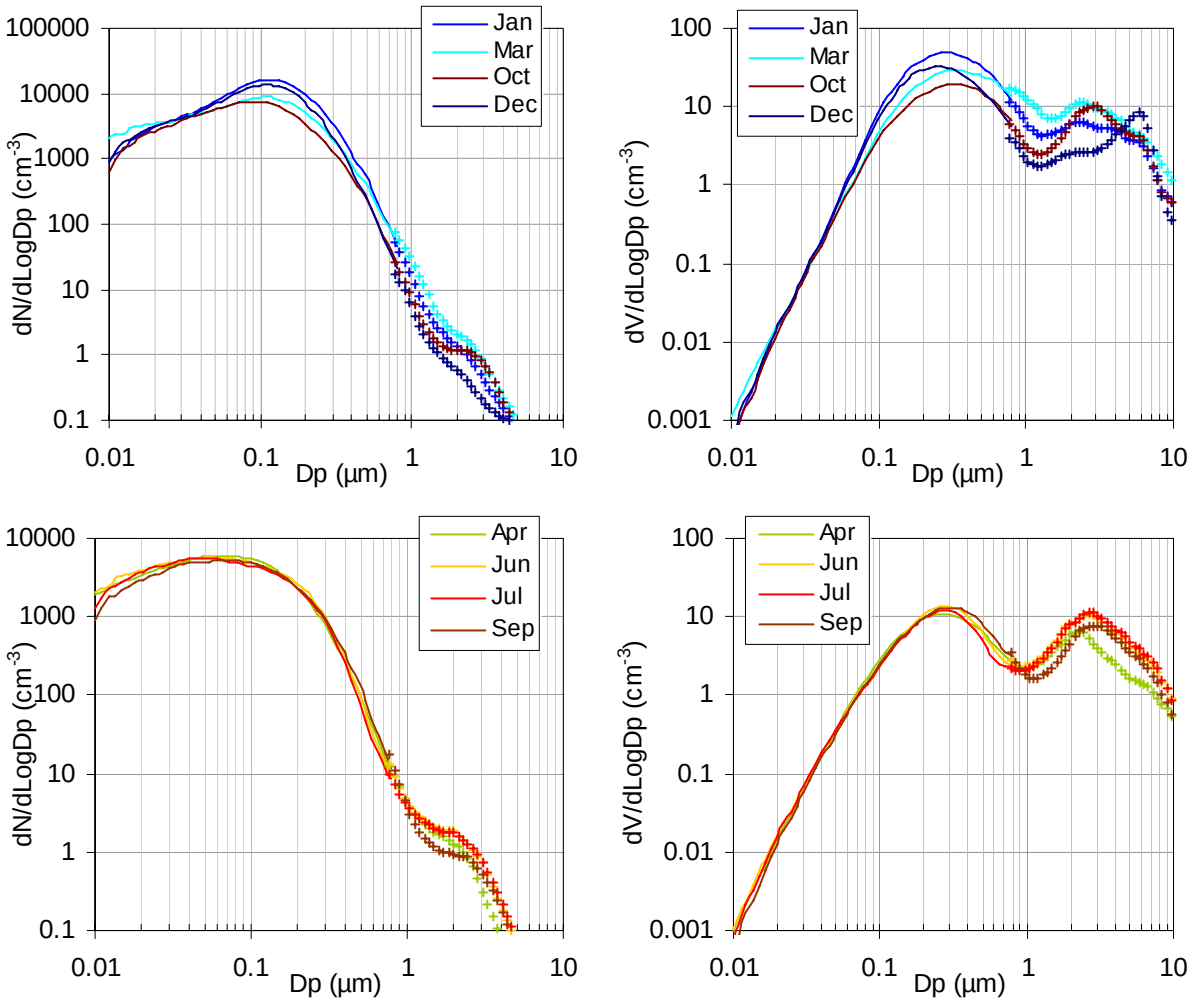

Fig. 32. *Monthly mean particle number (left) and volume (right) size distributions measured in 2012 with a DMPS (10-800 nm, solid lines) and an APS (0.85-10 µm, crosses). A density of* ***1.0 g cm*** $^{-3}$ *was used to convert aerodynamic to geometric diameters.*

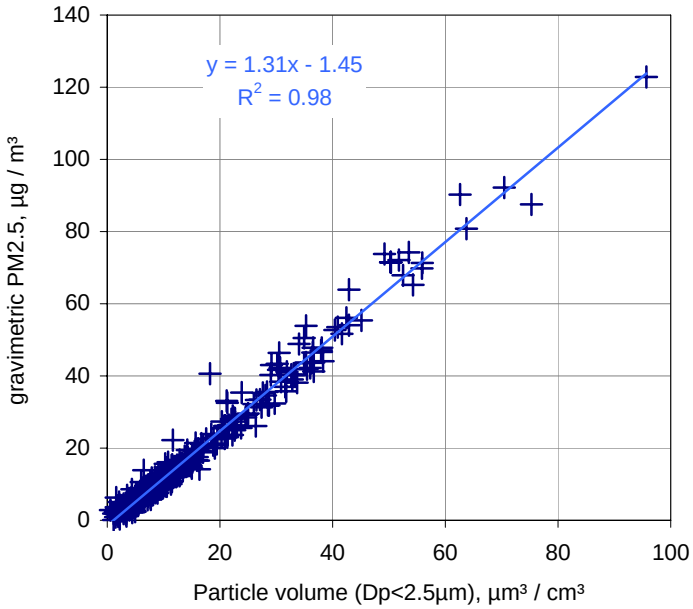

Fig. 33. *2012 regression between PM2.5 mass concentrations determined from gravimetric measurements at 20 % RH and particle volume (Dp < 2.5 µm) calculated from DMPS and APS measurements*

The apparent good agreement between particle number size distributions (Fig. 32) measured with the DMPS and the APS actually reveals a significant inconsistency between these two instruments, since the aerosol density (1.0 g cm^{-3}) used to convert aerodynamic diameters (measured by the APS) to mobility diameters (measured by the DMPS) is out of the range (1.6 ± 0.1 g cm^{-3}) expected for atmospheric particles (McMurry et al., 2002). This was already observed in December 2012, and may be due to over-counting for particles larger than 300 n, as also suggested by the 2013 DMPS intercomparison at the WCCAP in Leipzig.

The comparison between PM2.5 mass and aerosol volume concentration (for Dp < 2.5 µm) shows a good correlation (Fig. 33). The slope of the regression between PM2.5 at 20 % RH and particle volume suggests an aerosol density of 1.31 (to be compared to 1.37 and 1.38 in 2010 and 2011, respectively), i.e. lower than the value of 1.5 g cm^{-3} assumed to convert aerodynamic diameters to mobility diameters for particle volume calculation.

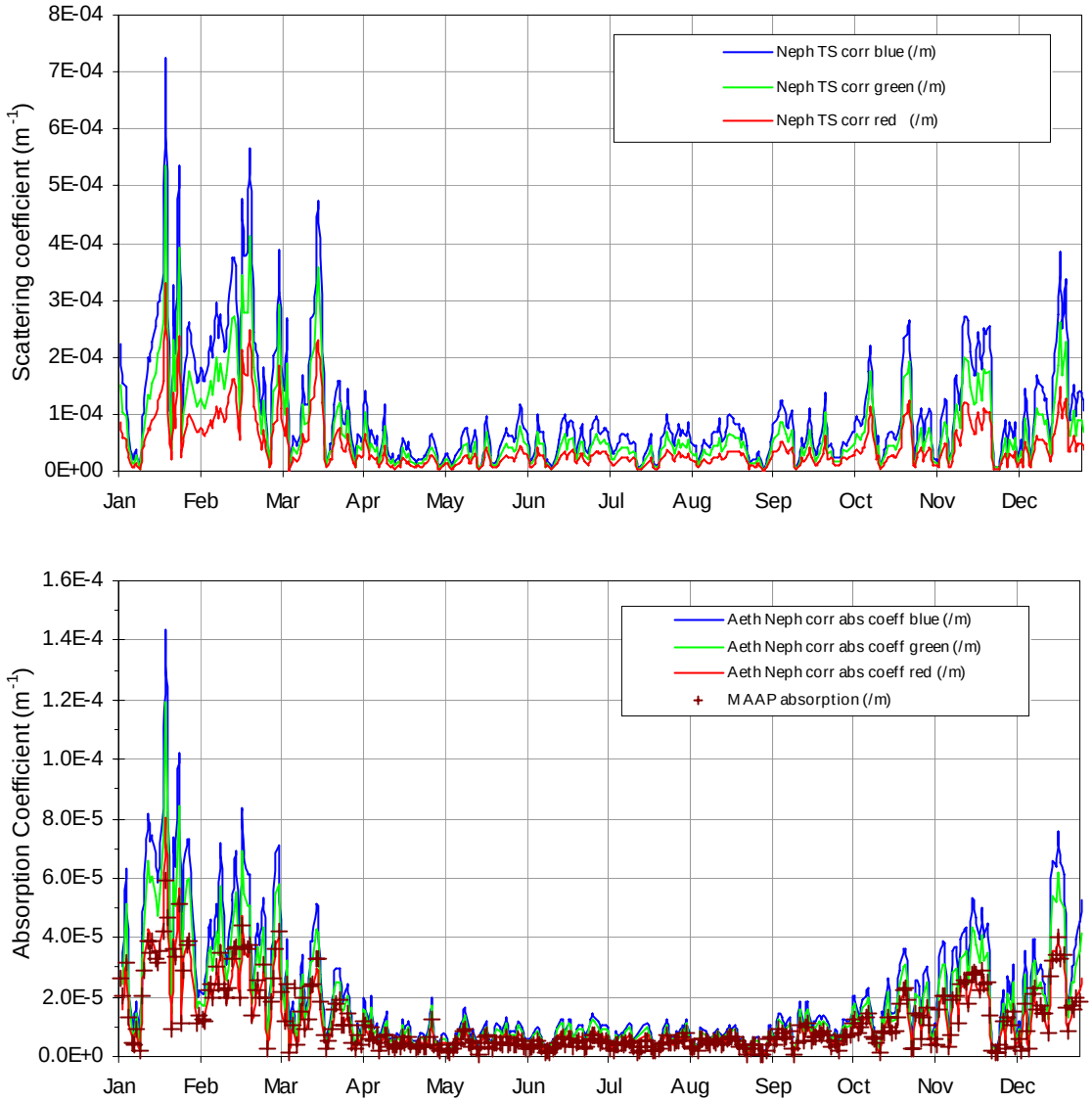

Fig. 34 *Daily mean atmospheric particle scattering (top) and absorption (bottom) coefficients at three wavelengths, derived from Nephelometer, Aethalometer and MAAP measurements (not corrected for RH) performed in 2012.*

Aerosol optical properties

Aerosol optical properties have been monitored continuously during 2012 (data coverage = 98%). Data from the Nephelometer (Fig. 34a) have been corrected for angular non idealities (truncation to 7 – 170°, slightly not cosine-weighted distribution of illumination) according to Anderson and Ogren (1998), but not for RH effects. Although a Nafion dryer is implemented to dry the air entering the nephelometer, RH > 40% commonly occurred between June 15th and Sep. 15th, 2012. At 40% RH, aerosol scattering is on average increased by 20% compared to 0% RH in Ispra (Adam et al., 2012).

Atmospheric particle absorption coefficients at 7 wavelengths (Fig. 34b) were derived from the Aethalometer AE-31 data corrected for the shadowing and multiple scattering effects when Nephelometer data were available, according to Weingartner et al (2003), making use of coefficients derived from Schmid et al. (2006), i.e. 3.60, 3.65 and 3.95 at 470, 520, and 660 nm, respectively.

Both scattering and absorption coefficients follow seasonal variations (Fig. 34) in line with PM mass variations, mainly controlled by pollutant dispersion rates.

The uncertainty of the multiple scattering correction factor may introduce a quite large uncertainty in the aerosol absorption coefficient values, since correction factors ranging from 2 to 4 have been proposed (Weingartner et al., 2003; Arnott et al., 2005). However, it should be noted that the use of the correction factors listed above leads to an aerosol absorption coefficient at 660 nm in good agreement with the absorption coefficient obtained from the Multi Angle Absorption Photometer (MAAP) for 670 nm (Fig. 35, R^2 = 0.98, slope = 1.04). Deviations from the 1:1 line are mainly observed for absorption coefficient values > 0.05 km^{-1}. This behavior strictly depends on the aerosol absorption and not on instrumental parameters such as the filter loading.

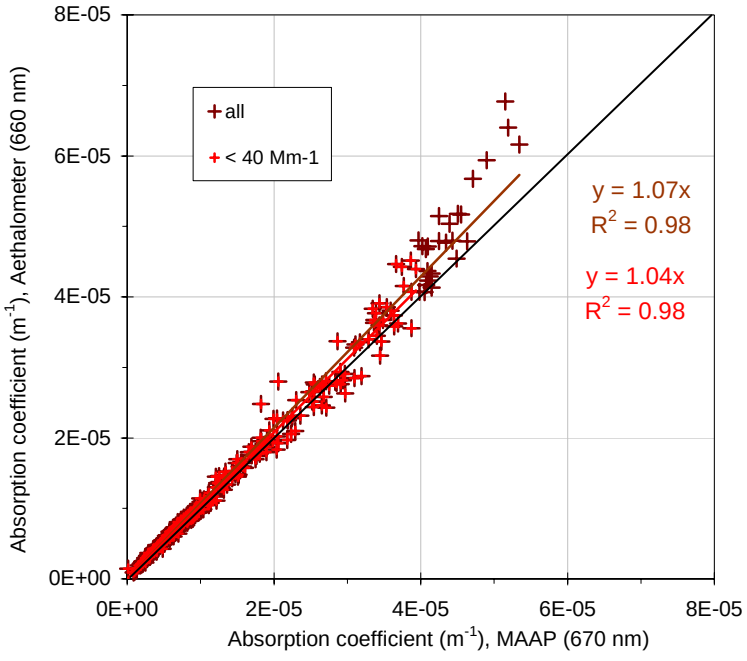

Fig. 35. *Comparison of Aethalometer and MAAP derived absorption coefficients at 660 and 670 nm, respectively. Data points are daily averages.*

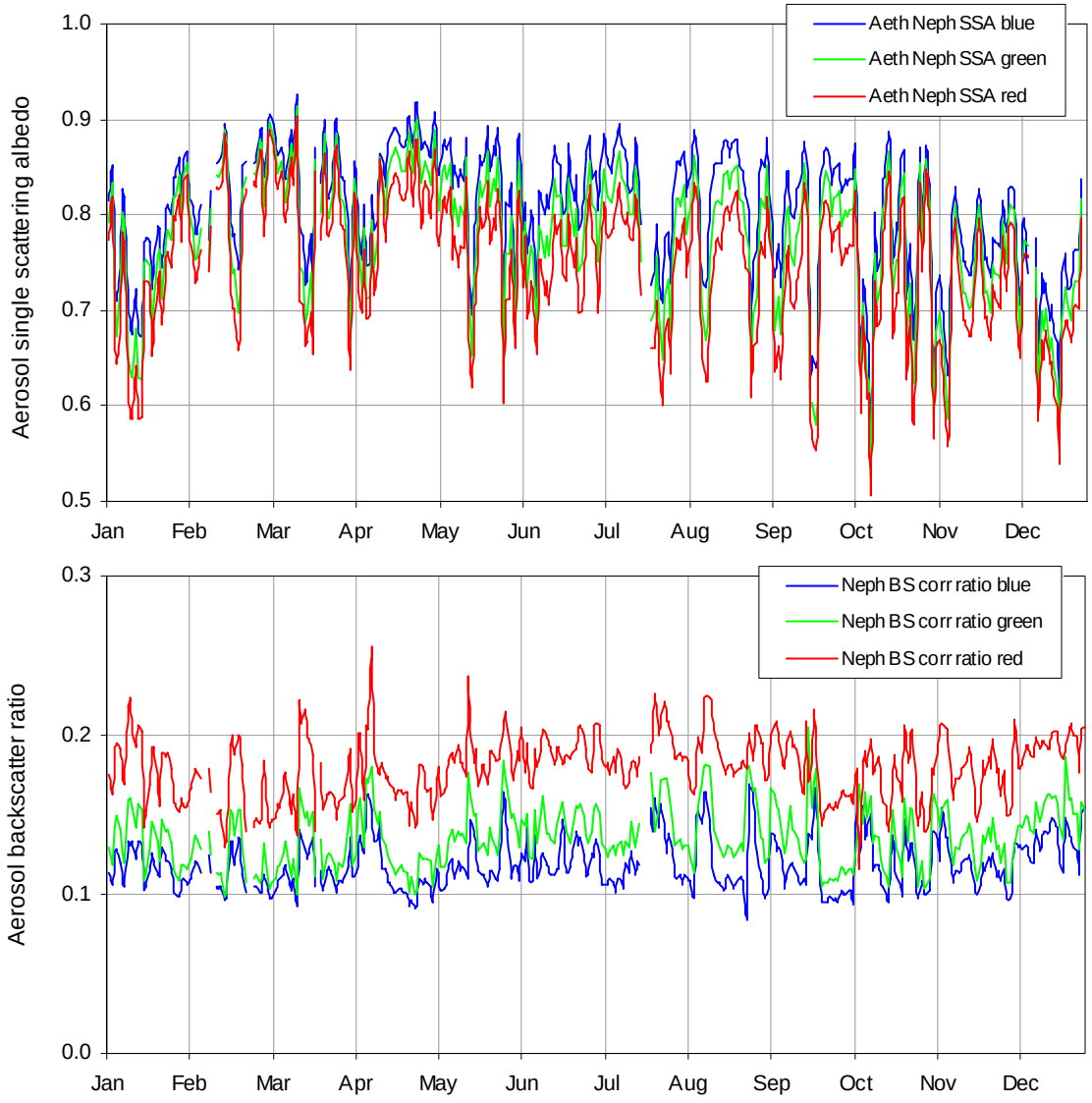

Fig. 36. Aerosol 24-hr average single scattering albedo and backscatter to total scatter ratio at three wavelengths corresponding to blue, green and red (RH generally < 40%).

The 24 hr averaged single scattering albedo at λ = 550 nm (at RH generally < 40 %) ranged from 0.61 to 0.92 (annual average 0.79), with generally higher values in summer compared to winter (Fig. 36a). In 2012, the aerosol single scattering albedo was slightly higher than in 2011 (0.77) and 2010 (0.75). The backscatter / total scatter ratio at 550 nm generally ranged from 9 to 19 % (Fig. 36b).

The aerosol extinction coefficient and particle mass or volume concentrations are rather well correlated (Fig. 37). The slope of the regression between extinction and mass shows that the extinction mass efficiency is on average 3.5 $m^2\ g^{-1}$, i.e. low compared with 4.2 $m^2\ g^{-1}$, the value calculated based on the aerosol mean chemical composition during 2012, and mass cross section coefficients for the various constituents found in the literature (see Table 7). The agreement between these two estimates of the aerosol extinction cross section deteriorated compared to 2010 and 2011. The slope of 5.5 observed in the extinction to volume correlation, together with the extinction to mass ratio (5.5/3.5 = 1.60), agrees marginally with the aerosol particle density of 1.31 found in Fig. 33).

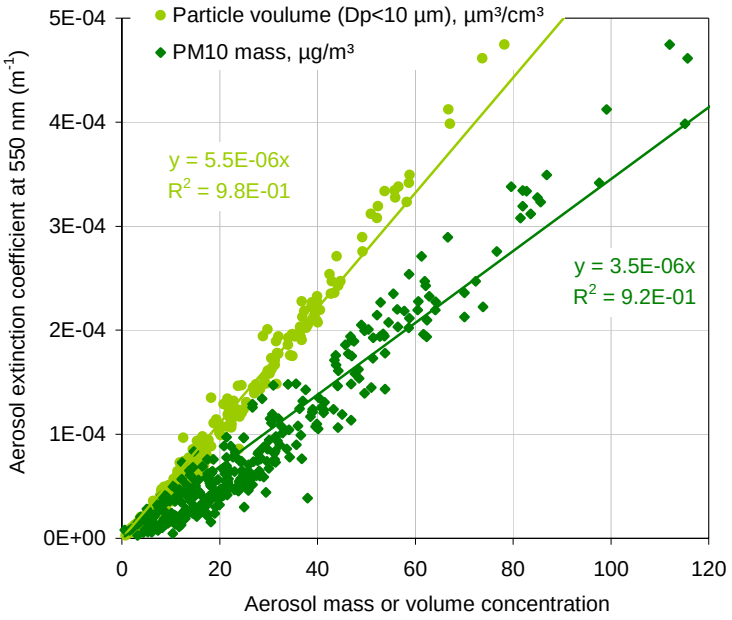

Fig. 37. *Regression between the aerosol extinction coefficient and PM10 mass (FDMS-TEOM) and volume (DMPS + APS) concentrations in 2012.*

Table 7. *Mean aerosol chemical composition (PM2.5) in 2012 and extinction efficiency.*

	2012 PM2.5 comp. (%)	σ_{ext} (m^2/g)	Reference (for σ_{ext})
"sea salt"	5	1.3	Hess et al., 1998
NH_4^+, NO_3^- and SO_4^{2-}	28	5.0	Kiehl et al., 2000
organic matter	42	3.6	Cooke et al., 1999
elemental carbon	6	11	Cooke et al., 1999
Dust	7	0.6	Hess et al., 1998
Total	**88**	**4.2**	

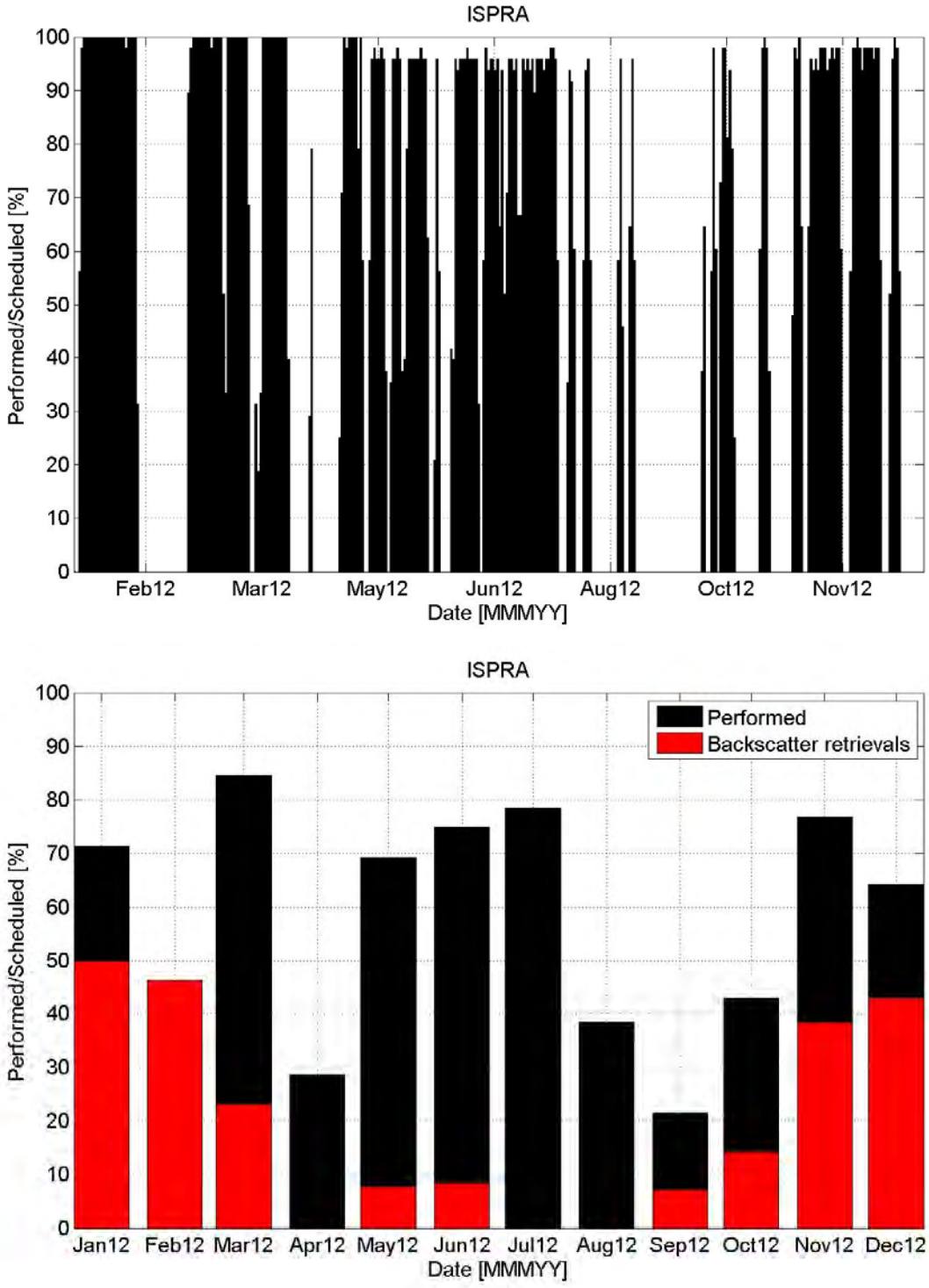

Fig. 38. *Performed/scheduled measurements for 2012 on daily (upper plot) and monthly bases.*

Aerosol vertical profiles

The backscatter LIDAR was operated almost continuously, weather permitting (no rainfall/snow, storm etc.). However, the laser power was low (34 mW on May 16th, 2012, compared to 60 mW on Aug 6th, 2009) and coupling into the fiber not excellent (56%). Laser power got extremely low between August 8th and September 25th, 2012, on which the laser was substituted (New laser power output 52 mW, 62% coupling into the fiber).

Among 105 scheduled measurements during the Earlinet slots, 76 were performed (72%) for the whole year 2012, of which 30 (29%) backscatter coefficients profiles were retrieved (Fig. 38). As for simultaneous measurements with Calipso, 62 measurements were performed out of 83 scheduled slots, of which 31 were inverted (37%). Not all the measured profiles are suitable for the inversion (in order to obtain the backscatter coefficient).

Fig. 39 shows an example of range corrected signal (no data inversion applied) recorded from Feb. 24th, 00:00 to Feb. 29th, 00:00, 2012. Thin white vertical lines correspond to 10-min periods during which the lidar is recovering. Patchy signals above 4 km are due to clouds. Low altitude signals (below 3 km) present a strong discontinuity: the profiles obtained between Feb. 24th and 26th, and on Feb. 28th-29th are as expected in winter, with a strong gradient and maximum concentration at the ground, while profiles recorded on Feb 26th-27th are weird, and probably due to an instrumental problem (e.g. loss of sensitivity at the ground due to change in the overlap function). This makes it difficult to invert the data obtained with this instrument automatically. This is why aerosol backscatter and extinction profiles have been retrieved so far mainly for the night-time measurements periods scheduled by Earlinet and for night-time Calipso overpasses.

Results derived from Lidar measurements performed in the past can be found in Barnaba et al., 2010.

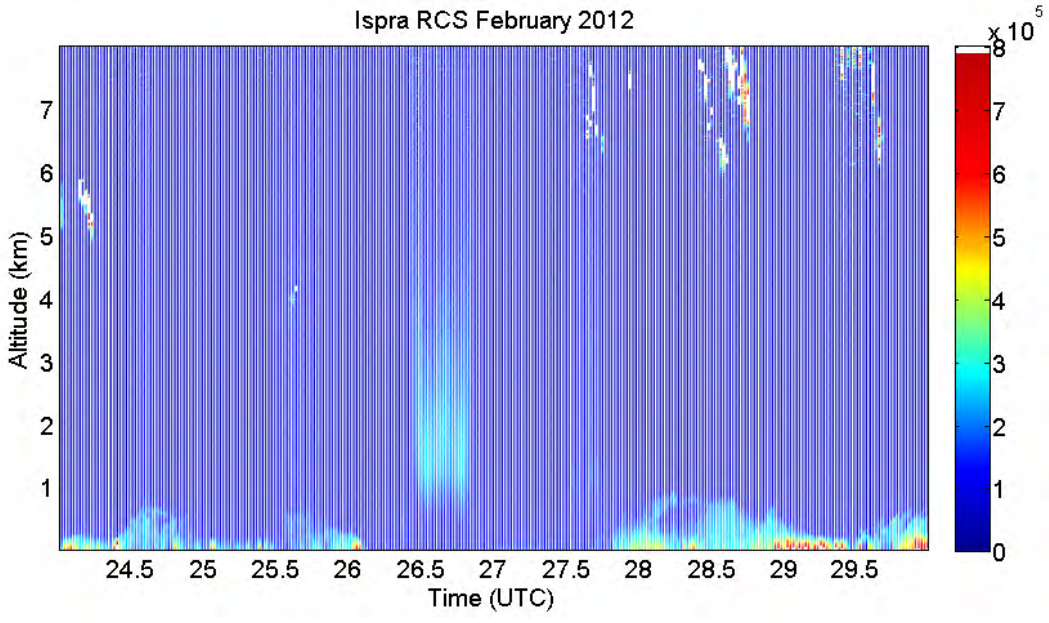

Fig 39: *Lidar signal obtained at ABC-IS on Feb. 24-29th, 2012, illustrating a possible instrumental problem on Feb.26-27th.*

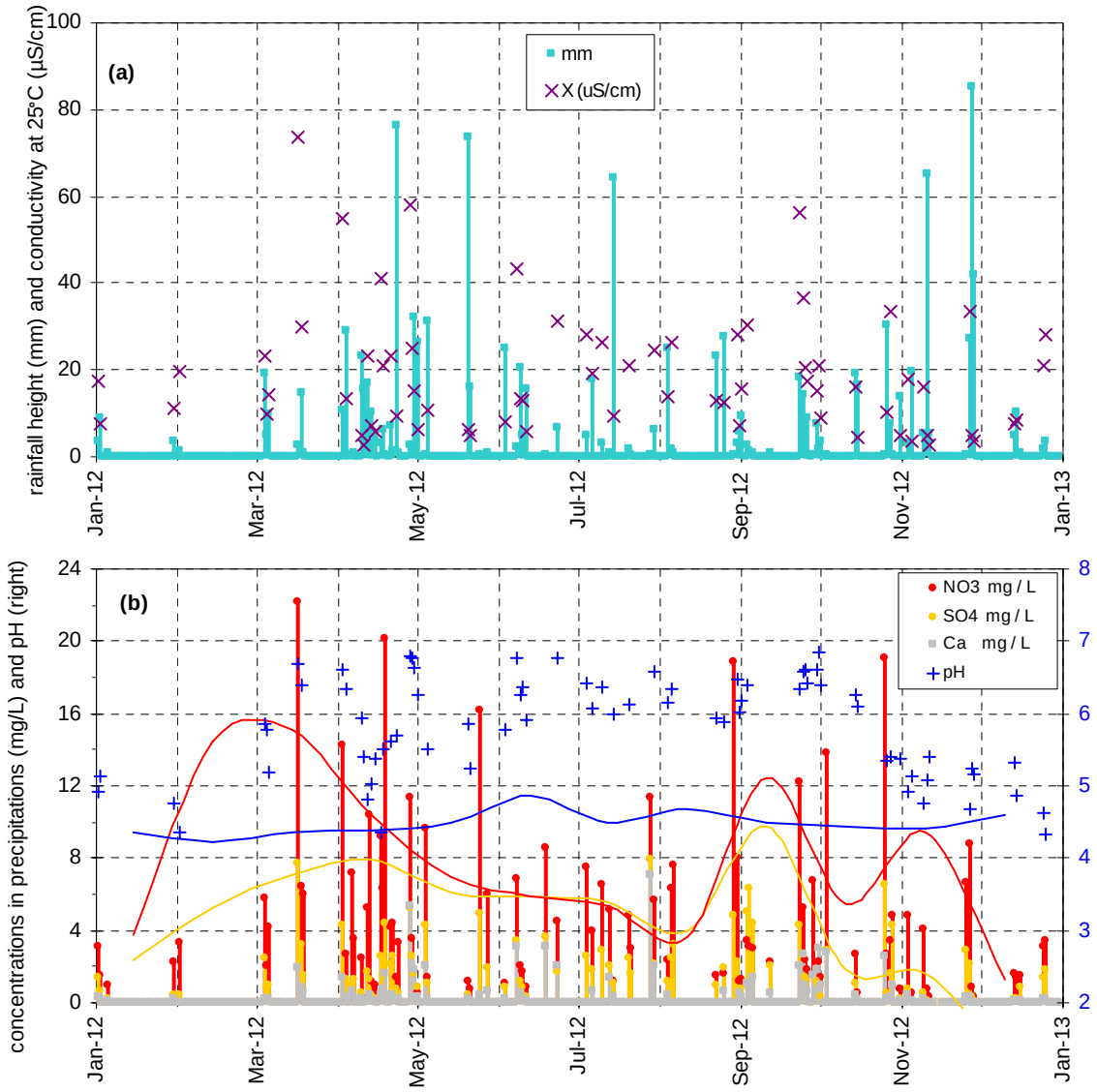

Fig. 40. *(a) Precipitation amount, conductivity and (b) concentrations of 3 major ions in precipitation and pH in 2012 (bars and crosses), and during the 1990-99 period (lines)*

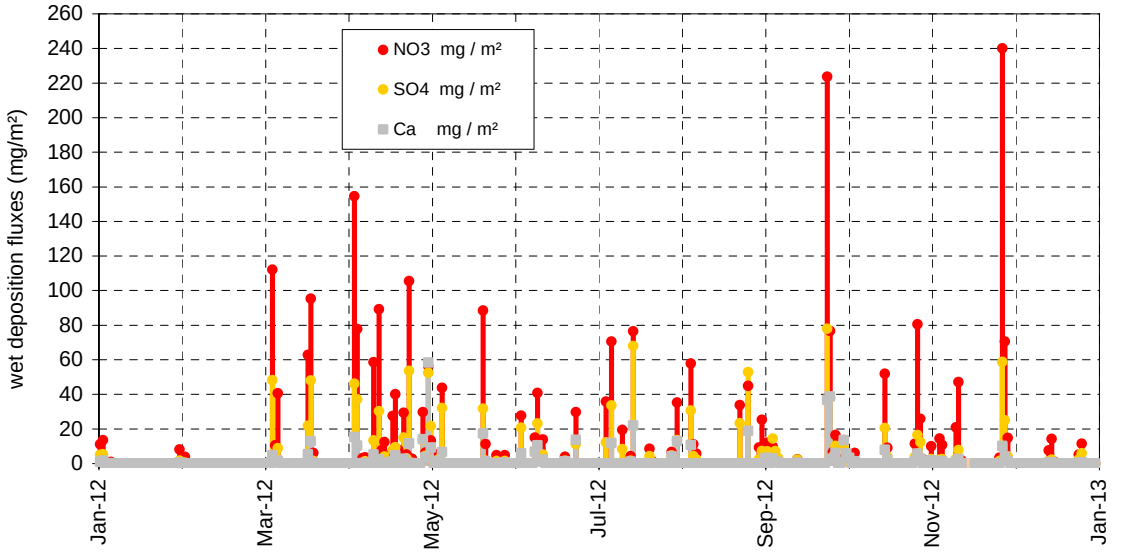

Fig. 40c. *Wet deposition fluxes of 3 main components in rain water in 2012.*

Precipitation chemistry

In 2012, 97 precipitation samples were collected and their ion content determined. Acidity (pH) and conductivity were also measured in 71 of those samples (not sufficient water volume was available for the remaining samples). The precipitation height of the collected events ranged from 0.3 to 85 mm (Fig. 40a) for a total of 1164 mm *vs.* 1141 mm detected by the rain sensor at the station (including data gap filling based on Bd 51 data). Two major rain events (> 1mm) were not sampled.

The ranges of concentrations measured in these samples are indicated in Table 9. Volume weighted mean concentrations of all species but Na^+ and Ca^{2+} were in 2012 smaller than the 1990-1999 averages. All precipitation samples collected in 2012 were acidic (pH < 7.0). However, pH<5.6 (equilibrium with atmospheric CO_2) was measured in 28 samples (compared to 17 in 2011) and pH < 4.6 in 3 samples only.

Wet deposition occurred mainly from March to November (Fig. 40c). The annual wet deposition flux of the main acidifying and eutrophying species was 1.2, 2.9, and 1.3 g m^{-2} for SO_4^{2-}, NO_3^-, and NH_4^+, respectively. These fluxes were significantly larger than in 2011 (0.9, 1.9, 0.8 g m^{-2}, respectively), and very close to values observed in 2010.

Table 9. *Statistics relative to the precipitation samples collected in 2012 (averages are volume weighted)*

	pH	cond.	Cl^-	NO_3^-	SO_4^{2-}	Na^+	NH_4^+	K^+	Mg^{2+}	Ca^{2+}
		µS cm^{-1}	mg l^{-1}	mg l^{-1}	mg l^{-1}	mg l^{-1}	mg l^{-1}	mg l^{-1}	mg l^{-1}	mg l^{-1}
Average	5.41	12.8	0.39	2.5	1.1	0.32	1.11	0.04	0.07	0.42
Min	4.34	2.5	0.02	0.3	0.04	0.02	0.04	<0.01	<0.01	<0.01
Max	6.86	31	25.8	22.2	7.9	11.2	8.2	1.0	1.4	7.1
1990-1999 average	4.40	73.6	0.44	3.9	3.1	0.23	1.3	0.09	0.06	0.45

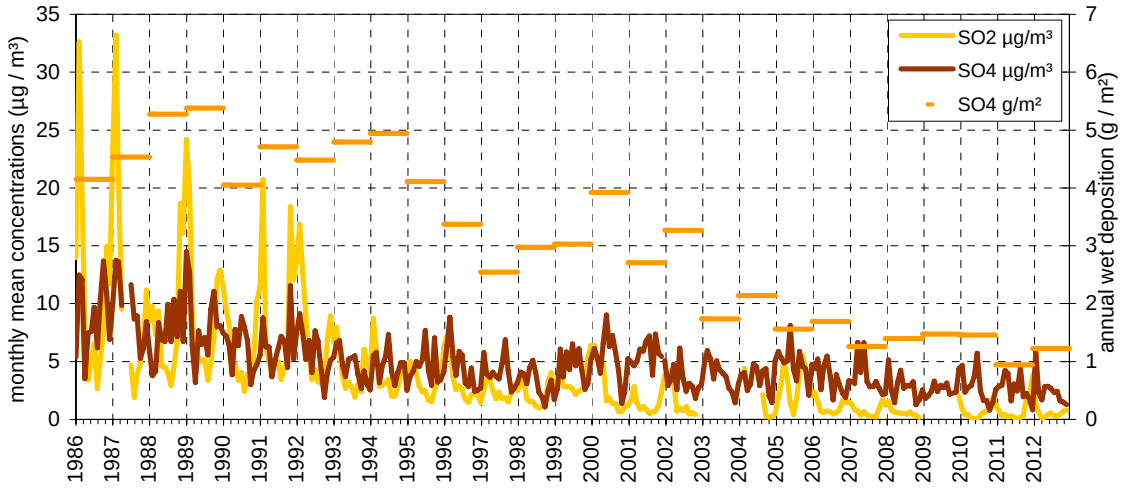

Fig. 41. Oxidized sulfur species monthly mean concentrations and yearly wet deposition.

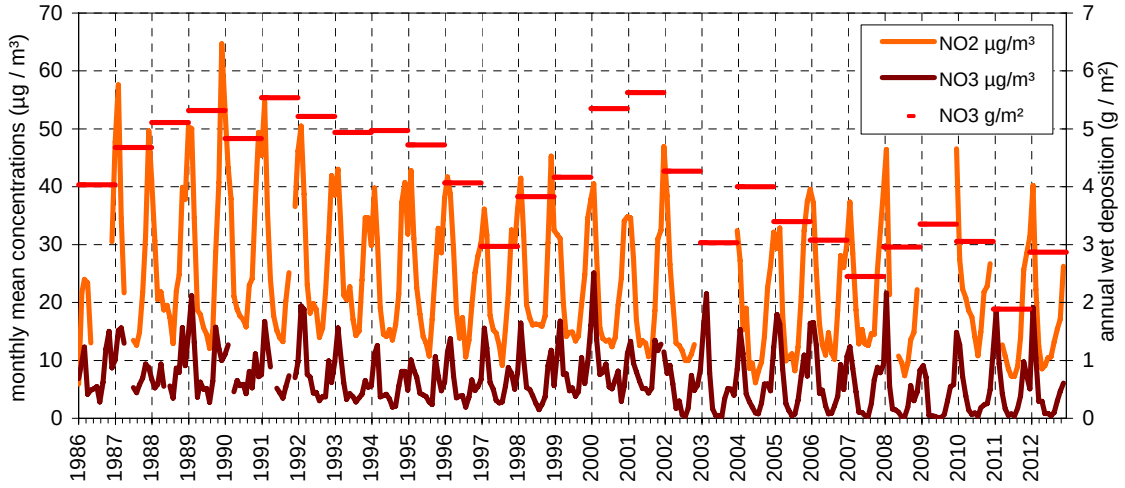

Fig. 42. Oxidized nitrogen species monthly mean concentrations and yearly wet deposition.

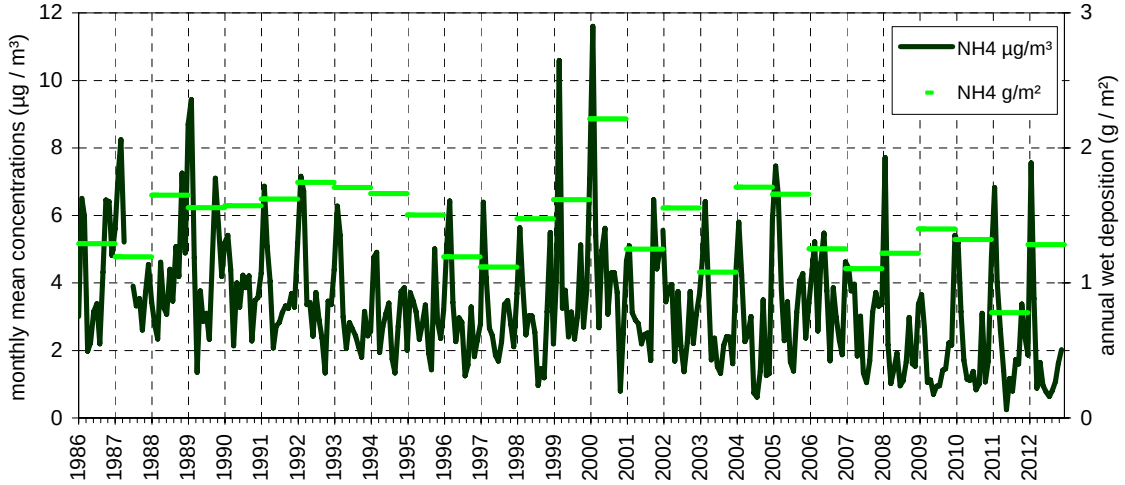

Fig. 43. Reduced nitrogen species monthly mean concentration and yearly wet deposition.

Results of year 2012 in relation to > 25 years of monitoring activities

Sulfur and nitrogen compounds

The 2012 yearly averages for particulate SO_4^{2-}, NO_3^-, and NH_4^+ in PM10 (estimates) were less than (SO_4^{2-} and NH_4^+) or similar as (NO_3^-) over the past 5 years (2.9, 4.8 and 2.4 µg/m³, respectively).

Annual mean particulate concentration SO_4^{2-} reached a historical minimum in 2013, after a 3-fold decrease from 1986 to 1998, followed by a stagnation around the mean 90's value (see Fig. 41). In contrast, both winter maxima and summer minima monthly mean concentrations of sulfur dioxide (SO_2) decreased by a factor of more than 10 over the past 20-25 years (Fig. 41) but remained roughly constant during the past 3 years. These data show that locally produced SO_2 decreased much more than possibly long-range transported SO_4^{2-} over the past 20-25 years, but no more for the past 3 years. It should be kept in mind that SO_4^{2-} concentrations were measured in PM10 or in PM2.5 from 2002 onwards, whereas it was measured in TSP (Total Suspended Particulate) from 1986 to 2001. However, simultaneous sampling of PM10 and TSP over 14 months showed that SO_4^{2-} in PM10 is generally less than 5 % lower than in TSP. It should also be mentioned that SO_4^{2-} is mainly present in the PM2.5 fraction (see Fig. 24). From 2005 onwards the calculations were as following SO_4^{2-}(PM10) = SO_4^{2-}(PM2.5) x <SO_4^{2-}(PM10)/ SO_4^{2-}(PM2.5)> (the average <SO_4^{2-}(PM10)/ SO_4^{2-}(PM2.5)> is calculated based on the 4-6 simultaneous PM10 and PM2.5 samples collected each month). SO_4^{2-} wet deposition in 2013 was the second lowest value (after 2012) ever recorded at the station.

Monthly mean concentrations of nitrogen dioxide (NO_2) do not show such a pronounced decreasing trend over the past 27 years (Fig. 42) as seen for SO_2. Wintertime NO_2 maxima indeed have remained quite constant since 1993, which does not reflect the 30 % abatement in NO_x emissions expected from emission inventories. Particulate NO_3^- wintertime concentrations observed in 2003 - 2012 are comparable to values observed earlier too. It should be noted that since October 2000, NH_4 and NO_3^- have been measured mostly from quartz fibre filters, which are known to lose NH_4NO_3 at temperatures > 20 °C. This might contribute significantly to the fact that NO_3^- summertime minima are particularly low since 2002. Furthermore, NO_3^- was measured from PM10 or in PM 2.5 from 2002, and no more from TSP, as over the 1986 to 2001 period. However, simultaneous sampling of PM10 and TSP over 14 months showed that NO_3^- in PM10 is generally less than 5 % lower than in TSP, like SO_4^{2-}. From 2005 and onwards the calculations were as following NO_3^-(PM10) = NO_3^-(PM2.5) x < NO_3^-(PM10)/ NO_3^- (PM2.5)> (the average < NO_3^-(PM10)/ NO_3^- (PM2.5)> is calculated based on the 4-6 simultaneous PM10 and PM2.5 samples collected each month. NO_3^- wet deposition annual flux observed in 2013 was the 3rd lowest ever recorded since 1986 in Ispra, but very close to the average over la last decade.

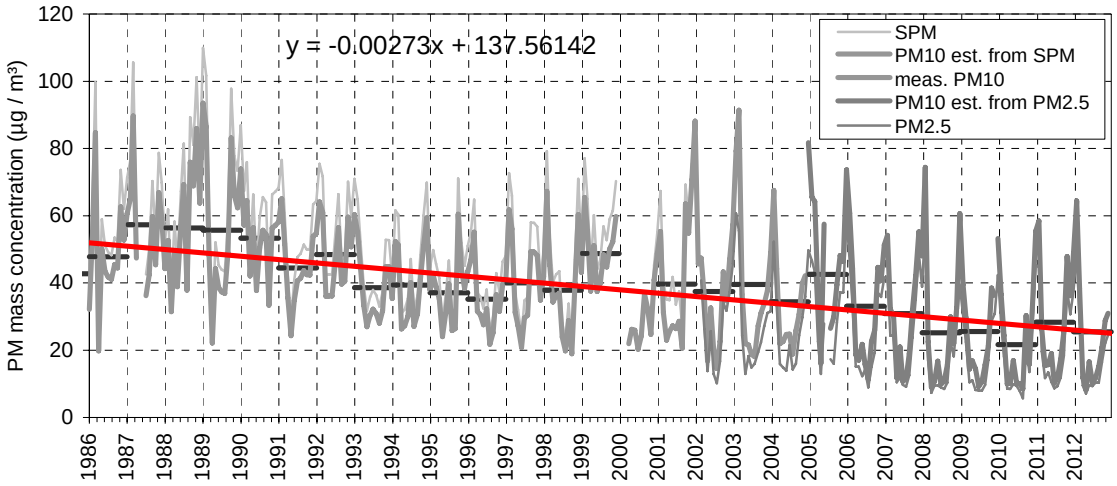

Fig. 44. Particulate matter mass concentration monthly (grey) and annual(black) averages. The red line is the long term trend over annual averages. All values in the figure are from gravimetric measurements or estimated from gravimetric measurements.

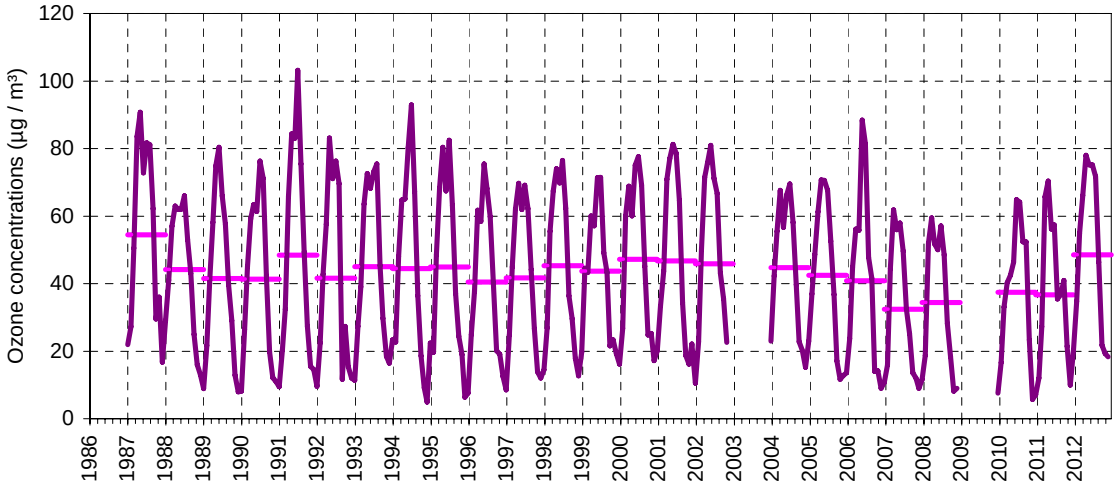

Fig. 45. Ozone yearly and monthly mean concentrations at JRC-Ispra.

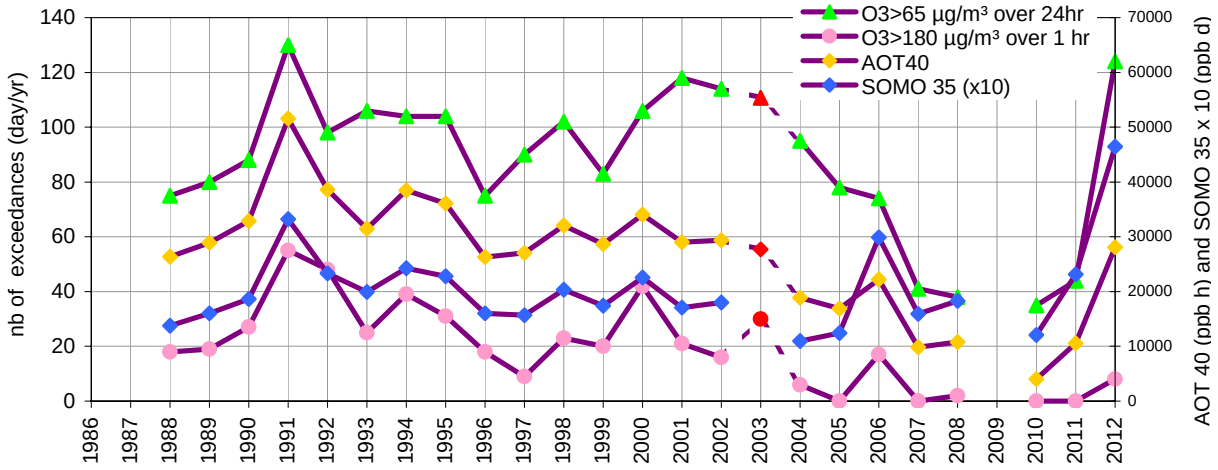

Fig. 46. AOT40, SOMO35 values, and number of days on which O_3 limit values were reached. The 3 red spots are data points from Malpensa.

Monthly mean concentrations of NH_4^+ in the particulate phase seem to have decreased slightly since 1986 (Fig. 43), especially because summertime minima decreased. Although winter-time maxima increased much since 2004, there is no significant long-term trend regarding NH_4^+.

It should be mentioned that from the year 2002 NH_4^+ was measured in the PM10 or in the PM2.5 fraction (from 2005 and onwards the calculations were as following NH_4^+(PM10) = NH_4^+(PM2.5) x < NH_4^+(PM10)/ NH_4^+(PM2.5)> (the average <NH_4^+ (PM10)/ NH_4^+(PM2.5)> is calculated based on the 4-6 simultaneous PM10 and PM2.5 samples collected each month). On average, NH_4^+ can neutralize close to 100% % of the acidity associated with NO_3^- and SO_4^{2-} in the particulate phase (see Fig. 21). NH_4^+ is also quite well correlated with NO_3^- + SO_4^{2-} in rainwater. NH_4^+ annual wet deposition was twice as large as in 2011, but very much in line with values recorded in Ispra since 2006.

Trace elements

Measurements of Pb, Zn, Fe, Cu, Mn, Cr and V were regularly performed in Ispra from 1987 to 1998. Little is known, however, on the analytical procedure apart that analysis was performed by EDX-RF. The annual average concentrations have decreased over the last 25 years, with reduction in the order of 80-95% for Mn, Zn, Cr, Pb and V, and 60% for Fe and 20% for Cu.

Concentration reductions are for the majority of elements so substantial (Fig. 47) that the lack of information on the comparability of the two techniques employed, i.e. EDX-RF and ICP-MS, does not affect the significance of these observations.

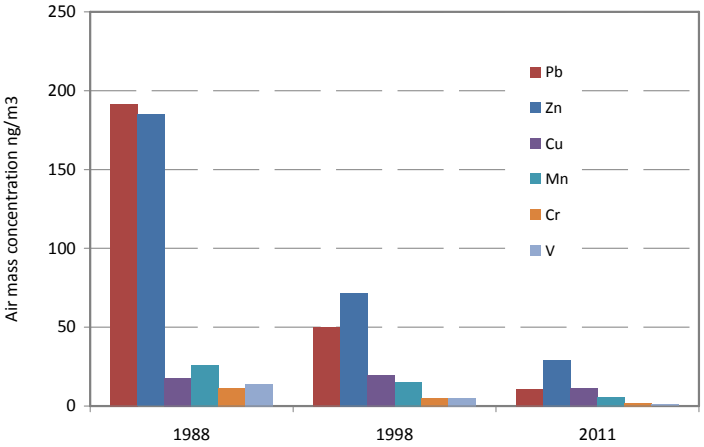

Fig. 47: *concentrations of selected trace elements for 3 selected years spanning 23 years*

Particulate matter mass

PM10 values observed in 2012 confirm the increasing trend in PM10 wintertime maxima observed since 2010 (Fig. 44), while summer time minima remain more or less constant: the 2012 annual average PM10 concentration (estimated from PM2.5 measurements) reached 25.5 µg/m³, i.e. les than 28.3 µg/m³ in 2011, but more than the historic minimum of 21.6 µg/m³ observed in 2010, and comparable to the 2008 and 2009 values. However, a linear fit indicates that PM10 has been decreasing by 1.0 µg m^{-3} yr^{-1} between 1986 and 2012. It should be kept in mind that PM10 concentrations were estimated from TSP mass concentration measurements (carried out by weighing at 60 % RH and 20 °C cellulose acetate filters sampled without any particle size cut-off and “dried” at 60 °C before and after sampling) over 1986-2000, based on a comparison between TSP and

PM10 over the Oct. 2000 - Dec. 2001 period (R^2 = 0.93, slope = 0.85), and based on measured PM2.5 values for years 2005-2011.

Ozone

Figure 45 shows monthly and yearly mean O_3 concentrations observed since 1987. It should be mentioned that ozone was not measured in 2009 and that there were an acquisition breakdown in 2003. The decreasing trends in wintertime minimums and summertime maximums observed since 2003 (2006 mini-heat wave peak excluded) are no more observed since 2009. On the contrary wintertime, summertime, and annual averages are all increasing again, getting back to values observed more than a decade ago.

As a consequence, all ozone indicators (Figure 46) have deteriorated. The number of extreme O_3 concentrations (days on which the limit of 180 µg/m³ over 1hr was exceeded) exceeded 1 / yr for the first time since 2008. Both indicators for the vegetation protection increased back to the highest values observed in the 1990's. Indeed, the number of days with a 24-hour mean O_3 concentration > 65 µg/m³ (vegetation protection limit) increased from 35 (2010) to 44 (2011) to 122. AOT40 (Accumulated Ozone exposure over a Threshold of 40 ppb), the vegetation exposure to above the O_3 threshold of 40 ppb - about 80 µg/m³), increased from 4000 ppb h (2010) to 10500 ppb h (2011) to 28100 ppb h (2012). The population exposure indicator SOMO 35 (Sum of Ozone Means Over 35 ppb, where means stands for maximum 8-hour mean over day) doubled from 2300 ppb d in 2011 to 4600 ppb d, the 2nd highest value observed since 1988, well above the values observed over the last decade.

Conclusions

In 2012, solar radiation was generally close to the climatologic average over 1990-1999. In contrast, 2012 was dryer and warmer that average. January, February, August and December were particularly dry, while June, July and August were particularly warm.

Dry and warm weather conditions may at least partly explain that various indicators for O_3 pollution very much increased compared to 2011. Actually, the annual mean concentrations of O_3, NOx and CO were also all quite high compared to the last decade. Just SO_2, annual average remained amongst the lowest ever observed at the EMEP-GAW station of Ispra.

Aerosol sampling on quartz fibre filter, and subsequent gravimetric and chemical analyses were also performed over the whole year. We collected PM2.5 daily and PM10 five times a month using two Partisol samplers, with and without a carbon monolith denuder, respectively. With the assumption used to estimate POM and dust from organic carbon (OC) and Ca^{2+}, respectively, the whole PM2.5 mass concentration could be explained rather well in 2012, except for a few days. PM2.5 average chemical composition was dominated by carbonaceous species (POM: 48%, EC: 9%), followed by secondary inorganics (NH_4^+:9%, NO_3^-: 13%, SO_4^{2-}: 15%). The contribution of sea-salt ions and mineral dust were about 3 %

each. However, there is a clear increase of NO_3^- contribution to PM2.5 when shifting from cleaner (PM2.5 < 10 µg/m³) to more polluted periods (PM2.5 > 25 µg/m³). Both PM2.5 and PM10 annual mean concentrations (19 and 28 µg/m³respectively) were below the EU annual limit value (25 and 40 µg/m³, respectively), but 51 exceedances (derived from TEOM measurements) of the 24-hr limit value (50 µg/m³) were observed. The long term time series still suggests a PM10 mass concentration decreasing trend of 1.0 µg m^{-3} yr^{-1} over the last 28 years of records. It should be noticed that the annual mean PM10 level in 2012 was amongst the three lowest values recorded since 1986, with 2008 and 2010 (see Figure 44).

The average particle number in 2012 (average: 7540 cm^{-3}, range 1950 – 18600 cm^{-3}) was larger than to the 2010 and 2011 values (~ 6900 cm^{-3}). Particle number size distributions were generally broadly bimodal, with a submicron mode at ca. 60-80 nm (dry) and a less pronounced coarse mode around 2 µm. The particle mean geometric diameter ranged 30 – 130 nm (maximum values observed in winter) and averaged 69 nm. Atmospheric aerosol scattering and absorption coefficients at various wavelengths were derived from Nephelometer and Aethalometer measurements in dried atmosphere (generally lower than 40%). The mean single scattering albedo at λ = 550 nm (not corrected for hygroscopic growth) was 0.79 in 2012 (vs 0.77 in 2011).

The aerosol extensive variables measured at JRC-Ispra (at ground level) all follow comparable seasonal variations with minima in summer. These variables are generally well correlated and lead to reasonable degrees of chemical, physical, and optical closures. However, the average aerosol density of 1.31 g/cm^3 derived from the gravimetric mass and DMPS + APS volume was still a bit low was as low in 2012 as in 2011 (1.32 g/cm^3), compared to 1.37 - 1.38 g/cm^3 in 2010-2011, and especially to the 2005 value of 1.50 g/cm^3. Also, the extinction-to-mass ratio of 3.5 m^2 g^{-1} observed in 2012 is lower than in 2011 (3.9 m^2 g^{-1}), and also low compared with the value that can be calculated from the mean PM2.5 chemical composition, which averages to 4.2 m^2 g^{-1} in 2011 (see Table 9).

Aerosol backscatter profiles were obtained with the CIMEL LIDAR across the whole seasons during 2012. Due mainly to unsuitable meteorological conditions, 138 out of the 188 profiles scheduled by EARLINET could be measured. Aerosol backscatter profiles were retrieved for 61 of these measurements (from January to October), but results are still being inspected before submission to the EARLINET data base.

The concentrations of all rainwater components (Cl^-, NO_3^-, SO_4^{2-}, NH_4^+, K^+, Mg^{2+}), but Na^+ and Ca^{2+} were lower in 2011 compared to the 1990-1999 average. The annual wet deposition flux of the main acidifying and eutrophying species were 1.2, 2.9, and 1.3 g m^{-2} for SO_4^{2-}, NO_3^-, and NH_4^+, respectively. These annual fluxes are larger than the 2011 values, and close to the values observed at the EMEP-GAW station in Ispra over the last decade.

The 2012 data listed by EMEP and ACTRIS as core parameters have been reported to EBAS in 2013, as requested by these networks.

Fig. 48: The 36 high self-standing tower at the ABC-IS Forest Flux Station

Atmosphere – Biosphere flux monitoring at the forest flux station in Ispra

Location and site description

The ABC-IS Forest Flux Station is part of the large ABC-IS infrastructure focussing on the measurement and monitoring of exchange processes of a forest ecosystem with the atmosphere predominantly relying on the use of the eddy covariance technique for flux measurements. The measurement site (45°48'45.68"N, 8°38'2.09"E) is located inside a small forest of approximately 10 ha that is part of the JRC Ispra premises. Situated in an almost flat area, this forest is unmanaged since the foundation of the JRC Ispra in the late 1950ies and therefore now characterized as a mixed, almost natural forest ecosystem. The tree species composition consists of ~80% Quercus robus, ~10% Alnus glutinosa, ~5% Popolus alba and ~3% Carpinus betulus. The predominant soil type is Regosol.

The ABC-IS Forest Flux Station comprises a 36 m high self-standing tower (see Fig. 48) as a platform to hold instruments, an air-conditioned container for instrumentation and IT infrastructure plus the surrounding forest where above and below ground sensors are installed. A detailed project documentation can be found at Gruening et al., 2011. After the erection of the tower in the second half of 2011, basic infrastructure installation, notably electricity, IT services and air conditioning in the container continued into the first quarter of 2012. Thereafter, the installation and testing of scientific instrumentation both on the tower and at the ground has started in view of the two projects the station participates in, i.e. the ESFRI initiative ICOS (International Carbon Observation System) and the FP7 project ECLAIRE (Effects of Climate Change on Air Pollution and Response Strategies for European Ecosystems). A report of the performance of the instruments at the site also in comparison with measurements from the EMEP station is given in Gruening et al, 2012.

Tab. 10: ICOS level 2 Ecosystem Station core parameters.

Core variables continuous	Core variables daily to monthly	Core variables yearly
CO_2, H_2O and energy fluxes	leaf area index	biomass (above ground)
wind speed and direction	CH_4, N_2O by manual chambers during sporadic short-term campaigns	soil carbon
CO_2 concentration vertical profile, normal precision	Phenology	stem diameter
net radiation: • incoming/reflected global radiation • incoming/outgoing longwave radiation • Albedo		above-ground Net Primary Production (NPP)
diffuse global radiation		litter fall
incoming / reflected under canopy Photosynthetic Active Radiation (PAR)		land-use history
temperature and relative humidity vertical profile		managements and natural disturbances
air pressure		C and N import and export on managed sites
precipitation, through-fall, snow depth		
soil heat flux		
ground water level		
soil temperature profile		
water content profile		

Measurement program

The ABC-IS Forest Flux Station has been projected as a platform to perform long-term monitoring activities with the additional possibility to engage in short-term research projects, mainly in the frame of international collaborations. The scientific activities are embedded at the moment into two major European programs: the ICOS initiative and the FP7 project ECLAIRE.

ICOS (Integrated Carbon Observation System, www.icos-infrastructure.eu) is one of the pan-European research infrastructure projects identified by the European Strategy Forum on Research Infrastructures (ESFRI) for implementation. After its preparatory phase planned for 2008 until 2012 with extension until 2013, during which monitoring infrastructure and technical procedures are developed, its operational phase will run for 20 years from 2014 until 2033.

Once in operational mode, greenhouse gas concentrations and fluxes will be monitored on a routine basis following a very strict quality controlled protocol, both in terms of measurement instrumentations required to be used and procedures to be followed. The JRC contributes with a level 2 Atmospheric Station (AS) for the high precision monitoring of greenhouse gas concentrations and two level 2 Ecosystem Stations (ES), the ABC-IS forest flux tower and the second installation in the Parco San Rossore near Pisa, for the monitoring of ecosystem fluxes. Level 2 stations provide data for less parameter compared to level 1 stations and thus require less investment for instrumentation and have lower running costs in terms of instruments and staff. The mandatory variables to be monitored at the level 2 Ecosystem Station ABC-IS forest flux tower are shown in Table 10.

ÉCLAIRE (Effects of Climate Change on Air Pollution and Response Strategies for European Ecosystems, www.eclaire.ceh.ac.uk) is a four year large scale integrating project funded by the EU's Seventh Framework Programme for Research and Technological Development (FP7) involving 39 partner institutions across Europe. It investigates the ways in which climate change alters the threat of air pollution on European land ecosystems including soils. Based on field observations, experimental data and models, it establishes new flux, concentration and dose-response relationships, as a basis to inform future European policies.

The ABC-IS flux tower is one of three forest ecosystem sites with a continuous measurement program from summer 2012 until the end of 2013 and several intensive periods in 2013 requiring more sophisticated instrumentation. In addition to the ICOS core parameters (see Table 10), the following measurements were performed continuously in 2012:

- atmospheric O_3 fluxes using eddy covariance technique
- soil NO / NO_2 fluxes with an automated dynamic chamber system

During the intensive measurement periods in 2013, VOC and especially Isoprene concentrations and fluxes will be determined in addition.

Measurements performed in 2012

The main parameters measured during 2012 are summarized in Table 10.

Fluxes of CO_2, H_2O, sensible heat and ozone were measured with eddy covariance technique using EddyMeas (Olaf Kolle, www.bgc-jena.mpg.de) for data acquisition and evaluated with the EdiRe software package from the University of Edinburgh (www.geos.ed.ac.uk/abs/research/micromet). For soil NO & NO_2 fluxes, an automated dynamic chamber system has been developed and deployed in the forest. The ancillary parameters (meteorology, radiation and soil) were obtained with respective sensors and the data quality checked for instrument malfunctioning, obvious outliers and consistency. In the following chapters, first the instruments used are described and then daily averages of the different parameters measured during the course of 2012 are presented.

Table 11: Parameters measured during 2012

FLUXES	CO_2, latent heat, sensible heat, ozone
METEOROLOGY	3D wind speed, temperature, relative humidity, pressure, precipitation
RADIATION	short & long wave incoming & outgoing, direct, diffuse & reflected photosynthetic active radiation
SOIL	temperature profile, water content profile, heat flux, water table height, respiration, NO / NO_2 fluxes
BIOLOGICAL	litter fall

Description of Instruments:

Infrastructural:

Sensor location

The instruments for the eddy covariance flux system, i.e. sonic anemometer and fast gas analysers, radiation and meteorological sensors plus gas inlets are mounted on the top of the 36 m high self-standing tower. Soil parameters including NO / NO_2 fluxes are measured at close vicinity to the tower on the forest ground approximately 20 m north.

Data acquisition

Eddy covariance flux data are acquired and stored with high frequency, i.e. 10 Hz, as chunks of 30 minutes on a local laptop connected to the sonic anemometer. Data from all other sensors are read every 10 s by a respective CR3000 data logger from Campbell Scientific (www.campbellsci.co.uk) which saves 30 minute averages of the acquired data.

For eddy covariance flux data, the start time of every 30 minutes measurement period is saved as the reference time, whereas for all other data, the end of the 30 minutes measuring period is used. The time reference for all measurements is UTC.

Ecosystem fluxes:

Sonic Anemometer for 3D wind direction Gill HS-50

Sonic anemometers determine the three dimensional wind vectors at high frequency using the speed of sound. The Gill HS-50 (www.gill.co.uk) emits ultrasonic pulses between its pairs of transducers, measures the flight time of the pulses to the paired transducer and calculates the wind speed in the direction of the transducer pair (see Fig. 49). Combining the results from

the three transducer pairs, the 3 dimensional wind speed is calculated at a frequency of 10 Hertz. After a rotation of the coordinate system during the data processing to align it with the north direction, horizontal and vertical wind speeds and the wind direction are calculated besides their use for flux calculations. As the speed of sound measured with the anemometer depends on the temperature, the so-called sonic temperature is reported by the instrument as well.

Due to the absence of moving parts and the fact that no calibration is required, the instrument is very robust and reliable. Instrument servicing is done at the manufacturer.

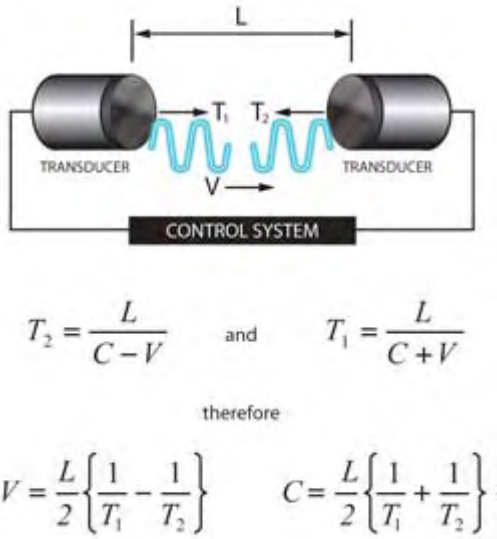

Fig. 49: Measurement principle of sonic anemometers, T: travelling time of sound pulses, L: distance between transducers, C: speed of sound, V: wind speed in direction of transducers (sketch from www.gill.co.uk)

Fast infrared gas analyser for CO_2 & H_2O concentration (IRGA) LI-7200 FM

For the determination of CO_2 and H_2O fluxes with the eddy covariance technique, fast analysers (10 to 20 Hertz) for concentration measurements of the gases of interest are obligatory. At the EMEP forest flux tower, a LI-7200 FM system from LI-COR (www.licor.com) has been installed, consisting of the LI-7200 enclosed CO_2/ H_2O analyser, the LI-7550 analyser interface unit and the LI-7200-101 flow module.

The LI-7200 is a high performance, non-dispersive, enclosed open path infrared CO_2/H_2O analyser based on the infrared absorption of CO_2 and H_2O at ambient conditions that provides concentration measurements at a frequency of up to 20 Hertz. With the flow module, ambient air is drawn into to analyser through the sample inlet at a set flow rate of 15 l/min. In the sample volume of 16.09 cm^3 (see figure Fig.50), light from the infrared source is absorbed at characteristic wavelengths for CO_2 and H_2O. This specific absorption is a function of the gas concentration in the sample volume. Using the absorption measurements at the CO_2 & H_2O wavelengths, at a non-absorbing wavelength plus calibration factors and measured temperature and pressure, the LI-7200 provides number-, mass densities or mole fraction of the two gases.

Zero and span checks and calibrations are done regularly using zero gas from a cylinder plus a dew point generator (LI-COR 610) and a CO_2 standard from a cylinder.

Fast ozone sensor - Sextant FOS

The measurement principle of the Fast Ozone Sensor (FOS), manufactured by Sextant Technology Ltd. (www.s-t.co.nz), is based on chemiluminescence. In a measurement chamber, ambient air containing ozone passes above a 25 mm diameter disc coated with coumarin. The dye coumarin reacts with ozone under the emission of light. This emission is proportional to the ozone concentration in the air and the reaction and the air exchange in the reaction chamber is sufficiently fast to allow 10 Hz measurements of ozone concentrations.

The sensitivity of the coumarin discs unfortunately changes within hours. Therefore an independent measurement of the absolute value of the ozone concentration is mandatory and realized with a Thermo Scientific 49C Ozone Analyser (see p 75 for instrument description) sampling air at vicinity of the FOS. A linear calibration of the FOS is automatically done in data post-processing using the 30 minute mean values of the FOS signal and the 49C concentration plus zero as offset. The lifetime of the coumarin-coated discs depends on the total ozone exposure and is limited to approximately two weeks.

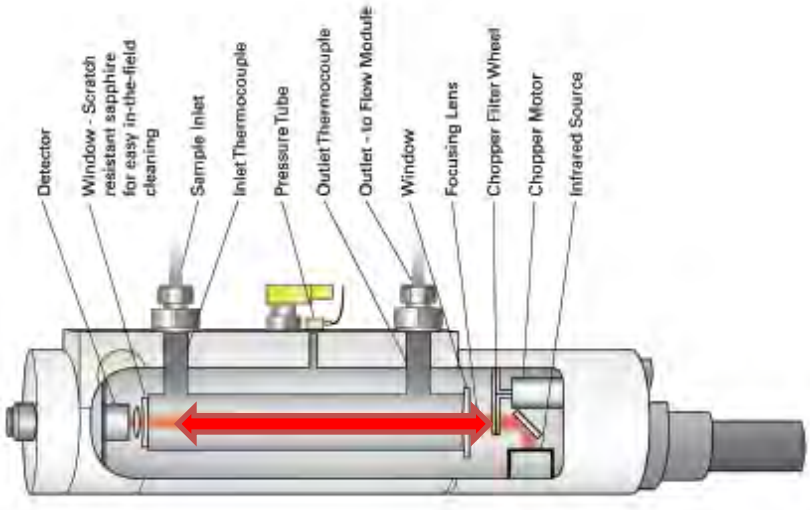

Fig. 50*: CO_2 and H_2O LI-7200 analyser head (from www.licor.com), arrow indicates sampling volume*

Radiation instruments

Net radiometer Kipp & Zonen CNR1

The net radiometer CNR1 from Kipp & Zonen (www.kippzonen.com) measures the energy balance between incoming and reflected radiation in the short (305 – 2800 nm) and long (5-50 µm) wavelength range to obtain the net radiation at the earth's surface. The short wavelength range is measured with two CM3 pyranometers, one facing upwards and one downwards. For the long range, two CG3 pyrgeometers facing opposite directions are used. The design of the instrument ensures a field of view of 180° upwards and downwards for the respective sensors.

The energy E_{short} of the short wave or so-called global (solar) radiation is calculated from the voltages provided by the CM3's using their sensitivity C_{CM3}: $E_{short} = V / C_{CM3}$. To calculate the energy E_{long} of the long wave radiation from the reported voltages, besides the sensitivities of the CG3's C_{CG3}, also the sensor temperature T measured with a PT-100 is needed: $E_{long} = V / C_{CG3} + 5.67 \cdot 10^{-8} \cdot T^4$. The net radiation over all wavelengths is then easily calculated by adding the respective energies: $E_{net} = E^{up}_{short} + E^{up}_{long} - E^{down}_{short} - E^{down}_{long}$. In addition, the Albedo of the earth's surface defined as the ratio of outgoing to incoming solar radiation can be obtained with the instrument as well: $Albedo = E^{downt}_{short} / E^{up}_{short}$.

Calibration and instrument checks at the factory are recommended every two years according to the manufacturer.

Photosynthetic active radiation Delta-T BF5

With the Sunshine Sensor BF5 from Delta-T (www.delta-t.co.uk), total (in the sense of direct plus diffuse) solar radiation, diffuse radiation and the sunshine state is measured as photosynthetic active radiation (PAR) of the solar spectrum, i.e. from 400-700 nm. To distinguish between direct and diffuse radiation, a set of seven photodiodes (PD) is arranged under a patterned hemispherical dome with 50% black bands such that at any position of the sun in the sky at least one photodiode is completely in the shade and at least one is fully exposed to direct sunlight. This design eliminates the necessity of frequent alignment of the shading parts to the position of the sun. The diffuse radiation is then given by $PAR_{diffuse} = 2 \cdot PD_{\min}$ and the direct by $PAR_{direct} = PD_{\max} - PD_{\min}$. The instrument reports $PAR_{diffuse}$, $PAR_{total} = PAR_{diffuse} + PAR_{direct}$ and sunshine state. The latter one indicates sunshine if

$PAR_{total} / PAR_{diffuse} > 1.25$ and $PAR_{total} > 50\ \mu mol \cdot m^{-2} \cdot s^{-1}$.

Meteorological sensors

Weather transmitter WXT 510 from Vaisala

A WXT510 weather transmitter from Vaisala (www.vaisala.com) records simultaneously the six weather parameters temperature, pressure, relative humidity, precipitation and horizontal wind speed and direction.

The wind data measurements utilise three equally spaced ultrasonic transducers that determine the wind speed and direction from the time it takes for ultrasound to travel from one transducer to the two others. The precipitation is measured with a piezoelectrical sensor that detects the impact of individual raindrops and thus infers the accumulated rainfall. For the pressure, temperature and humidity measurements, separate sensors employing high precision RC oscillators are used.

Soil instruments

Soil heat flux sensors HFP01 from Hukseflux

A set of 5 thermal sensors HFP01SC from Hukseflux (www.hukseflux.com) have been buried a few centimetres underground in the undisturbed soil around the tower to obtain a good spatial averaging of the soil heat flux. The determination of the heat flux is based on measuring the temperature difference of two sides of a plate that is exposed to a heat flow using a number of thermocouples connected in series (see Fig. 51). Ignoring possible errors, the temperature difference between the hot and cold side of the sensor is proportional to the heat flow. As the thermocouples provide a voltage proportional to the temperature, the voltage output of the sensor is proportional to the heat flow across the sensor.

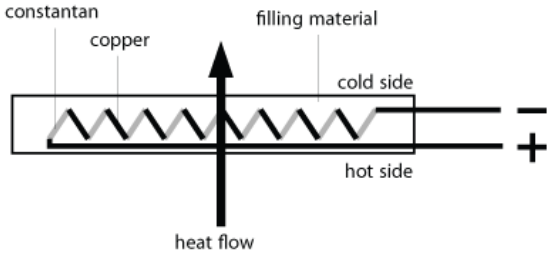

Fig. 51: Sketch of a soil heat flux sensor (drawing from www.wikipedia.org)

Soil water content vertical profile with TRIME-TDR from IMKO

Profile measurements of soil water content are performed using the TRIME-TDR (Time domain Reflectometry with Intelligent MicroElements with) from IMKO (www.imko.de). Based on Time-Domain-Reflectometry, the sensor generates high frequency electromagnetic pulses that propagate along a wave guide and reflected back into the sensor. Depending on the dielectric constant of the material surrounding the waveguide, the round trip time of the hf-pulses varies between some tens and thousand picoseconds. As the dielectric constant of soil and thus the round trip time strongly depends on the soil moisture content, measuring this time gives the water content of the soil surrounding the sensor. Burying several sensors at depths of 10, 30, 50, 120 cm below ground provides the soil humidity profile.

Soil temperature profile with Th3-v probe from UMS

For the measurement of soil temperatures at different depths, a Th3-v probe from UMS (www.ums-muc.de) is used. This probe features a convenient set of 6 temperature probes in a profile system buried at 5, 10, 20, 30, 50 and 100 cm below ground.

Ground water level Micro-Diver DI6xxx from SWS

The ground water level is monitored with Micro-Divers from Schlumberger Water Services (www.swstechnology.com). The device is placed in a water filled hole, 1 m below ground, and logs autonomously the pressure. Combining the measurement with the barometric pressure at the site gives the height of the water column above the sensor. Together with the known sensor depth below ground, the water table height can be easily calculated (see also **Error! Reference source not found.**32):

$$WL = TOC - CL - WC \text{ with } WC = 9806.65 \cdot \left(p_{Diver} - p_{baro}\right) / \rho \cdot g$$

With g = 9.81 m/s^2, ρ= 1.00 kg/m^3

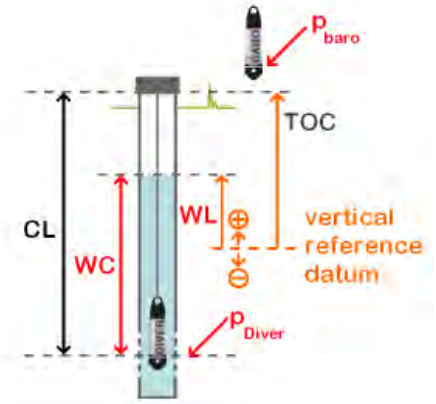

Fig. 32: Principle of water level calculation using the Diver (sketch from www.swstechnology.com). CL: cable length, TOC: top of container, WC: water column, WL: water level relative to a reference, p: pressure.

An automated dynamic chamber system for soil NO & NO_2 fluxes from ACU

During 2012, an automated dynamic chamber system to measure NO & NO_2 fluxes from the soil, based on Butterbach-Bahl et al., 1997, has been constructed at the JRC and subsequently deployed at the ABC-IS forest flux site (see Fig. 53). The setup consists of 5 replicate chambers measuring soil fluxes and one chamber that is closed to the ground and thus serves as a measurement blank. The analysers, pumps, control and data acquisition systems are installed in a small, air-conditioned trailer.

Fig. 53: Chamber system to measure NO & NO_2 fluxes from soil at the ABC-IS forest flux site.

The description of the system in a nutshell is the following: During a measurement cycle, the lids of one chamber are closed and that chamber is flushed with approx. 55 l/min for 6 minutes. At the same time, the concentrations of NO, NO_2 are measured with a Thermo Scientific 42C analyser at the outflowing air of chamber. The values of the first 3 minutes of each 6 minutes cycle are always discarded to allow for flushing and stabilization of the system. To account for concentration changes due to the reaction NO + O_3 = NO_2 + O_2 in the chamber and sampling lines, the concentration of O_3 is measured as well with a Thermo Scientific 49C analyser. In addition, the temperature and relative humidity in the chamber are recorded. Combining the measured concentrations, temperature, air flow and chamber size, raw soil fluxes of NO and NO_2 are calculated. In order to take chamber and sampling artefacts into account, the blank chamber, whose bottom part is closed to the ground, is measured in the same way before and after each soil chamber and the flux values calculated from that blank chamber are subtracted from the raw soil fluxes.

Flux data processing

Data evaluation for flux data is done using the free EdiRe software package developed at the micrometeorology group from the University of Edinburgh.

(www.geos.ed.ac.uk/abs/research/micromet/EdiRe/). As input data, EdiRe uses the 30 min raw flux data files in the binary *.slt format plus 30 minute averaged pressure, temperature and relative humidity data in ASCII format. As time convention, the start of the measurement period has to be assigned to the input data, the middle of the measurement period is assigned to the output data.

The main processing steps used within EdiRe to arrive at final, 30 minute averaged flux data that are corrected for various effects are the following:

Table 12: Processing steps for flux calculations using the EdiRe Software package.

EdiRe Process	**brief description**
Preprocessed Files	data from input file, gas concentrations as molar densities
Extract	all high speed data
Despike	all high speed data
Linear	conversion of raw data from voltages into physical variables
1 chn statistics	averages of 3D wind, sonic temperature and gas concentration
Gas conversion	conversion of molar densities to molar fraction
Filter – detrend	linear detrending of gas concentrations
Wind direction	align with geographic direction
Rotation coefficients	perform 3D coordinate rotation
Cross Correlate	gas concentrations with vertical wind speed
Remove Lag	remove time lag between anemometer and gas analyser
Friction Velocity	calculate u*
Sensible heat flux coefficient	
Latent heat of evaporation	
2 chn statistics	calculate covariances, i.e. uncorrected fluxes
Sonic T - heat flux correction	
Stability - Monin Obhukov	calculate z/L stability parameter
Frequency response	calculate high frequency correction for all fluxes
Webb correction	calculate water density fluctuation correction for all fluxes
Stationarity	perform stationarity test
Integral Turbulence	calculate integral turbulence
Cospectra	calculate co-spectra for all fluxes
Storage	calculate storage term
User defined	determine quality flag (0,1,2) for all flux data according to Carboeurope methodology

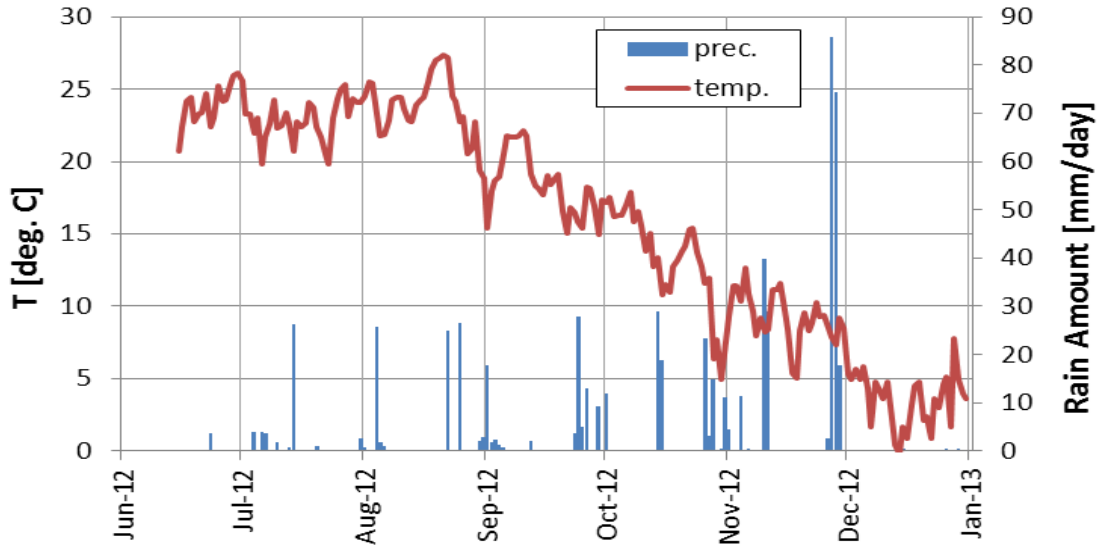

Fig. 54: Daily average of the air temperature (red) and daily sum of the precipitation (blue) measured at the tower top.

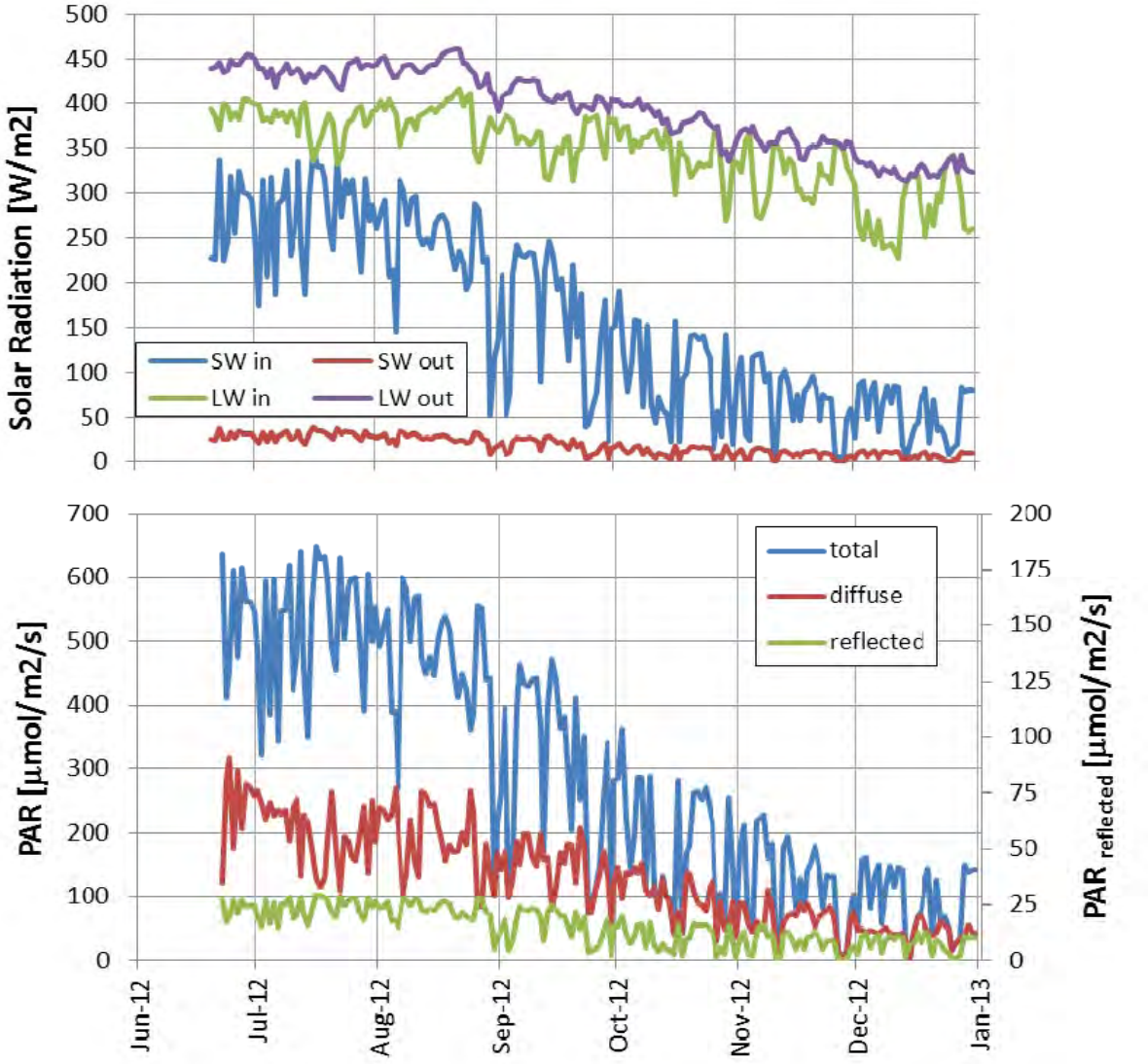

Fig. 56: Solar radiation parameters measured with the net radiometer (top) and the sensor for Photosynthetic Active Radiation (bottom).

Results of the year 2012

As the ABC-IS Forest Flux Station is on its way to be set-up as a long-term monitoring station, measurements with different sensors have started at different dates during the course of 2012. Therefore also the timelines of the different measurements presented below begin at different dates. For the same reason, annual statistics and analysis will be presented only in future reports.

Meteorology

Daily averages of the air temperature and daily sums of the precipitation measure at the top of the Forest Flux Tower in Ispra are shown in Fig. 54.

The wind measurements obtained with the 3D sonic anemometer indicate that north north-west is the predominant wind direction. Fig. 55 shows in red the frequency distribution of the wind directions for wind speeds > 0.5 m/s; the blue line indicates the average wind speeds per directional bin. Time periods with air coming from either east or west occur only during very few occasions and wind from the south is rather infrequent as well.

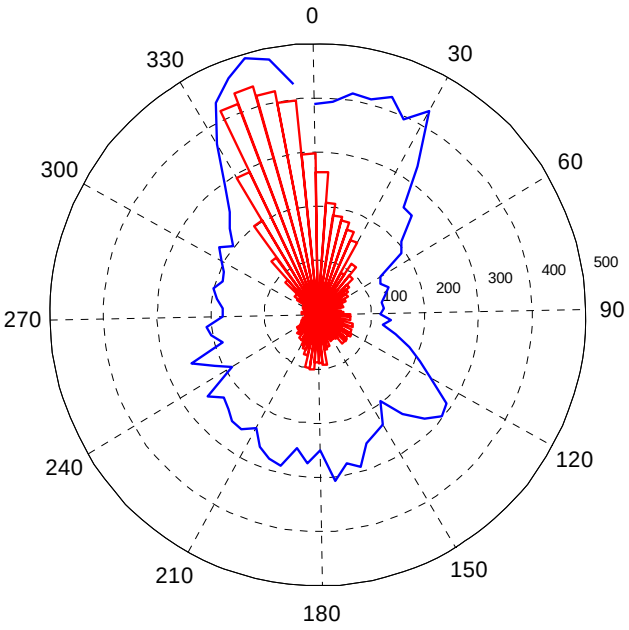

Fig. 55: Wind rose for 30 min. averages of wind measurements with wind speeds >0.5 m/s. Red: wind directions, blue: average wind speeds per direction interval in a.u.

Radiation

Different parameters regarding solar radiation are plotted in Fig. 56. On top, the daily averages of short & long wavelength incoming & outgoing radiation are plotted as measured with the CNR1 net radiometer above the forest canopy at 36 m. The surface albedo, i.e. the ratio between SWout and SWin (305 – 2800 nm) averages to approximately 0.11 for the summer period and 0.12 for the winter period of the measurement. On the bottom part of Fig. 56, the photosynthetic active radiation (PAR) part of the solar spectrum (approx. 400 – 700 nm) is shown as total & diffuse incoming (left axis) and reflected radiation (right axis). During the summer, i.e. vegetative period, the surface albedo at this part of the solar spectrum is approximately 0.04 and increases in winter up to 0.08 as the deciduous trees in the forest lose their leaves.

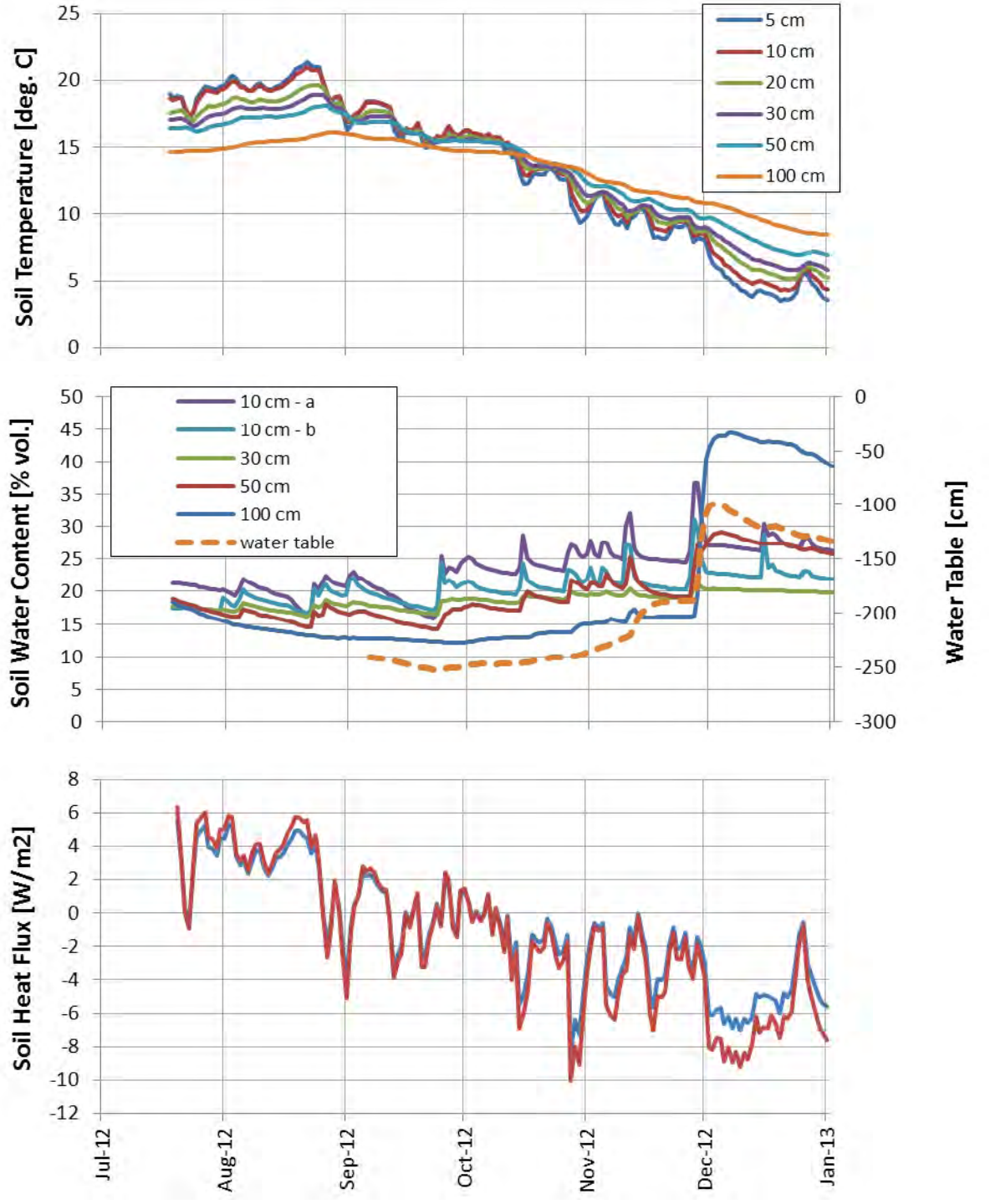

Fig. 57: *Timeline of daily averages of soil parameters measured at the ABC-IS forest flux site from top to bottom: soil temperature profile, soil water content profile plus water table below surface and soil heat flux at two replicates (10 cm below surface).*

Soil parameters

The soil parameters measured at the ABC-IS Forest Flux Station are shown in the three plots of Fig. 57. In the first one, daily temperature averages at 6 different depths are plotted. As expected, soil temperature decreases with measurement depth in summer. In the middle of October occurs the tipping period when the temperature profile is reversed.

The plot in the middle depicts the soil water content (SWC) at different depths (left axis) and the water table (right). Jumps in the daily averages of the SWC occur during precipitation events and thereafter the soil starts to dry again. The differences seen at the surface replicates at 10 cm give a glimpse on the heterogeneity of the soil and the forest environment. Due to little rainfall during summer 2012, the water table went down to 250 cm below the forest surface.

In the bottom plot of Fig. 57, the soil heat flux measured at two locations is presented. Obviously during summer time the soil heats up due to solar irradiation and in winter time it cools down. Again, the differences of the heat fluxes at the two sensor positions are due to different environmental situations at the two locations, i.e. different irradiance by the sunlight and to a lesser extend soil variation.

Fig. 58 illustrates fluxes of NO, NO_2 and O_3 from the soil as measured with the automated dynamic chamber system. Fluxes from the 5 replicate chambers are plotted on the left axis as hourly averages. During the entire measurement period the soil is a source for NO (dark blue) and for most times a sink for NO_2 and O_3 (red and green, respectively). The soil water content (SWC, yellow) and the soil temperature (light blue) are included as potential drivers for the release of NO and uptake of NO_2 by the soil.

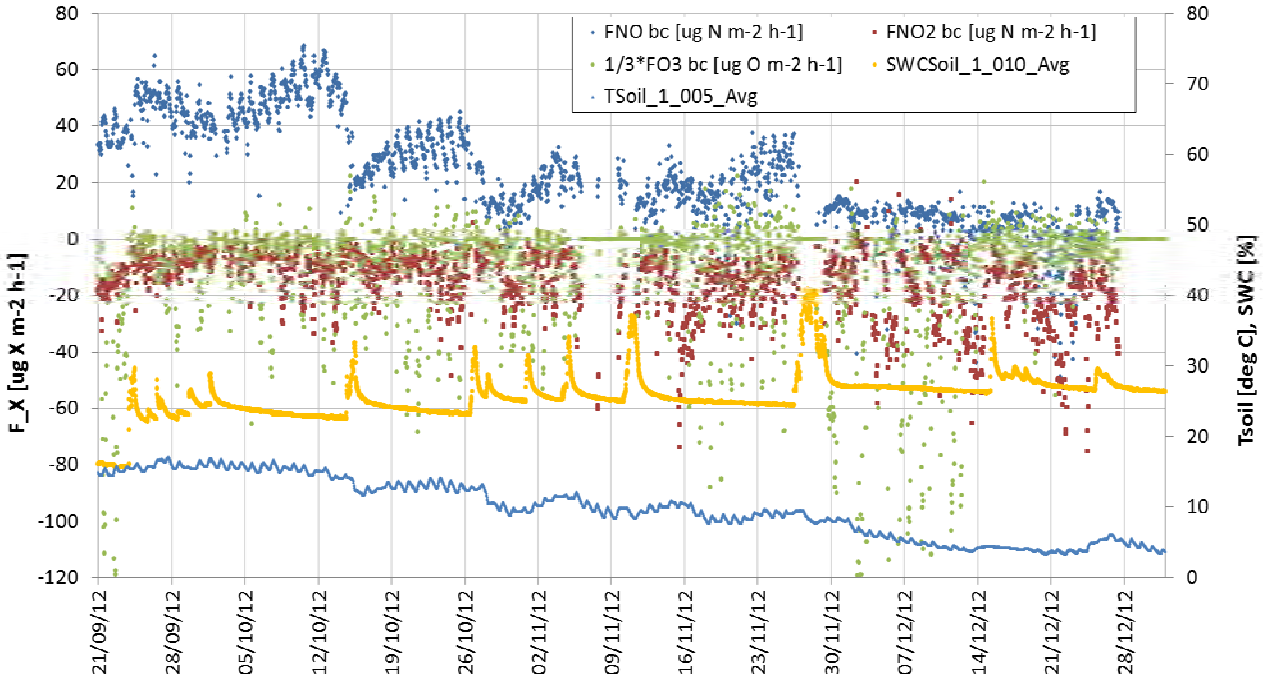

Fig. 58*: Hourly averages of soil fluxes measured with the 5 dynamic soil chambers.*

Tab. 11: Averages over all sampling points for soil respiration measurements plus standard variation.

measurement date	soil respiration CO_2 [g / m2 / h]	variability (standard deviation) CO_2 [g / m2 / h]
12/01/2012	0.21	0.28
29/02/2012	0.17	0.09
12/04/2012	0.33	0.23
15/06/2012	0.91	0.53
20/07/2012	0.71	0.40
31/08/2012	0.60	0.30
05/10/2012	0.79	0.50

Soil NO emission clearly go down as soil temperature decreases and the pattern changes as well significantly during and after rain events, indicated by a steep increase of the SWC. During rain events, the system was not measuring soil fluxes in order not to dry the soil covered by the chamber.

During the course of 2012, 7 measurements of soil respiration have been done in the forest. To obtain a good spatial representation, soil respiration at 25-34 locations inside the ABC-IS forest has been measured and averaged on each measurement date. The results are reported in Tab. 11, including the standard variation as an indication for the variability among the measurement locations. As expected, soil respiration is highest during the warm summer months and reduced during winter time.

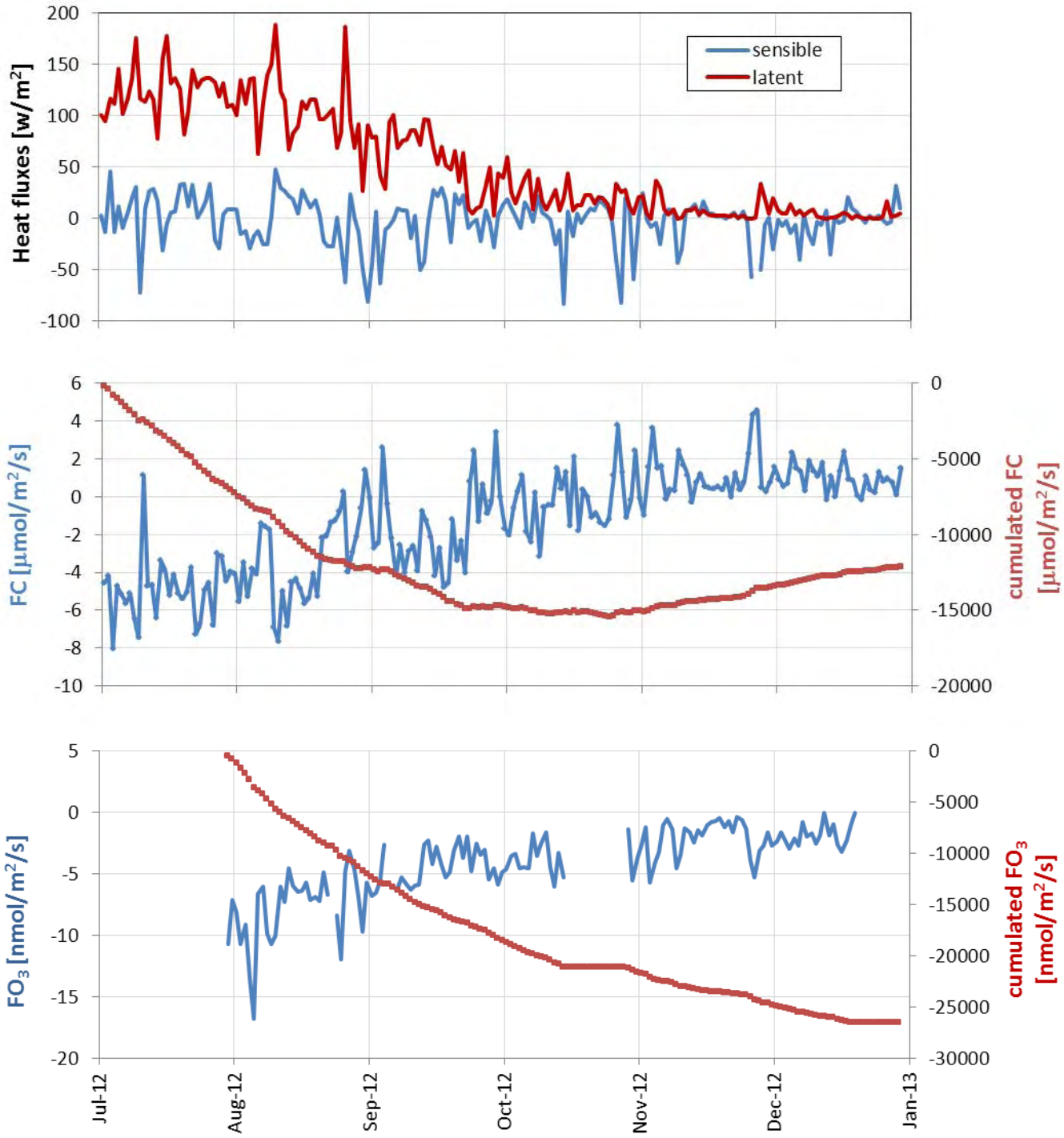

Fig. 59: Timelines of daily averages of fluxes calculated from data measured at the ABC-IS forest flux site, from top to bottom: sensible & latent heat flux, CO_2 flux & cumulated values, and ozone flux & cumulated values.

Eddy covariance fluxes

The timelines of 30 minute averages of CO_2, energy and O_3 fluxes calculated from measured data using EdiRe and following the Carboeurope methodology (no correction for storage) are shown in Fig. 59: from top to bottom H – sensible heat flux, LE – latent heat flux, FC – CO_2 flux plus its cumulated value, FO_3 – O_3 flux plus its cumulated value.

From the FC plot and the cumulated values one clearly observes the 3 periods when (1) the forest acts as a CO_2 sink, i.e. until early October, (2) when photosynthesis and ecosystem respiration are approximately balanced, early October until early November, and (3) from then the respiration dominates, turning the forest into a CO_2 source for the rest of the year. The latent heat fluxes LE and to a lesser extend the sensible heat flux H show a seasonal behaviour as well with higher values during the summer period and lower during winter.

O_3 fluxes were measured since August and indicate that the forest is a significant sink for ozone during the entire measurement period. From early October, the O_3 flux values become lower. This coincides with a lower ozone concentration in the atmosphere compared to the situation in the summer, the reduction of air uptake by the trees and the autumnal leaf loss of the trees.

An assessment of the applicability of the eddy covariance (EC) method to measure fluxes at any time is given by the stationarity and integral turbulence tests. They are combined in the Carboeurope methodology into a quality flag (QF) for every data point. A value of 0 indicates strong turbulence and good stationarity, giving reliable EC flux values. A QF = 1 indicates acceptable quality and flux data with QF = 2 are unreliable and thus should not be used in further calculations. For the measurements at the ABC-IS station, the distribution of quality flags for all flux data are given in Table 114. The table shows that 60 – 68 % of the data depending on the flux type are usable for further data evaluation and interpretation.

Table 14: Total number of flux data points and percentage of data points with quality flags according to the Carboeurope methodology.

	H [%]	LE [%]	FC [%]	FO_3 [%]
data points	8809	8809	8809	7366
QF = 0	12	9	10	10
QF = 1	55	51	52	53
QF = 2	33	40	38	37


Fig. 60: left: Trailer mast old pinus pinaster site that holds the sonic anemometer and Infra Red Gas Analyser (IRGA) used for flux measurements (in retracted configuration for service). Right: newly erected tower at the pinus pinea site that will hold the measurement equipment.

Atmosphere – Biosphere flux monitoring at San Rossore

Location and site description

The measurement site 'San Rossore' (43°43.68'N, 10°17.04E, 6 m a.s.l.), operated by the Air and Climate Unit, is located in the Parco San Rossore (www.parcosanrossore.org), approximately 9 km west of Pisa and 500 m east of the seashore in a Mediterranean forest ecosystem (see Fig. 60). The Climate Change and Air Quality Unit operates the site in the Parco San Rossore site since 1999.

The measurement site is situated in an almost flat area with a morphology characterized by the presence of sandy dunes. The vegetation in the direct vicinity is a pinewood established in 1953 following artificial seeding and it is dominated by the evergreen tree Pinus pinaster with sparse trees of Pinus pinea and Quercus ilex. The average canopy height is approximately 18 m. The understorey vegetation is confined to the forest edges and canopy gaps.

The area has a Mediterranean – type climate within the sub-humid zone, with a mean annual rainfall of 876 mm yr^{-1} and a range of 534 – 1270 mm for the period 1980 – 2005. The long term data were obtained from a meteorological station located at a distance of approximately 10 km and managed by the Regional Hydrologic Service of Tuscany. Rain falls mainly during autumn and winter with about 50% occurring between September and November, while the driest months are July and August. The average annual temperature is approximately 15 °C with the average temperature of the coldest month (January) being 7 °C and that one of the warmest month (August) being 25 °C. The wind regime is characterized by a sea – land breeze circulation, i.e. the air flows quite predictable from the west (sea) during day and from east (land) during night.

Starting in 2009, major clear cuts of the forest in the vicinity of the measurement site were initiated as a response of the park management to the infection of the Pinus pinaster with 'Matsucoccus feytaudi' (see Fig. 61). As it is obvious from the satellite picture, the cuts destroy the homogeneity of the canopy around the measurement site (red circle). This inhomogeneity of the ecosystem in the fetch of the flux tower now renders eddy covariance measurements of ecosystem fluxes almost meaningless. It has therefore been decided to move to a new location within the park that is not threatened by the 'Matsucoccus feytaudi' and has a homogeneous canopy suitable for micrometeorological measurements. The new site has been identified in 2011 (blue circle in Fig. 62), approximately 700 m away and within a quite homogenous stand of Pinus pinea. The new tower (see Fig. 59) for eddy covariance measurements of fluxes has been erected in autumn 2012 and equipping the site with instrumentation has started as well. First test measurements of a few parameters run since end of November 2012. After a period of overlapping meteorological measurements performed in parallel at the old and new sites, shutting down and dismantling of the old site has started in the first half of 2013.

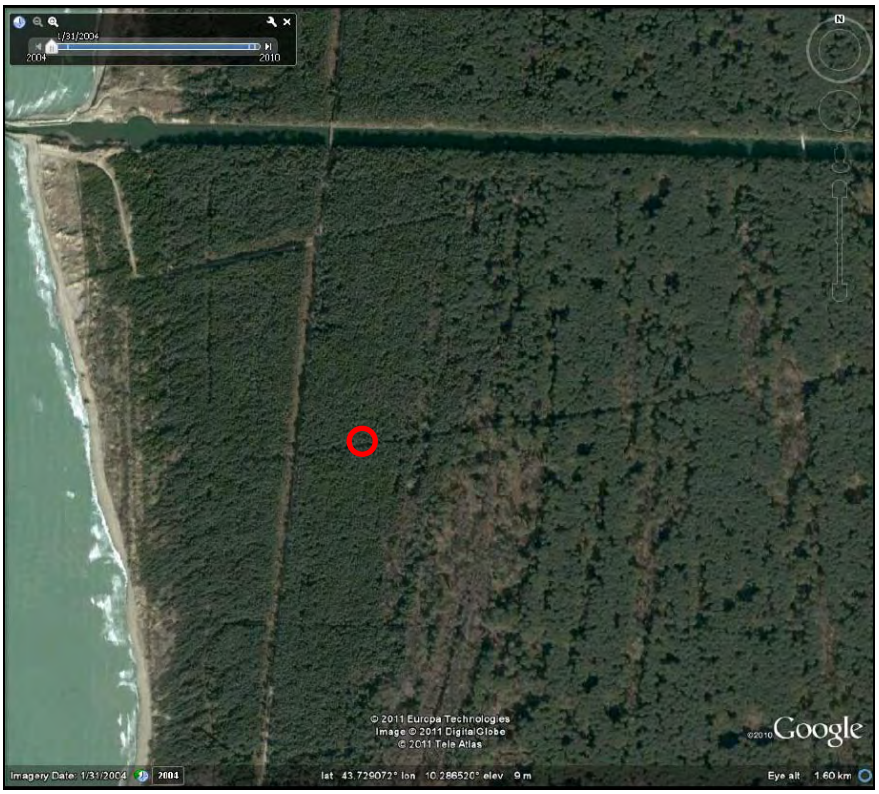

Fig. 61: Location of the measurement site in the Parco San Rossore (red circle). The picture from Google Earth taken on 31.01.2004 shows a homogenous canopy around the flux tower.

Fig. 62: The picture of the vicinity around the measurement site from Google Earth taken on 04.08.2011 visualizes the severe cutting of tries due to infection with 'Matsucoccus feytaudi'. The blue circle shows the location of the new tower at ~700 m distance.

With regards to data reporting as in the previous years, quality checked data for 2012 have been submitted for the last time under the station name IT-SRo to the Fluxnet database at the European Fluxes Database Cluster at www.europe-fluxdata.eu (ex IMECC Terrestrial Carbon Data Centre).

Monitoring program

The new measurement site in the Parco San Rossore will also be a level 2 Ecosystem Station within ICOS. For a brief description of ICOS and the obligatory parameters to be measured, please refer to the respective chapter in the description of the ABC-IS Forest Flux Station, Table 10 on page 70.

Despite the unfortunate circumstances of tree cutting activities described in the preceding chapter, the measurement program at the San Rossore site continued also in 2012 for the last year of measurements at that site. The main parameters measured are summarized in Table 15. In addition, sensors already installed for sap flow and stem temperature measurements continued to record data.

Table 15: parameters measured during 2012

FLUXES	CO_2, latent heat, sensible heat
METEOROLOGY	3D wind speed, temperature, relative humidity, pressure, precipitation
RADIATION	short wave incoming, direct & diffuse photosynthetic active radiation
SOIL	temperature profile, water content profile, heat flux, water table height
BIOLOGICAL	litter fall

In the same way as it is done at the ABC-IS Forest Flux Station, fluxes of CO_2, H_2O and sensible heat were measured with eddy covariance technique and evaluated using the EdiRe software package from the University of Edinburgh (www.geos.ed.ac.uk/abs/research/micromet). The ancillary parameters (meteorology, radiation and soil) were obtained with respective sensors and the data quality checked for instrument malfunctioning, obvious outliers and consistency. Daily averages of the different parameters measured during the course of 2012 are presented in the following section as an overview.

The measurement techniques

Infrastructural:

Sensor location

The instruments for eddy covariance flux system, i.e. sonic anemometer and fast gas analyser, are mounted on the top of a temporary trailer mast with a height of 22 m. Soil parameters are measured at close vicinity to the trailer on the forest ground. Radiation and meteorological sensors are placed on top of a scaffold tower structure at a distance of approximately 800 m from the main measurement site.

Data acquisition

Eddy covariance flux data are stored with high frequency, i.e. 10 Hz, as chunks of 30 minutes on a local laptop connected to the sonic anemometer. Data from all other sensors are read every 10 s by a DL2e data logger from Delta-T Devices (www.delta-t.co.uk) which saves 30 minute averages of the acquired data.

For eddy covariance flux data, the start time of every 30 minutes measurement period is saved as the reference time, whereas for all other data, the end of the 30 minutes measuring period is used. The time reference used for all San Rossore measurements is local time, not corrected for summer time.

Ecosystem fluxes:

Sonic Anemometer for 3D wind direction Gill R3-50

Sonic anemometers determine the three dimensional wind vectors at high frequency using the speed of sound. As the Gill R3-50 (www.gill.co.uk) is an instrument very similar to the Gill HS used at the ABC-IS Forest Flux Station, please refer to the instrument description on page 75.

Fast infrared gas analyser for CO_2 & H_2O concentration (IRGA) LI-7500 A

For the determination of CO_2 and H_2O fluxes with the eddy covariance technique, fast analysers (10 to 20 Hertz) for concentration measurements of the gases of interest are obligatory. At San Rossore, a LI-7500A Open Path CO_2/ H_2O Analyser from LI-COR (www.licor.com) has been installed.

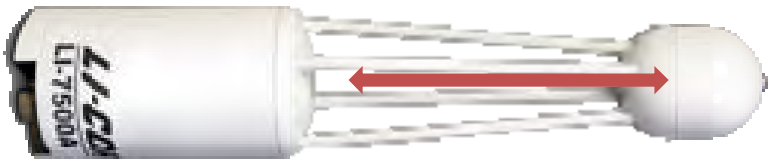

Fig.63: LI-7500A analyser head (from www.licor.com), arrow indicates sampling volume

The LI-7500A is a high performance, non-dispersive, open path infrared CO_2/H_2O analyser based on the infrared absorption of CO_2 and H_2O at ambient conditions that provides concentration measurements at a frequency of up to 20 Hertz. In the sampling volume (see figure Fig.), light from the infrared source is absorbed at characteristic wavelengths for CO_2 and H_2O. This specific absorption is a function of the gas concentration in the sampling volume. Using the absorption measurements at the CO_2 & H_2O wavelengths, at a non-absorbing wavelength plus calibration factors and measured temperature and pressure, the LI-7500A provides number-, mass densities or mole fraction of the two gases.

Zero and span checks and calibrations are done regularly using zero gas from a cylinder plus a dew point generator (LI-COR 610) and a CO_2 standard from a cylinder.

Radiation instruments

Short wavelength incoming radiation Li-Cor Li-200 Pyranometer

The incoming short wavelength solar radiation is measured with a Li-200 Pyranometer from Li-Cor (www.licor.com). It is a low price device compared to first class thermopile-type pyranometers such as the CM11 used et the EMEP station. The LI-200 features a silicon photovoltaic detector mounted in a fully cosine-corrected miniature head. Current output, which is directly proportional to solar radiation, is calibrated against an Eppley Precision Spectral Pyranometer (PSP) under natural daylight conditions in units of watts per square meter (W m-2). Under most conditions of natural daylight, the deviation of the Li-200 compared to the reference instrument is <5%.

Photosynthetic active radiation Delta-T BF3

With the Sunshine Sensor BF3 from Delta-T (www.delta-t.co.uk), total (in the sense of direct plus diffuse) solar radiation, diffuse radiation and the sunshine state is measured as photosynthetic active radiation (PAR) of the solar spectrum, i.e. from 400-700 nm. The BF3 is the predecessor of the BF5 used in Ispra, therefore please refer to page 75 for further details.

Soil instruments

Soil heat flux sensors Hukseflux HFP01

A set of 5 thermal sensors HFP01SC from Hukseflux (www.hukseflux.com) have been buried a few centimetres underground in the undisturbed soil around the tower to obtain a good spatial averaging of the soil heat flux (see page 77 for description).

Soil water content vertical profile with TRIME-TDR from IMKO

Profile measurements of soil water content are performed using the TRIME-TDR (Time domain Reflectometry with Intelligent MicroElements with) from IMKO (www.imko.de). Please refer to the instrument description for ABC-IS on page 77 for details. In San Rossore the sensors are buried at depths of 10, 50, 120 cm below ground to provide the soil humidity profile.

Soil temperature profile with PT-1000

For the measurement of the soil temperature profile, three PT-1000 temperature sensors with 3 cable wiring setup are buried at 3 cm, 15 cm and 50 cm below ground.

Ground water level Micro-Diver DI6xxx from SWS

The ground water level is monitored with Micro-Divers from Schlumberger Water Services (www.swstechnology.com). As the same device is used at ABC-IS in Ispra, please refer to page 77-78 for details.

Flux data processing

The evaluation of flux data is performed in the same way as at the ABC-IS Forest Flux Station in Ispra. Therefore please refer to page 78-79 for a detailed description. The only difference, due to the use of an open path sensor in San Rossore in contrast to the closed path sensor in Ispra in Ispra, is a so-called Webb-correction of the CO_2 and H_2O flux data. This is needed because of high-frequency pressure fluctuations in the sampling volume of the open-path sensor.

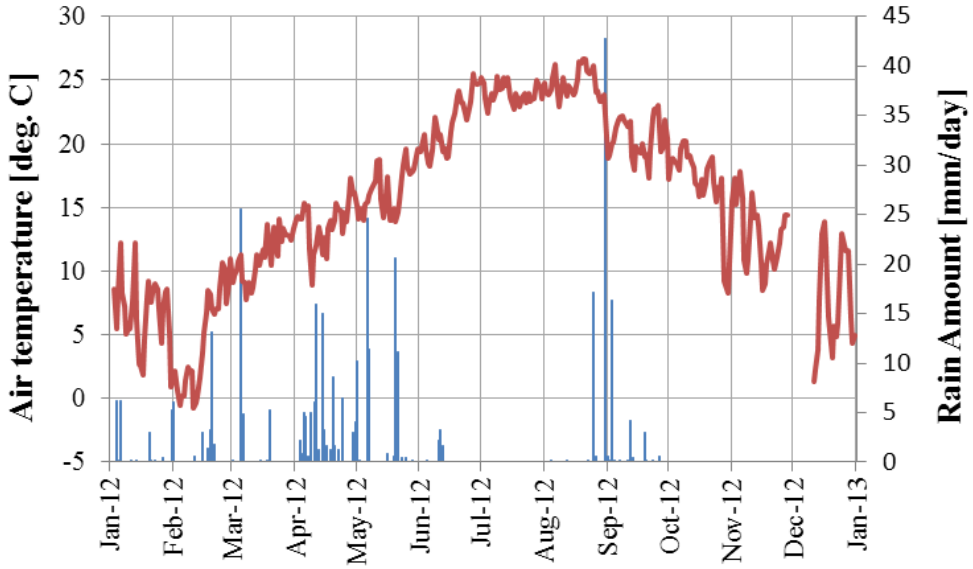

Fig. 64: Daily averages of air temperature (red) and daily sum of precipitation (blue) as measured in the Parco San Rossore. Gaps in the temperature curve show periods with missing data.

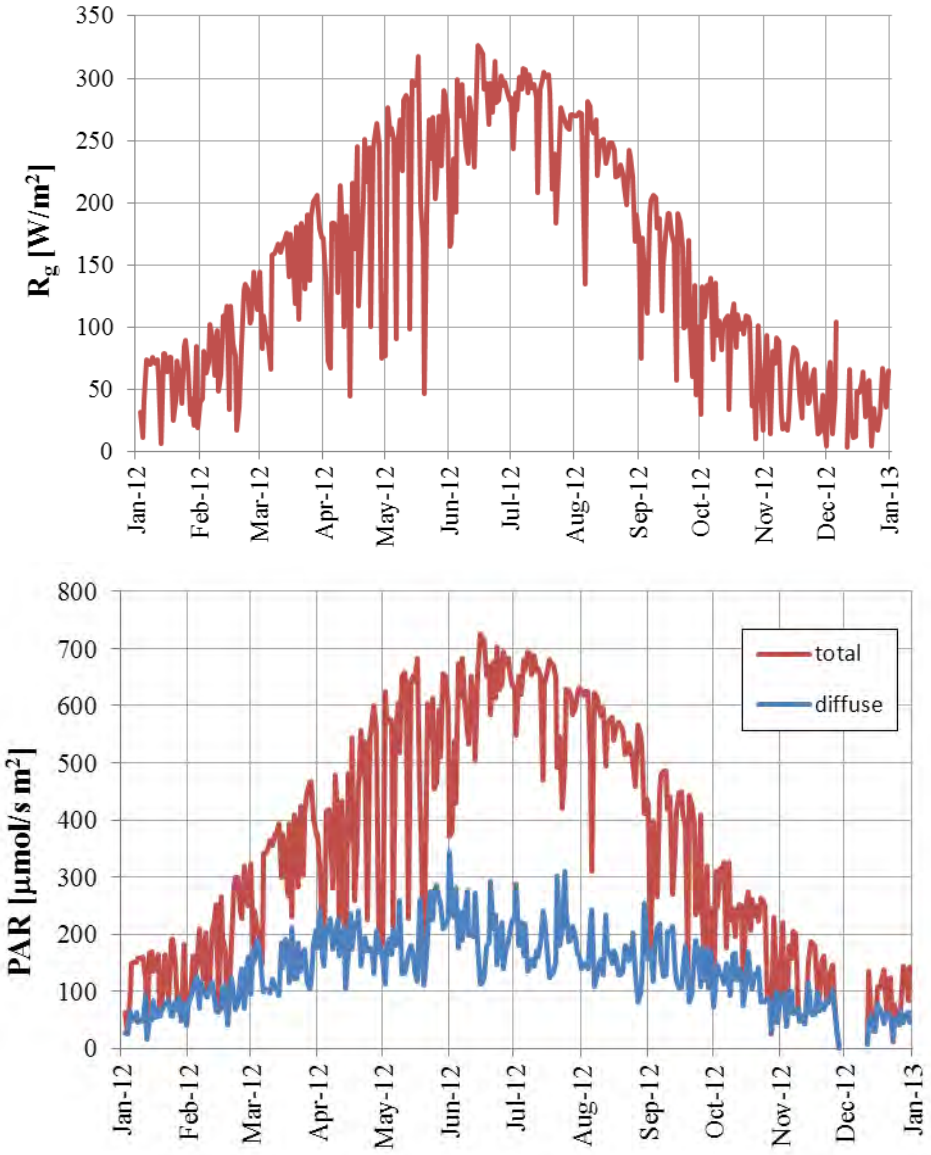

Fig. 66: *Daily averages of short wave incoming radiation (top) and incoming photosynthetic active radiation (bottom).*

Results of the year 2012

Meteorology

Daily averages for the annual cycle of air temperature and precipitation are shown in Fig. 64. Taking the data gap in December into consideration, the annual mean temperature for 2012 is an upper limit and results in 15.3° C. The total measured rainfall was 350 mm. Due to a severe sensor failure, the rain sensor stopped working properly on 27.9.2012 and thus the measure amount is only a fraction of the total annual rainfall. The mean annual rainfall for San Rossore is 876 mm yr^{-1}.

The predominant sea – land breeze wind circulation can be seen from the statistical evaluation of the 3D wind direction measurements and is shown in Fig. 65 The red plot shows the frequency distribution of the wind directions for winds speed > 0.5 m/s; the blue line indicates the average wind speeds per directional bin.

Radiation

In Figure 66, the annual cycle of short wave incoming radiation is shown on the top graph, the photosynthetic active radiation (PAR) in terms of total and diffuse contribution on the bottom.

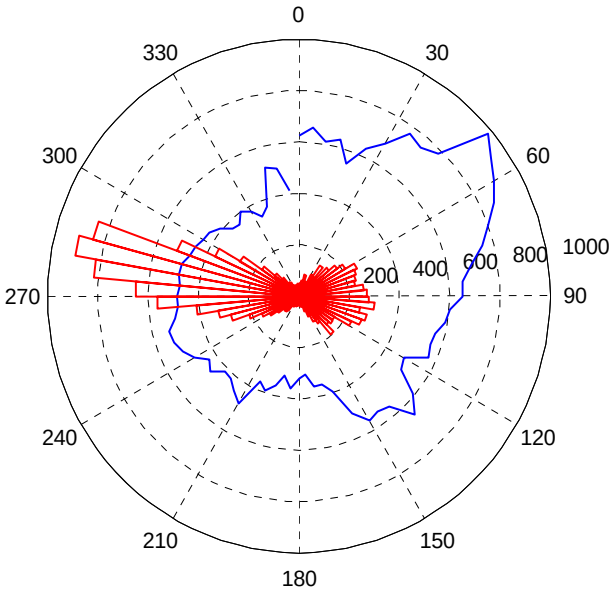

Fig. 65: Wind rose for 30 min. averages of wind measurements with wind speed >0.5 m/s. Red: wind directions, blue: average wind speeds per direction interval in au.

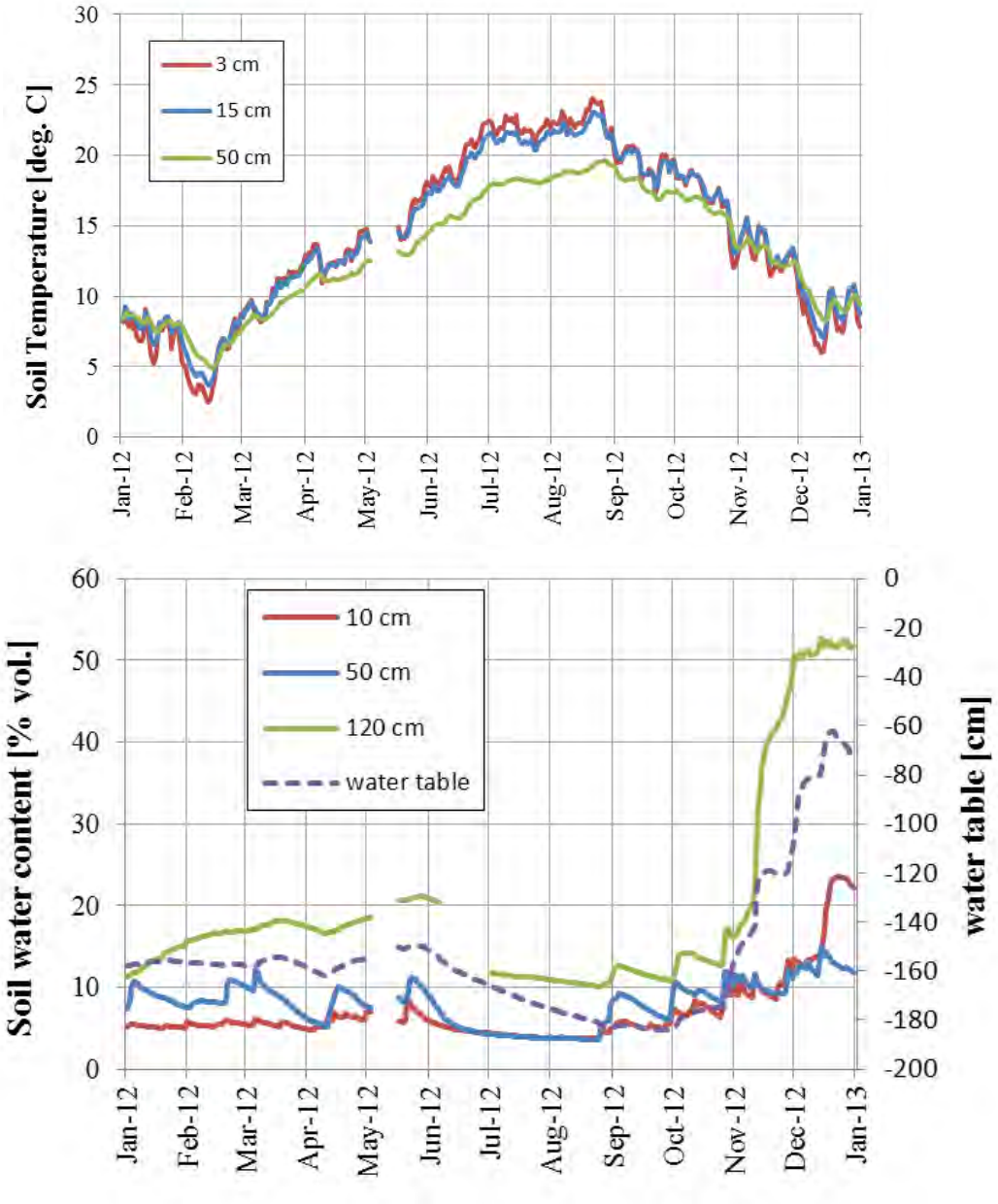

Fig. 67: Profiles of soil temperature (top) and soil water content plus water table (bottom) measured as daily averages.

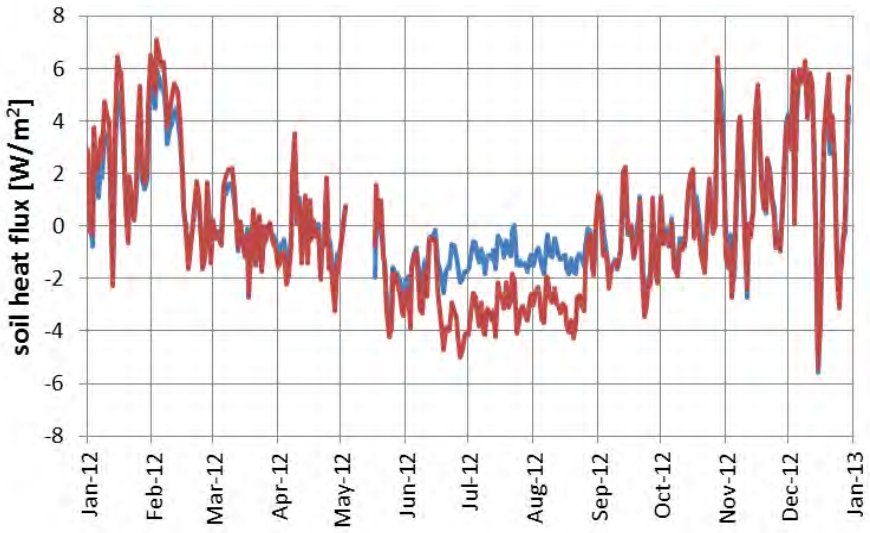

Fig. 68: Soil heat fluxes measured with two identical sensors located some meters apart.

Soil parameters

Soil parameters monitored in 2012 were the temperature at three different depths (3, 15 and 50 cm), soil water content profile (10, 50 and 120 cm) plus water table depths. Daily averages of these values are illustrated in Fig. 6767. As it was the case already in 2011, also 2012 continued to be a very dry year as indicated in the low soil water content at -120 cm and a low water table staying between -140 cm and -180 cm until middle of November 2012.

The soil heat flux measured with two identical sensors located a few meters apart in the forest soil is shown in Fig. 68. The differences between the two sensors originate from the different light intercept by the canopy at the two locations and the soil inhomogeneity.

Flux measurements

The daily averages of CO_2 and heat fluxes measured during 2012 are shown in Fig. 69 and Fig. 72, respectively. To obtain the eddy covariance flux data for the 30 minute measurement periods, the high frequency data from the LiCor 7500A open path CO_2 and H_2O analyser have been evaluated together with the anemometer data using the EdiRe software package from the University of Edinburgh. Using the Carboeurope quality classification for the 17568 flux data points for 2012, only 3% of the CO_2 fluxes are of good quality (class 0), 51% middle quality (class 1), 24% low quality (class 2) and 22% are missing due to instrument malfunctioning or rain conditions. The quality of flux measurements has deteriorated significantly compared to the past, e.g. 64% of the data points in 2011 were of good quality. As this quality classification is based on criteria derived from micrometeorological conditions, it is rather clear sign that the measurement site becomes unsuitable for eddy covariance flux measurements due the clear-cutting in the vicinity of the site.

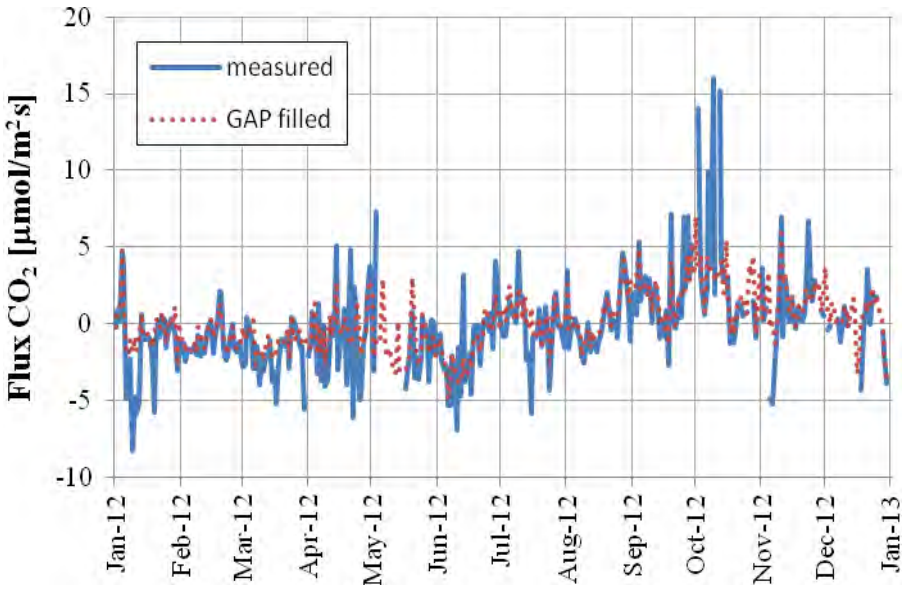

Fig. 69: Daily averages of measured (blue) and gap filled (red) CO_2 fluxes.

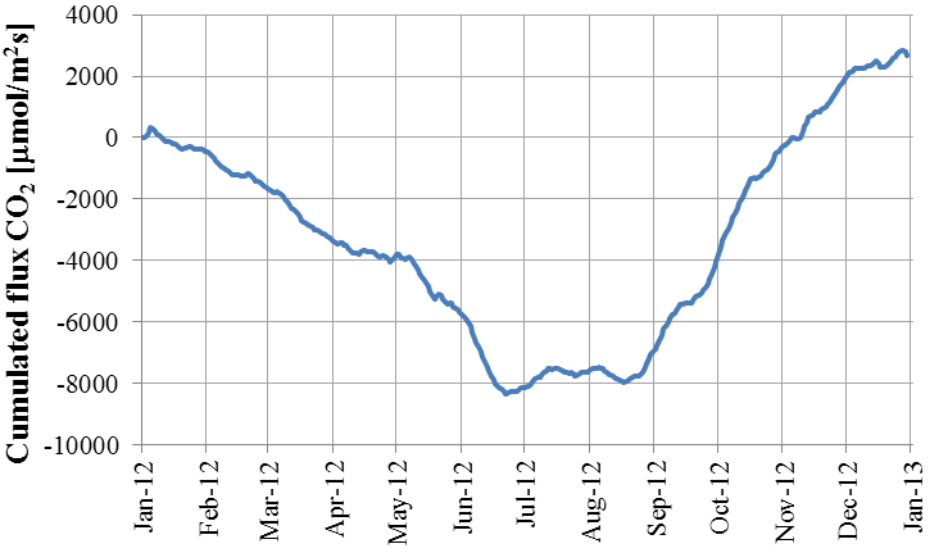

Fig. 70: Cumulated sum of 30 min averages of gap filled CO_2 fluxes.

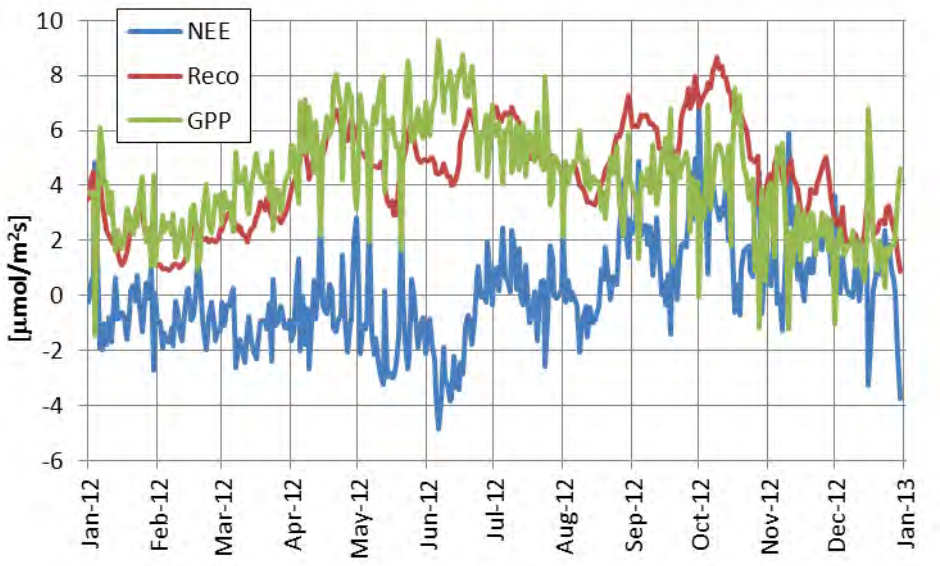

Fig. 71: daily averages of NEE, GPP and Reco for 2012.

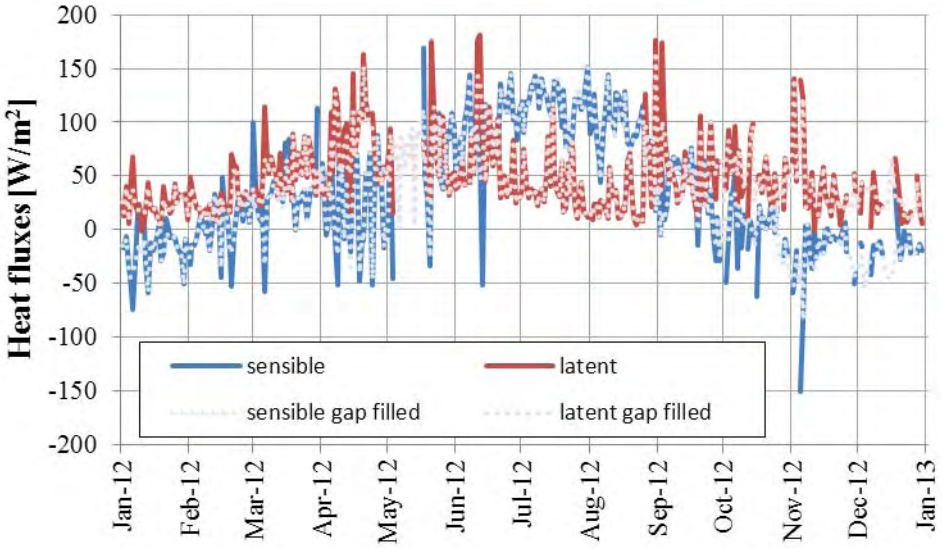

Fig. 72: Daily averages of latent (red) and sensible (blue) heat fluxes.

Gap filling of the dataset has been performed without u* filtering using the 'Eddy covariance gap-filling & flux-partitioning tool' online available at: www.bgc-jena.mpg.de/~MDIwork/eddyproc/ for missing and quality class 2 data. The cumulated sum of the gap filled 30 min. CO_2 fluxes is shown in Fig. 70. Using the flux partitioning module of the above mentioned online tool, the Net Ecosystem Exchange (NEE), i.e. the CO_2 flux measured, has been partitioned into Gross Primary Production (GPP) and Ecosystem Respiration (Reco) and plotted as daily averages in Fig. 71. Calculating the budget for 2012, NEE sums up to +54 g C m^{-2} $year^{-1}$ (-322 g C m^{-2} $year^{-1}$ in 2011), GPP to -1593 g C m^{-2} $year^{-1}$ (-1734 g C m^{-2} $year^{-1}$ in 2011) and Reco to 1646 g C m^{-2} $year^{-1}$ (1412 g C m^{-2} $year^{-1}$ in 2011).

Compared to the preceding years and also to 2011, the measurement site transformed from a sink for CO_2 to a source of CO_2, indicated by a positive NEE. Despite the deterioration of the quality of the eddy covariance flux measurements as mentioned in the previous paragraph, both the decrease in GPP and increase of Reco compared to e.g. 2011 are clearly result of the clear-cutting (see Fig. 61) around the measurement site.

Fig. 72 shows the latent (red) and sensible (blue) heat fluxes for 2012 as daily averages. The dry situation especially in summer can be seen here as well, the latent heat flux is much smaller than the sensible one.

Fig.73: Costa Magica and the cabin on Deck 14 with the JRC air monitoring station.

Air pollution monitoring from a cruise ship

Introduction

Measurements of air pollutants over the Western Mediterranean have been carried out regularly since the autumn of 2005 during spring, summer and autumn from a monitoring station placed in a cabin on cruise ships belonging to the fleet of the Italian cruise line Costa Crociere. The basis for this monitoring activity is a collaboration agreement between Costa Crociere and the JRC. The scope of this activity is to obtain information about the concentration levels of air pollutants in this area, to improve the understanding of their sources and to test the performance of air pollution chemical transport models. Further, as this is intended as a long term monitoring activity, it is also potentially useful for analysis of trends and changes related to introduction of new legislation. So far three scientific papers have been published based on the data obtained from this monitoring activity (Marmer et al. 2009, Velchev et al. 2011 and Schembari et al. 2012).

In order to obtain a dataset that allows us to observe year-to-year variations, the measurements have, as far as possible, been performed on ships that follow the same weekly route in the Western Mediterranean. This implies that the monitoring station occasionally must be moved from one Costa Crociere ship to another. In 2012 the intention was to continue to perform the measurements on Costa Concordia, which was going to follow the same route as it did in 2011. Thus part of the instrumentation was left on board of this ship and was there, when it grounded in January 2012. For this reason, the start of the measurements was seriously delayed, the measurement period in 2012 was very short (from August 6 to October 4) and only a reduced set of measurements were performed (only gaseous compounds were measured).

Measurement platform location

The measurements of air pollutants in 2012 were performed on the cruise ship Costa Magica, which was following a fixed weekly route in the Western Mediterranean (see e.g. Fig. 74).

Table 16. *Time schedule for Costa Concordia in 2011during the period of the measurements (August 6 – October 4)*

Day of the week	Harbour	Arrival	Departure
Monday	Savona	09:00	17:00
Tuesday	Barcelona	13:30	19:30
Wednesday	Palma	09:00	18:00
Thursday	*At sea*		
Friday	Malta	08:00	18:00
Saturday	Catania	08:00	14:00
Sunday	Naples	08:00	14:00

The route differed thus from the one followed by Costa Concordia the year before on two points: the Sicilian harbour was Catania instead of Palermo and the last harbour before Savona was Naples instead of Civitavecchia (see Fig. 74 and Table 16).

Ambient air was sampled from inlets placed at the top front of the ship (see Fig. 73) at appr. 50 m height a.s.l. In order to test if this sampling point was equivalent to the ideal sampling point at the very front of the bow of the ship, a series of measurements of ozone and particle size distributions were carried out in July 2005 by the beginning of this monitoring activity. The results showed excellent agreement between ozone concentrations measured at the front of the bow and at the top of the cabin on Deck 14. For the aerosols, the agreement was generally also very good, discrepancies were only found in harbours with strong local emission sources and in a situation with fog and thus strong stable layering of the atmosphere.

Instrumentation

On-line measurements

The automatic monitoring station on Costa Magica hosts the following measurement equipment

- Ozone Analyser (Model C49, Thermo Electron Instruments Inc., USA, S/N 0503110497),
- Trace level SO_2 Analyser (Model 43i-TLE, Thermo Electron Instruments Inc., S/N 0724324323)
- Trace level NOx-analyser (Model 42i-TL, Thermo Electron Instruments Inc., S/N 0710820808).
- Carbon monoxide IR analyser (Model 48, Thermo Electron Instruments Inc., S/N 68275-360).
- Delta Ohm HD2003 ultrasonic anemometer (S/N 10007572); the built-in compass in this instrument allowed also to obtain the course of the ship.
- GPS Evermore SA320 instrument.

The measurement principle of these instruments is described in the chapter "Measurement techniques" (p. 20-22). The inlets to the gas and Aethalometer have a cut-off respectively at 1 µm and 10 µm particle diameter by a homemade inertial impactor. Before entering the gas analysers the air passes through 5 µm pore size PTFE Millipore membrane filters in order to remove particles. The measurement procedure complies with the recommendations in the EMEP manual (EMEP, 1996). The anemometer as well as the GPS were placed at the top of the cabin housing the other instruments.

Data quality control and data processing

Calibrations are performed by use of certified standards of NO, CO and SO_2 from Air Liquide and zero air generated by a Breitfuss zero air generator. Before being brought on the ship, the Air Liquide standards were certified by comparison to VSL (National Metrology Institute of The Netherlands) primary standards in the ERLAP laboratory in Ispra. Calibrations were performed automatically during the week while the measurements were running unattended. NOx and SO_2 were calibrated once per week while CO zero calibrations were performed daily because of rapid baseline drift. CO span calibration was performed

once per week. Ozone was calibrated by comparison to a portable primary standard (Thermo Electron 49C PS).

The ozone analyser (Model C49) showed good stability: it was calibrated before the start of the measurements, during the measurements period and after getting back to the laboratory; in all cases all span and zero calibrations gave results within +/- 1 ppbV of the initial values. This stability is related to the fact that the instrument is using a two-channel system: one channel measures ambient air while the other channel measures ambient air, filtered by an ozone scrubber, and thus it provides a continuously updated zero point for the measurements.

Also the NOx and SO_2 analysers were stable: NOx calibrations gave a zero value (+/- one standard deviation) of -0.06±0.06 ppbV and 0.04±0.02 for NO and NO_2, respectively; the measured span gas multiplication correction factor ($C_{measured}/C_{certified}$) was 1.15±0.03. For SO_2, the calibrations gave zero values of 0.01±0.02 ppbV while the measured span gas calibration multiplication factor was 1.13±0.01. CO showed by far the largest drift of the zero point (8 ppbV per day). In addition, the CO measurements were influenced by variations in the internal temperature; the instrument response showed a linear dependence on temperature. Correction for the zero point drift as well as the temperature related variations were performed.

Raw data are averaged over 10 minute intervals and stored in a computer in an ACCESS database, using a LABVIEW software developed by NOS S.r.l. (Fabrizio Grassi).

Measurement program in 2012

Measurements were carried out continuously from August 6 until October 4 apart from interruptions of, altogether, approximately 6 measurements days due to various technical problems. The measurements were stopped because the ship started following a different route.

The information on course and speed of the ship as well as on wind speed and direction, obtained from the ultrasonic anemometer, was used to identify situations where the measurements might be influenced by emissions from Costa Magica: in all cases where the inlets to the measurement station were downwind of the stack of the ship within an angle of ± 40 degrees the data were discarded because of the risk of contamination from the stack.

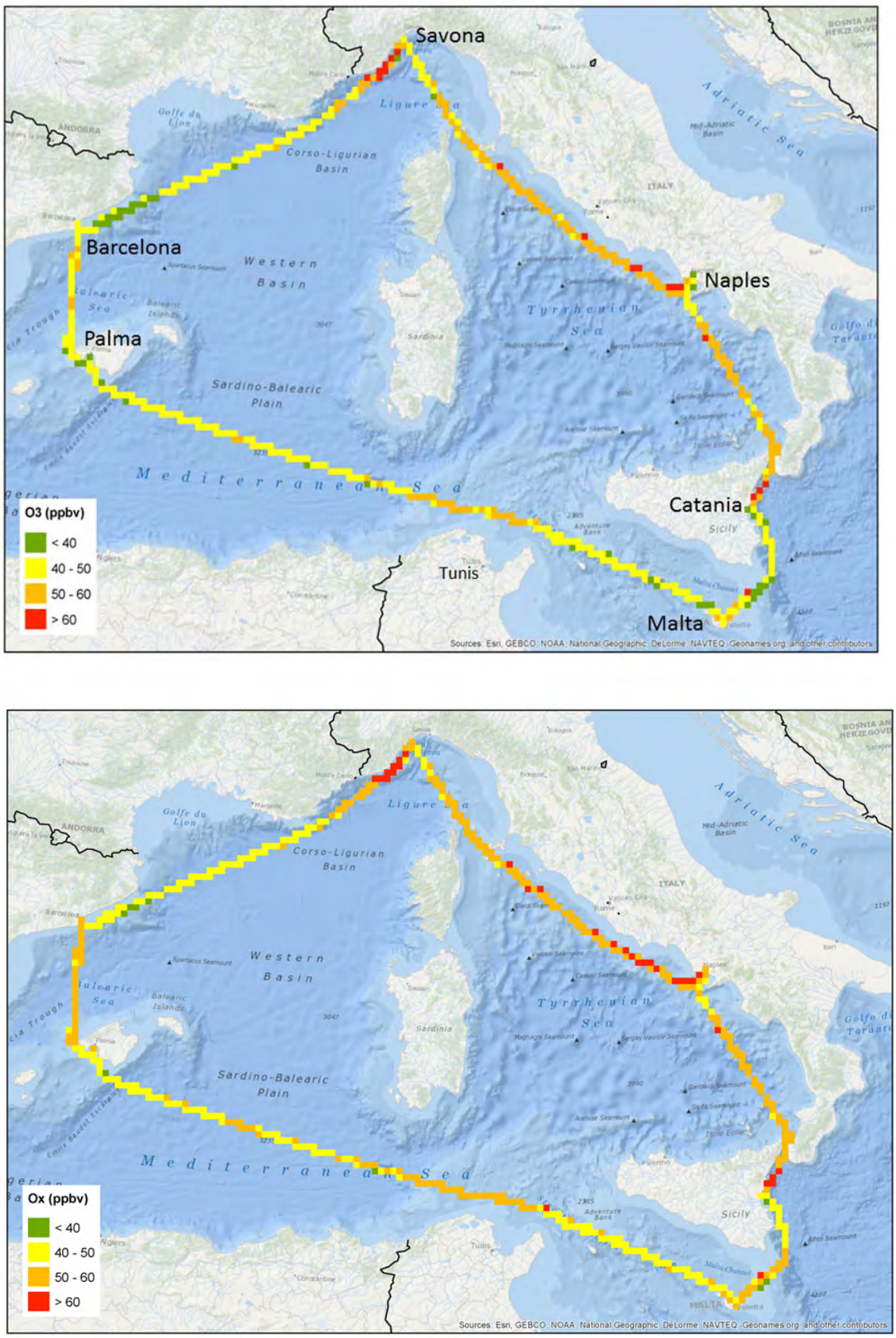

Figure 74. Ozone and Ox concentrations measured over the Western Mediterranean during the period August 6 – October 4, 2012.

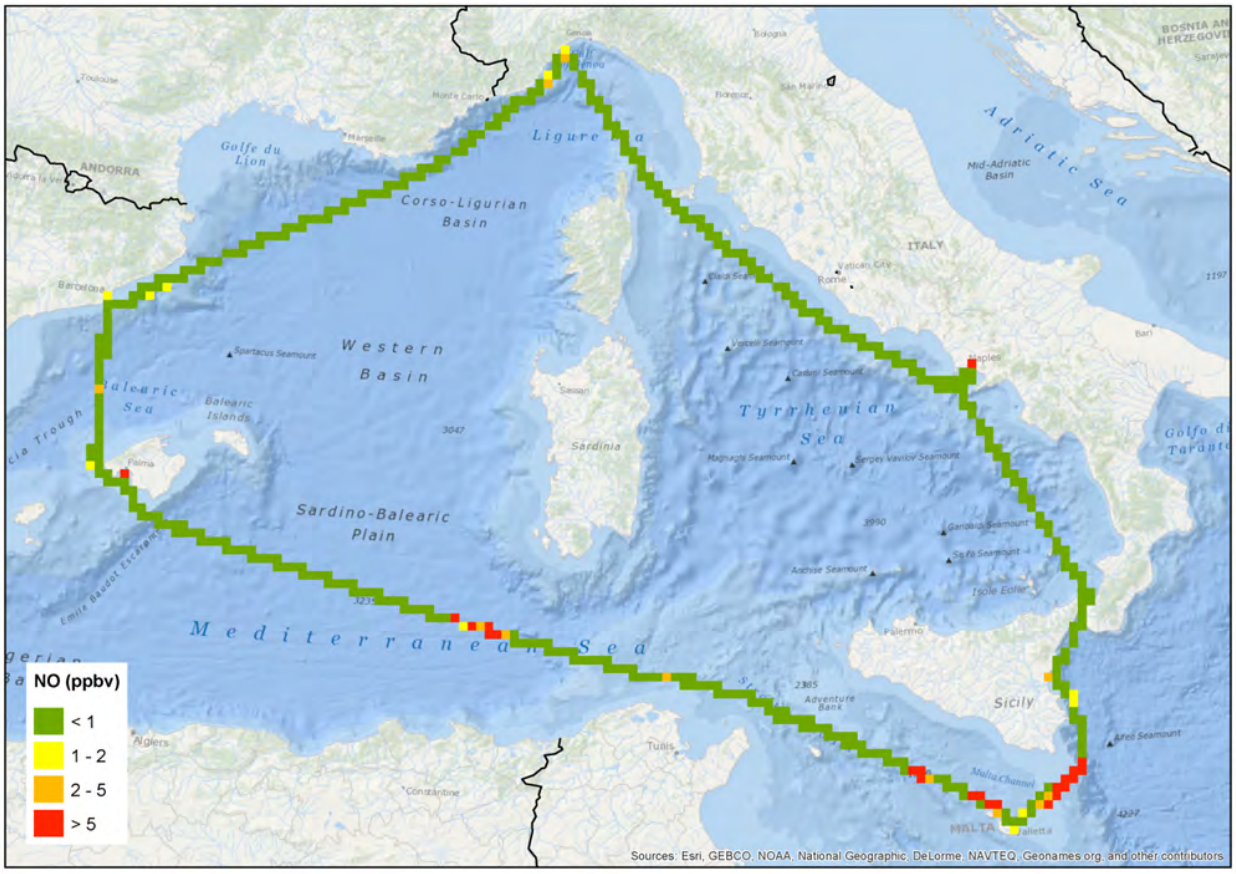

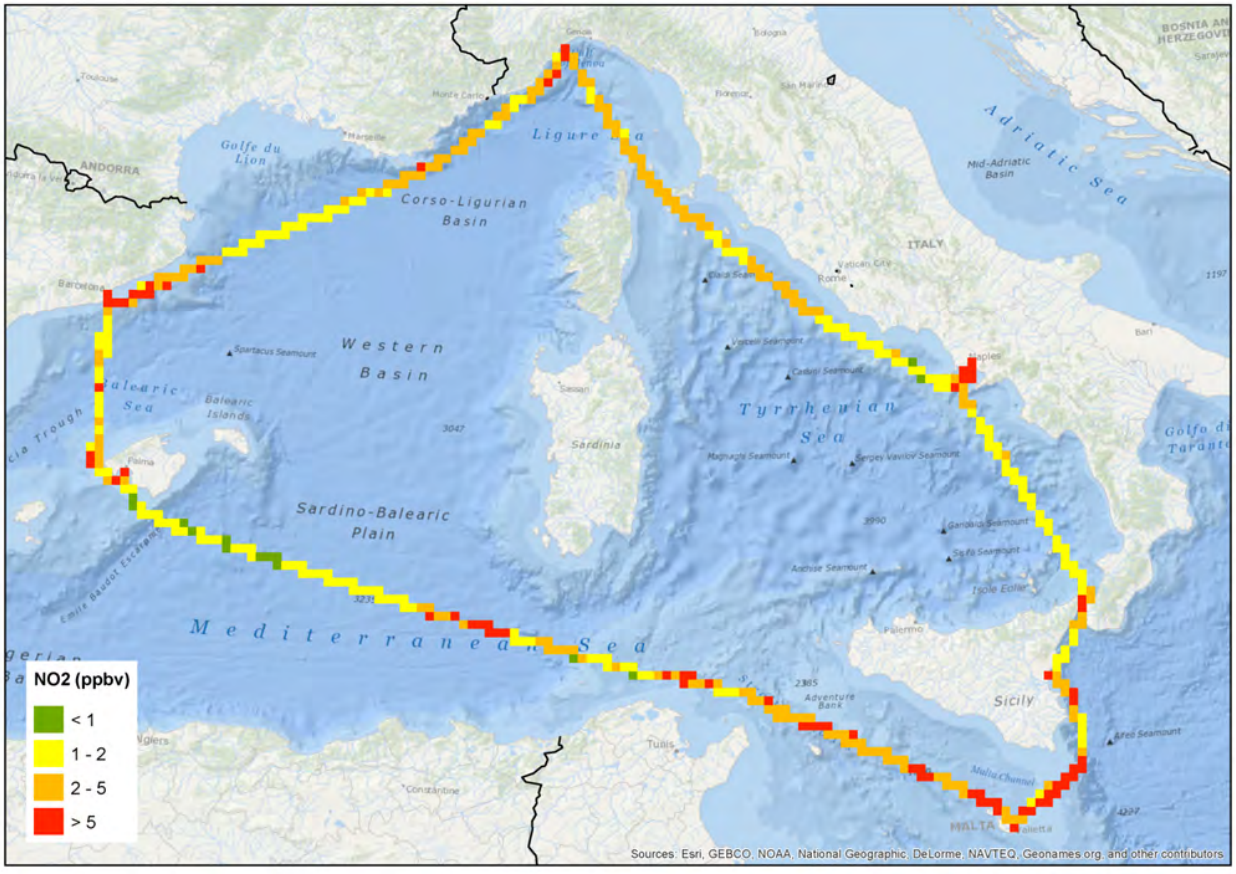

Figure 75. The average concentrations of NO and NO_2 measured over the Western Mediterranean during the period August 6 – October 4, 2012.

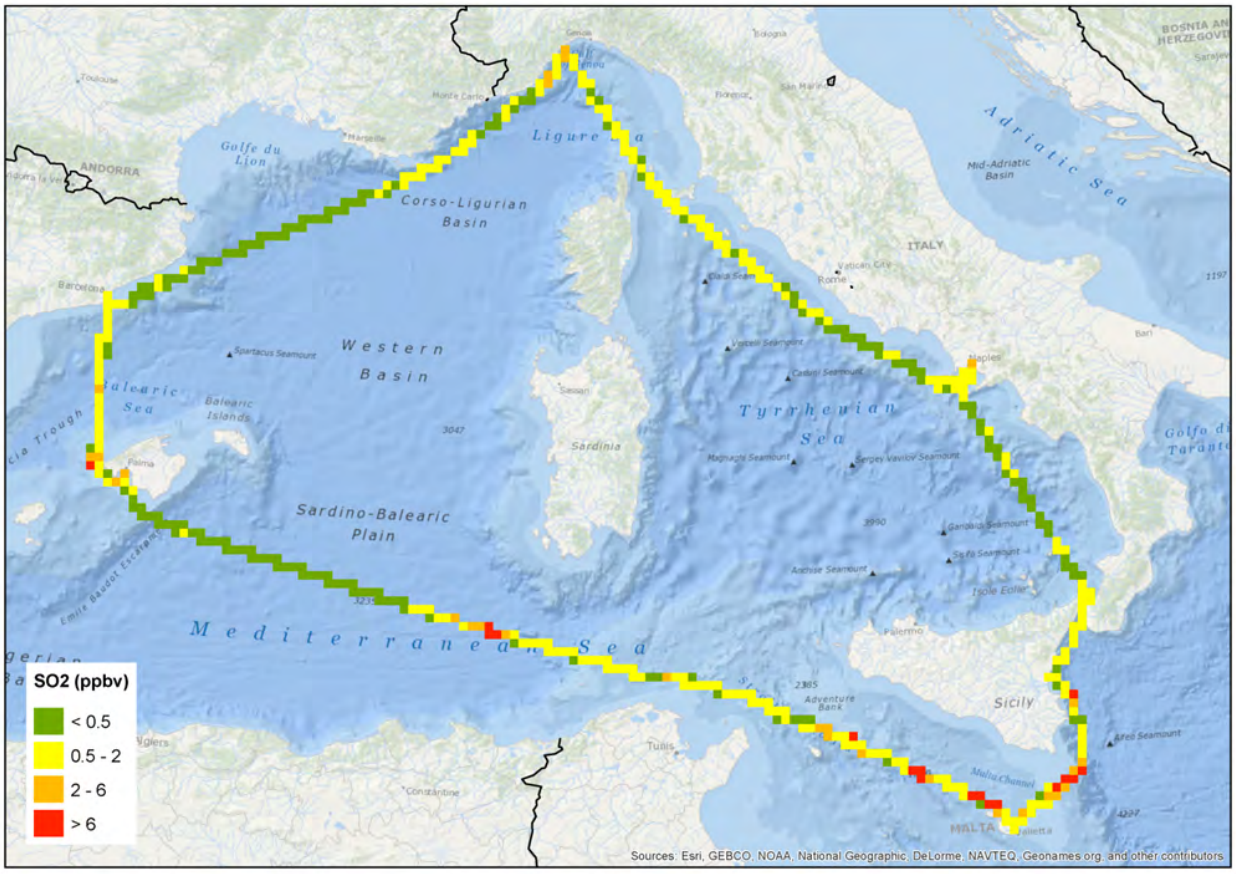

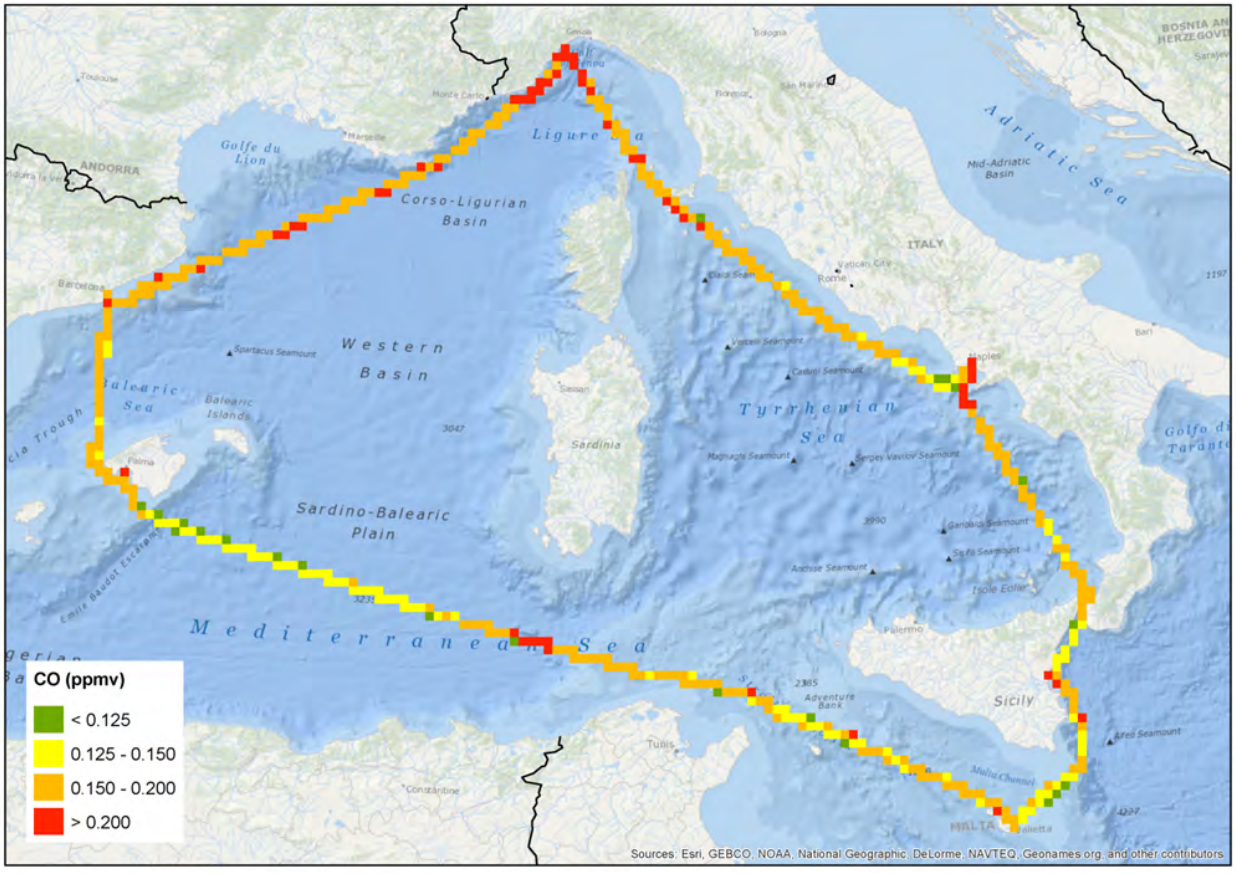

Figure 77. The average concentrations of SO_2 and CO measured over the Western Mediterranean during the period August 6 – October 4, 2012.

Results from 2012

The average concentrations observed during the period of the measurements have been plotted as a function of geographical position at a 10 x 10 km² grid scale using the ArcGIS software with the kind collaboration of Filipe Natista e Silvar**.** The data have been 'filtered' for measurements with a risk of contamination from the ship as described above.

The ozone and Ox concentrations are shown in Figure 74. 'Ox' , ozone plus NO_2, is a useful parameter to look at because it is insensitive to the impact of nearby, local NO-sources (normally combustion sources) that can have a strong influence on ozone because of the fast reaction

$$NO + O_3 \rightarrow NO_2 + O_2$$

It is seen, that during this period the highest ozone and Ox-levels were found at the eastern part of the route of the ship, particularly along the coasts of Lazio and Campania and close to the Gulf of Genova. As ozone is formed as a secondary pollutant by photochemical reactions, it is not expected to have exactly the same distribution as NOx and other primary pollutants, although there is a relationship, because NOx, and other compounds emitted from combustion of fossil fuels, are precursors of ozone.

The measured NO and NO_2 concentrations show, as expected, maxima in harbours and close to large urban centres like Genova, Barcelona and Naples (Fig. 75). However, relatively high concentrations are also found along the legs Palma-Malta and Malta Catania in areas that are not expected to be strongly influenced by emissions from the coast. This can be explained by the impact of NOx emissions from ships: as illustrated in Fig. 76, the EDGAR inventory predicts high levels of ship emissions along the main ship route that goes from the Strait of Gibraltar to the Suez Channel; this coincides with the area where high NOx concentrations were found along the route of Costa Magica. Ship traffic appears to be an important source of air pollution over the Western Mediterranean. Actually, 30% of all international sea-borne trade by volume is originating from or directed to Mediterranean ports or passing through its waters, where the oil tanker traffic is particularly intense.

The map of measured SO_2 concentrations (Fig. 77) shows the same features as the NO_x map, but here the highest concentrations are all found along the legs Palma-Malta and Malta-Catania. This is in agreement with the fact that ships generally use fuels with much higher sulphur content than what is used for transport on land and thus they are particularly strong sources of SO_2.

The concentrations of CO (Fig. 77) may be taken as an indication of the influence of combustion sources. It is thus to be expected that it may show a similar pattern as NO_x and SO_2 that also stem from combustion sources. However, the distribution of CO is seen to differ from that of SO_2 and NO_x because there are more frequent high concentrations in the northern part of the ship route and less along the legs between Palma, Malta and Catania. This is in line with the notion that ship emissions, compared to other combustion sources, typically have higher contents of NO_x and SO_2 compared to CO, due to the characteristics of

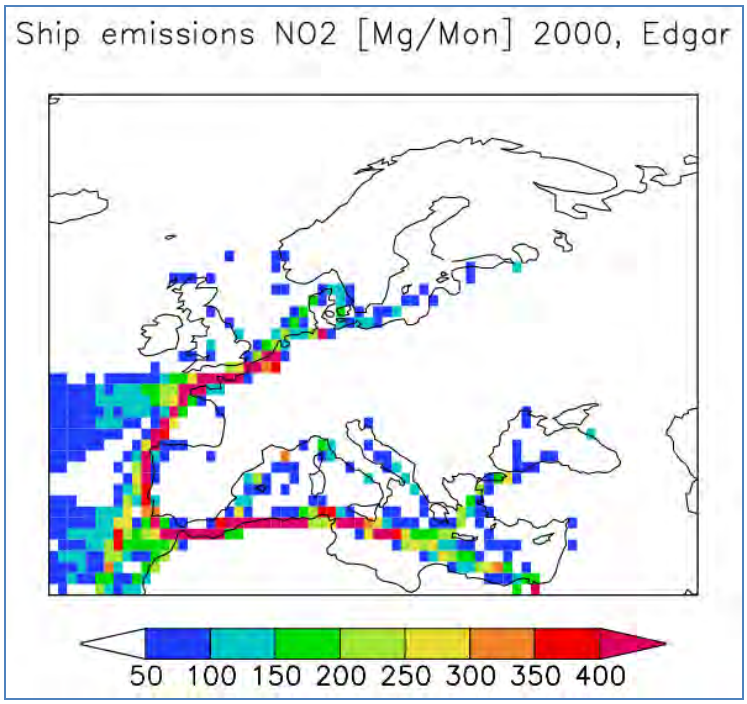

Fig. 76. Ship emissions of NO_2 according to the EDGAR emission inventory (from Marmer et al., 2008).

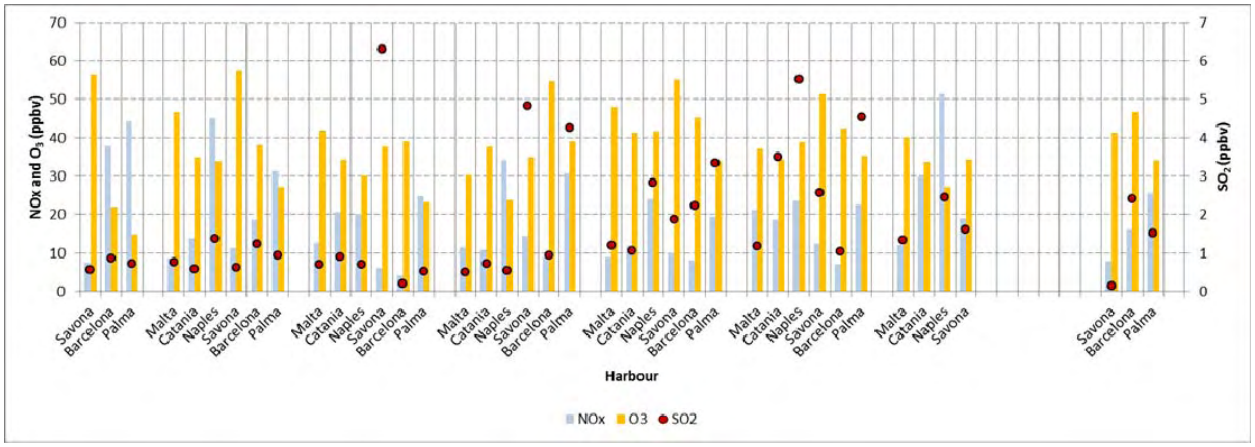

Fig. 78. The average concentrations of NOx, O_3 and SO_2 measured week by week during the stay of the ship in in harbours.

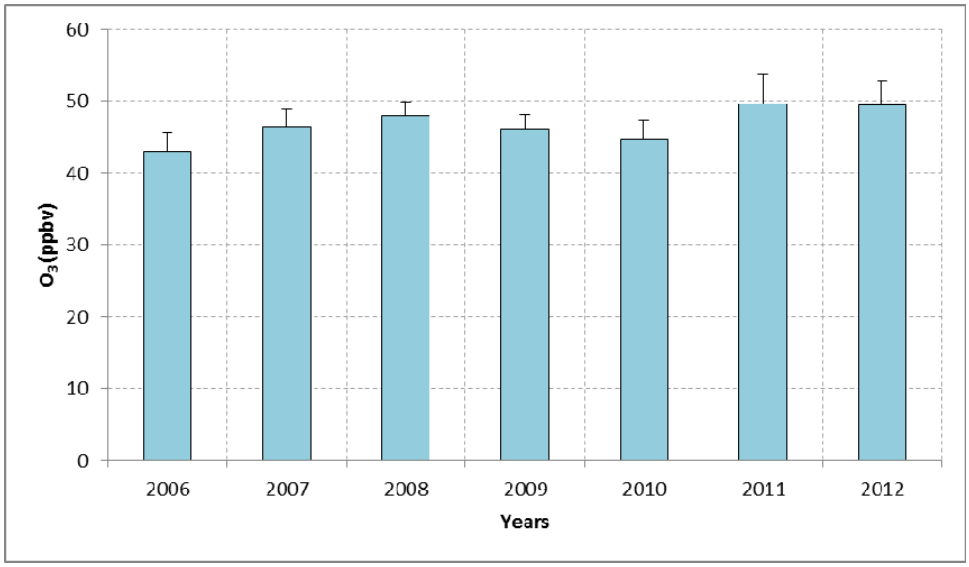

Fig. 79. The average concentration of O_3 measured during the month of September for the open sea route Palma-Tunis (see text).

the ship engines and the fuels they use. Furthermore, the CO distribution is different because this species has a longer atmospheric lifetime than NOx and SO_2.

The measurements from the cruise ship do also allow us to observe air pollution in harbours (Fig. 78). High levels of NOx are often observed while the average ozone values tend to be relatively low because of the impact of the destruction of ozone by the above mentioned reaction with NO. The concentrations of SO_2 have been found to be significantly reduced since the EU directive 2005/33/EC imposed a strong reduction of the sulphur content of fuels from the beginning of 2010, as discussed by Schembari et al. (2012). The values of SO_2 and NOx shown here are higher than the values reported by Schembari et al. because in the latter case, peak values from nearby sources (typically other ships) were filtered out.

The leg Palma-Tunis is important for these studies because it is the only part of the route where the ship is sailing for ~24h in open sea and far from the influence of coastal sources of pollution.

From Figure 79, it seems that the average concentrations of O_3 have been generally increasing along this route over the years, but it is important to tell that in the last two campaigns (2011 and 2012), the ship has altered its route, namely the harbor of Tunis was replaced by the harbor of La Valletta in Malta. For this comparison, only the first part of the route Palma-Malta, until the point nearest to Tunis, has been taken into account. This is only a slight change of the route, but we do not know if it can explain the fact that the ozone concentrations in 2011 and 2012 are higher than the previous ones.

Conclusion

Measurements of gaseous pollutants and meteorological variables were carried out continuously on board *Costa Magica* from August 6 to October 4 of the year 2012. The shorter dataset obtained for the year 2012 (due to the incident of Costa Concordia) proved to be nevertheless useful for obtaining a picture of air pollution over the Western Mediterranean, showing the pollution levels in harbors and the distribution of air pollutants along the route of the ship for the analyzed period. The observations gave evidence of an impact of emissions from ships on the measured air pollutants. The data will be useful for further analyses and for comparison with global and regional atmospheric models applied to the Western Mediterranean Basin.

References

Adam, M., J. P. Putaud, S. Martins dos Santos, A. Dell'Acqua, and C. Gruening, Aerosol hygroscopicity at a regional background site (Ispra) in Northern Italy, Atmos. Chem. Phys., 12, 5703–5717, 2012

Anderson, T.L., and Ogren, J.A., Determining aerosol radiative properties using the TSI3563 integrating nephelometer, *Aerosol Sci. Technol.*, **29**, 57-69, 1998.

Arnott, W.P., Hamasha, K., Moosmüller, H., Sheridan, P.J., and Ogren, J.A., Towards aerosol light-absorption measurements with a 7-wavelength Aethalometer: Evaluation with a photoacoustic instrument and a 3 wavelength nephelometer., *Aerosol Sci. Technol.*, **39**, 17-29, 2005.

Barnaba, F., Putaud, J.P., Gruening, C., Dell'Acqua, A., Dos Santos, S., Co-located in-situ, total-column and height-resolved aerosol observations: Implications for ground-level PM estimation from remote sensing. *J. Geophys. Res.*, **115**, D10204, doi:10.1029/2009JD012451, 2010.

Bates T., Calhoun J., Wang Y., Quinn P., variations in the methanesulphonate to sulphate molar ratio in submicrometer marine aerosol particles over the South Pacific Ocean, Journal of Geophysical research 1992, 97, 9859-9865.

Butterbach-Bahl K., R. Gasche, L. Breuer & H. Papen, Fluxes of NO and N_2O from temperate forest soils: impact of forest type, N deposition and of liming on the NO and N_2O emissions, Nutrient Cycling in Agroecosystems 48: 79–90, 1997.

Cavalli, F., Putaud, J.P., Toward a standardised thermal-optical protocol for measuring atmospheric organic and elemental carbon: the EUSAAR protocol, *Atmos. Meas. Tech.*, **3**, 79-89, 2010.

Cooke, W.F., Liousse, C., Cachier, H., and Feichter, J., Construction of a 1x1°fossil fuel emission data set for carbonaceous aerosol and implementation and radiative impact in the ECHAM4 model, *J Geophys. Res.*, **104**; 22,137-22, 1999.

Dell'Acqua, A., Putaud J.P., Gruening, C., Study of the JRC-Ispra EMEP site representativeness for short-lived atmospheric species measurements, *JRC report* EUR 24312 EN, 2010.

EMEP manual for sampling and chemical analysis (1995). *EMEP/CCC-Report 1/95.* (*Revised 1996; 2001; 2002).* 1995.

European Directive 2008/50/EC. On ambient air quality and cleaner air for Europe. 2008.

Gruening C., Goded I., Jensen N.R., Cescatti A., Cieslik S., Project Document ABC-IS forest flux tower, ARES(2011)1288711, (2011)

Gruening C., Goded I., Cescatti A., D. Fachinetti, I. Fumagalli, M. Duerr, ABC-IS Forest Flux Station, Report on Instrumentation, Operational Testing and First Months of Measurements, EUR 25705 EN, (2012), JRC76928

Hess, M., Koepke, P. Schult, I., Optical Properties of Aerosols and Clouds: The Software Package OPAC, *Bull. of Am. Meteorol. Soc.*, **79**; 831-844, 1998.

Jensen, N. R., Gruening, C., Adams, M., Cavalli, F., Cavalli, P., Grassi, F., Dell'Acqua, A., Martins Dos Santos, S., Roux, D., Putaud, J.-P. JRC Ispra EMEP – GAW regional station for atmospheric research, 2009 report, *EUR 24678 EN*, (2010), *JRC62602*.

Kiehl, J. T., Schneider, T. L., Rasch, P. J., Barth, M. C., Wong, J., Radiative forcing due to sulfate aerosols from simulations with the National Center for Atmospheric Research Community Climate Model, Version 3 (Paper 1999JD900495), *J. Geophys. Res.,* **105**; 1441-1458, 2000.

Marmer, E., Velchev , K., Hjorth, J., Vignati, E., Cavalli, F., Dentener, F., v. Aardenne,J., Raes, F. , Assessment of Impact of Ship Emissions Over the Summertime Mediterranean Sea, *Second International Conference on Harbours, Air Quality and Climate Change (HAQCC),*Rotterdam, the Netherlands, 29-30 May 2008.

Marmer, E., Dentener, F., Aardenne, J, Cavalli, F., Vignati, E., Velchev, K., Hjorth, J., Boersma, F. and Raes, F.: What can we learn about ship emission inventories from

measurements of air pollutants over the Mediterranean Sea, Atmos. Chem. Phys., 9, 6815-6831, 2009

McMurry, P., Wang, X., Park, K., and Ehara, K. The relationship between mass and mobility for atmospheric particles: A new technique for measuring particle density, *Aerosol Sci. Tech*., **36**, 227–238, 2002.

Mira-Salama, D., Van Dingenen, R., Gruening, C., Putaud, J.-P, Cavalli, F., Cavalli, P., Erdmann, N., Dell'Acqua, A., Dos Santos, S., Hjorth, J., Raes, F., Jensen, N.R. Using Föhn conditions to characterize urban and regional sources of particles, *Atmospheric Research* **90**, 159–16, 2008.

Pépin, L., M. Schmidt, M. Ramonet, D.E.J. Worhty and P. Ciais, Notes des Activités Instrumentales, A new gas chromatographic experiment to analyze greenhouse gases in flask samples and in ambient air in the region of Saclay, Institut Pierre-Simon Laplace (2001), http://www.ipsl.jussieu.fr.

Petzold, A., H., Schönlinner, M., Multi-angle absorption photometry - A new method for the measurement of aerosol light absorption and atmospheric black carbon, *Journal of Aerosol Science*, **35** (4), 421-441, 2004.

Putaud, J.-P., et al. (21 authors), 2004, A European aerosol phenomenology—2: chemical characteristics of particulate matter at kerbside, urban, rural and background sites in Europe. *Atmospheric Environment*, **38**, 2579-2595.

Putaud, J.-P., et al. (39 authors), 2010, A European aerosol phenomenology—3: Physical and chemical characteristics of particulate matter from 60 rural, urban, and kerbside sites across Europe. *Atmospheric Environment*, **44**, 1308-1320.

Russell, L.M.: Aerosol organic-mass-to-organic carbon ratio measurements, *Environ. Sci. Technol.*, **37**, 2982-2987, 2003.

Schmid, O., et al., Spectral light absorption by ambient aerosols influenced by biomass burning in the Amazon Basin I: comparison and field calibration of absorption measurements techniques, *Atmos. Chem. Phys.*, **6**, 3443-3462, 2006.

Scheeren, H. A., P. Bergamaschi, N. R. Jensen, C. Gruening, I. Goded, and J. van Aardenne, First results from the new JRC greenhouse gas monitoring site at Ispra, Italy. In Willi A. Brand (ed.) Report of the 15th WMO/IAEA Meeting of Experts on Carbon Dioxide, Other Greenhouse Gases and Related Tracers Measurement Techniques, Jena, Germany, 7-10 September 2009, WMO GAW report N. 194, 2010.

Scheeren, H. A., P. Bergamaschi et al., An analysis of four years of CO_2, CH_4, N_2O and SF_6 observations and ^{222}Radon-based emission estimates from the monitoring station at Ispra (Italy), for submission to Atmos. Chem. Phys. Discuss., 2013.

Schembari, C., F. Cavalli, E. Cuccia, J. Hjorth, G. Calzolai., N. Pérez, J. Pey, P. Prati, F. Raes: Impact of a European directive on ship emissions on air quality in Mediterranean harbours, Atmospheric Environment (2012), doi: 10.1016/j.atmosenv.2012.06.047

Stratmann, F., Wiedensohler, A. A new data inversion algorithm for DMPS-measurements. *J. Aerosol Sci.*, **27** (Suppl 1), 339-340, 1996.

Van Dingenen, R., et al. (28 authors), 2004, A European aerosol phenomenology –1: Physical characterization of particulate matter at kerbside, urban, rural and background sites in Europe, *Atmospheric Environment*, **38**, 2561-2577.

Velchev, K. ., Cavalli F., Hjorth J., Vignati E., Dentener F., Raes F., Ozone over Western Mediterranean Sea-results from two years of shipborne measurements., Atmospheric Chemistry and Physics, 11, 675-688, 2011.

Weingartner, E., Saathoff, H., Schnaiter, M., Streit, N., Bitnar, B., and Baltensperger, U., Absorption of light by soot particles: determination of the absorption coefficient by means of aethalometers, *J. Aerosol Sci.*, **34**, 1445-1463, 2003.

Weitkamp, C. (editor), LIDAR Range-Resolved Optical Remote Sensing of the Atmosphere, *Springer*, New York, 2005.

WHO, Health risks of ozone from long-range transboundary air pollution, 2008.

Worthy, D. E. F., I. Levin, N. B. A. Trivett, A. J. Kuhlmann, J. F. Hopper, and M. K. Ernst, Seven years of continuos methane observations at a remote boreal site in Ontario, Canada, J. Geophys. Res., 103 (D13), 15995-16007, 1998.

Zahorowski, W., S. D. Chambers, A. Henderson-Sellers, Ground based radon-222 observations and their application to atmospheric studies, J. Environm. Radioact., 76, 3-33, 2004.

Links

ACTRIS, *www.actris.net*

ARPA Lombardia, *ita.arpalombardia.it/ITA/qaria/doc_RichiestaDati.asp*

Calipso, *www.nasa.gov/mission_pages/calipso/main*

Chemical Co-ordinating Centre of EMEP, *www.nilu.no/projects/ccc*

CLRTAP, *www.unece.org/env/lrtap/welcome.html*

EARLINET, *www.earlinet.org*

ECLAIRE: www.eclaire-fp7.eu

EMEP, *www.emep.int*

EPTR, European Pollutant Release & Transfer Register, prtr.ec.europa.eu/MapSearch.aspx

European Committee for Standardisation (CEN), *www.cen.eu/cen/pages/default.aspx*

EUSAAR, *www.eusaar.net/*

Global Atmosphere Watch (GAW), *www.wmo.int/pages/prog/arep/gaw/gaw_home_en.html*

ICOS, www.icos-infrastructure.eu

WDCA, *www.gaw-wdca.org*

World Meteorological Organization (WMO), *www.wmo.int/pages/index_en.html.*

Executive Summary

The ABC-IS annual report 2012 provides an overview of the Atmosphere-Biosphere-Climate integrated monitoring activities performed by the Air and Climate Unit of the Joint Research Centre (H02). It presents results obtained in 2012 on long lived greenhouse gases concentrations (CO_2, CH_4, N_2O, SF_6), air ⇆ biosphere fluxes (CO_2, H_2O, heat,O_3), short lived climate forcers (O_3, aerosols) and their precursors (NOx, SO_2, CO), as well as other regulated species (PM_{10}, $PM_{2.5}$, heavy metals). These data extend the long time series in key pollution metrics (> 25 years) and climate forcers (5-10 years), in one of the most polluted areas in Europe.

We measure greenhouse gas concentrations and ^{222}Rn activity in Ispra (regional background in Northern Italy), atmosphere ⇆ terrestrial biosphere fluxes in Ispra (unmanaged temperate forest) and San Rossore (semi-managed Mediterranean forest), and O_3, aerosols and their precursors in Ispra and from a cruise ship in Western Mediterranean. Data quality is our priority. It is assured through our participation in international projects (ICOS, InGOS, ECLAIRE, ACTRIS) and programs (EMEP, GAW, AQUILA), in which standard operating procedures are applied, certified scales are used and inter-laboratory comparisons are organized regularly.

Our data can be downloaded from international data bases (www.europe-fluxdata.eu, www.ingos-infrastructure.eu, ebas.nilu.no, www.eclaire-fp7.eu), and can also be directly obtained from ABC-IS' staff. Five years of continuous greenhouse gas monitoring show that CO_2, CH_4, N_2O, and SF_6 concentrations are close to marine background under clean air conditions, with annual increments ranging 0.2 - 6%. Deviations from background concentrations provide key information about regional and larger scale European greenhouse gas sources. Analyses of rainwater revealed only 3 very acid (pH<4.6) rain event in 2012. In contrast, measurements of PM_{10} confirm the high level of particulate air pollution in the area of Ispra (Northwest of the Po Valley): 51 exceedances of the 24hr limit value (50 µg m^{-3}) were observed in 2012. However, PM concentrations have decreased by 1 µg m^{-3} yr^{-1} on average for more than 25 years. The main constituents of $PM_{2.5}$ are currently organic matter (48%), ammonium sulfate (21%), ammonium nitrate (17%), and elemental carbon (9%). The contribution of ammonium nitrate to $PM_{2.5}$ increases during pollution events. Ozone concentration decreased during 2001 – 2008, but increased for the third consecutive year in 2012. As a consequence, few indicators (e.g. SOMO35) reached or exceeded their historical maximums record at Ispra since 1988. However, the frequency of extreme events (1hr concentration > 180 µg m^{-3}) remains low compared to the past 25 years. Atmosphere ⇆ vegetation flux measurements in the forest on the JRC-Ispra premises were initiated in June 2012. During June-December 2012, atmospheric turbulence was such that 60 to 68% of the flux measurements were of good to acceptable quality. "Our" forest is clearly a sink for CO_2 in summer, and for O_3 the whole year round. As for the forest soil, it is a significant source of NO in summer, and a sink of NO_2 especially in winter. In San Rossore, pests' attacks led to massive tree cutting which forced us to stop measurements at

the current site. A new site was set up 700 m away in autumn 2012. The measurements from the cruise ship were resumed with a limited program in August this year, due to Costa Concordia's wreck. They clearly show the impact of ship emissions on NOx and SO_2 concentrations in the Western Mediterranean.

Long-term accurate measurements produce datasets which are essential to assess the impact of European Directives and international protocols, and develop future air quality and climate change mitigation policies. Conclusions arising from further analyses of our measurements include:

- evaluation of regional greenhouse gas emissions using inverse modeling and model-independent analyses using the ^{222}Rn tracer.
- abatement in sulfur emissions have been efficient in solving the acid rain issue and decreasing PM levels in our area. PM levels still remains too high though
- air quality policies are dimming the climate cooling effect of aerosols at our site
- measures for abating tropospheric ozone, which had a positive impact on concentrations and various indicators in the early 2000's, were partly compensated during the 3 last years
- temperate and Mediterranean forest can be an important sink for CO_2 and O_3. In contrast, the emission of NO from forest soils is significant.
- Directive 2012/33/EC on sulfur content of ship's fuel had a measurable impact on air quality in big European harbors around the Mediterranean. Out at sea, ships still emit massive amounts of pollutants, including O_3 precursors.
- The scope of these conclusions is certainly limited by the spatial representativeness of our measurements, which depends on the atmospheric lifetime of the studied species. This is why our measurements are performed in the framework of international collaborations. This ensures a privileged near real time access to the data produced on regional and global scales by the networks in which we participate.

European Commission
EUR 26571 EN – Joint Research Centre – Institute for Environment and Sustainability

Title: JRC – Ispra Atmosphere – Biosphere – Climate Integrated monitoring Station. 2012 report

Author(s): J.P. Putaud, C. Belis, P. Bergamaschi, F. Cavalli, A. Cescatti, D. Daou, A. Dell'Acqua, K. Douglas, M. Duerr, I. Goded, F. Grassi, C. Gruening, J. Hjorth, N. R. Jensen, F. Lagler, G. Manca, S. Martins Dos Santos, R. Passarella, V. Pedroni, P. Rocha e Abreu, D. Roux, B. Scheeren

Luxembourg: Publications Office of the European Union

2014 – 116 pp. – 21.0 x 29.7 cm

EUR – Scientific and Technical Research series – ISSN 1831-9424 (online)

ISBN 978-92-79-33603-4 (PDF)

doi: 10.2788/38242

Abstract

The Institute for Environment and Sustainability provides long-term observations of the atmosphere within international programs and research projects. These observations are performed from the research infrastructure named ABC-IS: Atmosphere – Biosphere – Climate Integrated monitoring Station. Most measurements are performed at the JRC-Ispra site. Observations are also carried out from two other platforms: the forest station in San Rossore, and a ship cruising in the Western Mediterranean sea. This document reports about the measurement programs, the equipment which is deployed, the data quality assessment, and the results obtained for each site. Our observations are presented, compared to each other, as well as to historical data obtained over more than 25 years at the Ispra site.

LB-NA-26571-EN-N

JRC Mission

As the Commission's in-house science service, the Joint Research Centre's mission is to provide EU policies with independent, evidence-based scientific and technical support throughout the whole policy cycle.

Working in close cooperation with policy Directorates-General, the JRC addresses key societal challenges while stimulating innovation through developing new methods, tools and standards, and sharing its know-how with the Member States, the scientific community and international partners.

Serving society
Stimulating innovation
Supporting legislation

doi: 10.2788/38242
ISBN 978-92-79-33603-4